

4 Puck's action plane fracture criteria

4.1 Fiber fracture criteria

Fiber fracture is primarily caused by a stressing σ_{\parallel} which acts parallel to the fibers. For $(\sigma_1, \sigma_2, \tau_{21})$ -combinations the use of a simple maximum stress formulation is recommendable. Such a formulation was already proposed by Puck in 1969 [Puck 1969, Puck and Schneider 1969]. It expresses the physical idea that fiber fracture under multiaxial stresses in a UD-lamina occurs when its stress parallel to the fibers σ_1 is equal to or exceeds the stress necessary for a fracture under uniaxial stress σ_1 . From this hypothesis follows the simple FF-condition

$$\begin{aligned} \frac{\sigma_1}{R_{\parallel}^t} &= 1 & \text{for } \sigma_1 > 0 \\ \frac{\sigma_1}{(-R_{\parallel}^c)} &= 1 & \text{for } \sigma_1 < 0 \end{aligned} \quad (\text{Eq. 14})$$

If σ_1 is a tensile stress, the strength R_{\parallel}^t is used in (Eq. 14). If σ_1 is a compressive stress, R_{\parallel}^c is used instead. Strengths are always defined as positive values. This is the reason for using the “-” sign at R_{\parallel}^c in (Eq. 14). If σ_1 reaches the fracture stress $\sigma_{1fr} (= R_{\parallel}^t \text{ or } -R_{\parallel}^c)$ the fracture condition is fulfilled.

(Eq. 14) can easily be transformed to a fracture criterion being formulated with the stress exposure $f_{E,FF}$:

$$\begin{aligned} f_{E,FF} &= \frac{\sigma_1}{R_{\parallel}^t} & \text{for } \sigma_1 \geq 0 \\ f_{E,FF} &= \frac{\sigma_1}{(-R_{\parallel}^c)} & \text{for } \sigma_1 < 0 \end{aligned} \quad (\text{Eq. 15})$$

For a preliminary analysis this simple fracture criterion is sufficient. However, for a precise analysis a more sophisticated formulation can be

useful which takes into account secondary effects, too. These effects are discussed in the following:

A uniaxial σ_2 -stress (or σ_3 -stress, respectively) leads – due to a Poisson's effect – to an additional micro-mechanical strain in fiber direction ε_1 . The effect is enlarged locally by the circumstance that the stress in the matrix is inhomogeneously distributed and effectively larger than the transverse stress σ_2 (σ_3 , respectively) on the lamina-level.

This effect of stress and strain magnification can best be explained using the common model of serial springs. If a thin UD-lamina (which consists alternately of fibers and matrix) is stressed transverse to the fiber direction, the load is – on an intersection without fibers – carried by the matrix alone. On a neighboring intersection, the load is carried by the fiber alone [Puck and Schneider 1969]. From this simple model follows that the stress σ_2 is the same in fiber and matrix and that the micro-mechanical strain is different due to the different Young's moduli. However, close to the interface between fiber and matrix there is additional biaxial strain in the matrix. This effect is taken into account by the use of a magnification factor $m_{\sigma,f}$. Puck proposes $m_{\sigma,f} = 1.3$ for GFRP and $m_{\sigma,f} = 1.1$ for CFRP¹⁶ [Puck 1996, Fischer 2003].

Puck based his more sophisticated FF-condition on the following fracture hypothesis [Puck 1996, Puck and Schürmann 1998, Puck and Schürmann 2002]:

Fiber fracture of a UD-lamina under combined stresses will occur when in the fibers the same stress σ_{1f} is reached which is acting *in the fibers* at an FF of the lamina caused by uniaxial tensile stress σ_1^t or a uniaxial compressive stress σ_1^c respectively.

The starting point is the strain ε_{1f} of the fibers caused by the combined stresses $\sigma_1, \sigma_2, \sigma_3$:

$$\varepsilon_{1f} = \frac{\sigma_{1f}}{E_{\parallel f}} - \frac{\nu_{\parallel \perp f}}{E_{\perp f}} \cdot m_{\sigma f} \cdot (\sigma_2 + \sigma_3) \quad (\text{Eq. 16})$$

Using $\nu_{\parallel \perp f}/E_{\perp f} = \nu_{\perp \parallel f}/E_{\parallel f}$, and $\varepsilon_{1f} = \varepsilon_1$, the stress σ_{1f} in the fibers acting in their longitudinal direction can be calculated from

$$\sigma_{1f} = E_{\parallel f} \cdot \varepsilon_1 + \nu_{\perp \parallel f} \cdot m_{\sigma f} \cdot (\sigma_2 + \sigma_3) \quad (\text{Eq. 17})$$

¹⁶ The value for CFRP is smaller because the transverse Young's modulus of carbon fibers is lower than that of glass fibers.

From (Eq. 17) a new fracture condition can be derived. First ε_1 and the fiber stress σ_{1f} are replaced by the elastic law of the UD-lamina and the fracture resistance $R_{\parallel f}$ of the fibre, respectively:

$$\varepsilon_1 = \frac{\sigma_1}{E_{\parallel}} - \frac{\nu_{\perp\parallel}}{E_{\parallel}} (\sigma_2 + \sigma_3) \quad (\text{Eq. 18})$$

$$R_{\parallel f} = E_{\parallel f} \cdot e_{\parallel} ; R_{\parallel} = E_{\parallel} \cdot e_{\parallel} \quad \text{with } e_{\parallel} = \text{fracture strain from uniaxial } \sigma_1 \text{ of both fiber and UD-lamina} \quad (\text{Eq. 19})$$

Based on this the FF-condition for the UD-lamina is:

$$\frac{1}{\pm R_{\parallel}^{t,c}} \left[\sigma_1 - \left(\nu_{\perp\parallel} - \nu_{\perp\parallel f} m_{\sigma f} \frac{E_{\parallel}}{E_{\parallel f}} \right) (\sigma_2 + \sigma_3) \right] = 1 \quad \text{with} \quad (\text{Eq. 20})$$

$$\begin{aligned} R_{\parallel}^t & \text{ for } [\dots] > 0 \\ -R_{\parallel}^c & \text{ for } [\dots] < 0 \end{aligned}$$

This fracture condition (Eq. 20) is homogeneous of grade 1 and can thus easily be transformed to a formulation for the stress exposure $f_{E,FF}$:

$$f_{E,FF} = \frac{1}{\pm R_{\parallel}^{t,c}} \left[\sigma_1 - \left(\nu_{\perp\parallel} - \nu_{\perp\parallel f} m_{\sigma f} \frac{E_{\parallel}}{E_{\parallel f}} \right) (\sigma_2 + \sigma_3) \right] \quad \text{with} \quad (\text{Eq. 21})$$

$$\begin{aligned} R_{\parallel}^t & \text{ for } [\dots] \geq 0 \\ -R_{\parallel}^c & \text{ for } [\dots] < 0 \end{aligned}$$

Here, $f_{E,FF}$ is the FF-stress exposure of the UD-lamina, $\nu_{\perp\parallel}$ is the major Poisson's ratios of the UD-lamina, and $\nu_{\perp\parallel f}$ the major Poisson's ratio of the fiber. In general the definition of the Poisson's ratios is a well known source of misunderstandings, because there are different definitions used. In the US for instance, it is common standard to define the indices of ν the other way round (the first index for the direction of the stress which leads to the Poisson effect).

In the above Equations E_{\parallel} is the longitudinal modulus of the lamina parallel to the fibers and $E_{\parallel f}$ the longitudinal modulus of the fibers. $m_{\sigma f}$ is a magnification factor for the transverse stress in the fibers (GFRP $m_{\sigma f} \approx 1,3$ and for CFRP $m_{\sigma f} \approx 1,1$). Puck has found that in case of plane (σ_1 , σ_2 , τ_{21})-stress, the results of (Eq. 15) and (Eq. 21) differ only by a few percent. However, the influence of transverse stresses on FF can become important in the region of combined $\sigma_2 < 0$ and $\sigma_3 < 0$ of similar magnitude, where $|\sigma_2|$

and $|\sigma_3|$ can exceed the transverse compressive strength R_{\perp}^c by a factor of up to 3 or 4 [Kopp 2000]).

The maximum stress criteria (Eq. 15) and (Eq. 21) presented above were put into question by Hart-Smith [Hart-Smith 1998a, Hart-Smith 1998b] who proclaimed that the fracture stress σ_{ifr} is considerably reduced in the presents of high transverse strains with a different algebraic sign compared to the strain in fiber direction ε_1 . Hart-Smith based this on some experimental work [Hart-Smith 1984]. However, this hypothesis has – at least for monotonously increasing loads – been disproved by sophisticated experimental work [Fischer 2003; Mannigel 2007] which approves the appropriateness of maximum stress criteria.

A further aspect to be considered is the influence of shear stresses on the fiber fracture. Whereas tensile stressing in fiber direction σ_{\parallel}^t leads unquestionably to fiber rupture, the fracture mode is not as obvious in the case of compressive stressing σ_{\parallel}^c . In principle, several forms of fiber fracture are possible. The dominant failure mode is kinking of the fibers due to shear stresses in the fiber [Schürmann 2004; Pinho et al 2006]. Consequently, longitudinal shear stressing of the UD-lamina $\tau_{\perp\parallel}$ reduces the compressive fracture strength $\sigma_{\perp\parallel}^c$. In [Puck 1996] and [Fischer 2003] pure empirical formulations are given to account for this effect. Mannigel [Mannigel 2007] quantified the effect for the first time by intensive experimental investigations. He found that for relatively small shear stresses there is no influence of τ_{21} on the fiber fracture. If the shear stress surpasses a threshold and leads to microdamage, the compressive fracture strength is significantly reduced. Mannigel found a linear (degressive) influence of the shear stress on the compressive fracture strength above the threshold. A calibration can be made with the experimental results published in [Mannigel 2007].

A further influence on the fiber fracture which is not taken into account by the maximum stress criteria (Eq. 15) and (Eq. 21) is the effect IFF has. Especially under cyclic loading IFF reduces the fiber fracture stress σ_{ifr} considerably. However, the UD-lamina can in this case no longer be used as an isolated model. Instead, IFF in adjacent lamina influences FF [Knickrehm 2000]. In this case a more sophisticated analysis of the gradual failure process is necessary.

4.2 Inter fiber fracture (IFF) criteria

4.2.1 Motivation

The major motivation for the development of Puck's Inter Fiber Fracture criteria is experimental evidence. Fracture criteria are used to predict the

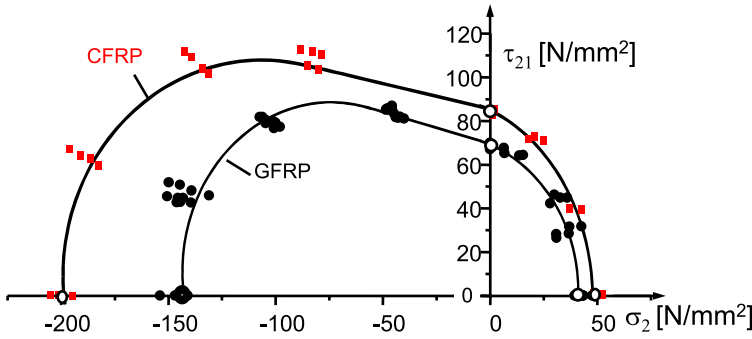


Fig. 23. Fracture limits for (σ_2, τ_{21}) -stress combinations

strength of a material for arbitrary states of multiaxial stress with the preliminary knowledge of only some easy to measure strength values. One can best compare different criteria by taking experimental results that do exhibit some kind of “uncommon” or special material behavior. For carbon (squares) and glass fiber reinforced plastics (circles) Fig. 23 shows such test results obtained in a large German research project [Cuntze et al. 1997].

Some remarkable observations can be made here:

- The stresses σ_2^t and τ_{21} interact. That means that – when σ_2^t and τ_{21} act at once – fracture occurs before $\sigma_2^t = R_{\perp}^t$ or $\tau_{21} = R_{\perp\parallel}$ respectively are reached.
- Shear fracture is impeded by moderate transverse compressive stress σ_2^c . In other words: Higher shear stress τ_{21} can be sustained without fracture, when τ_{21} and moderate σ_2^c act simultaneously.
- A third aspect becomes obvious when looking at Fig. 24: When σ_2^c and τ_{21} act simultaneously and the ratio $|\sigma_2^c/\tau_{21}|$ exceeds a certain value, fracture occurs under an angle $\theta_{fp} \neq 0^\circ$. The fracture angle increases with growing stress ratio $|\sigma_2^c/\tau_{21}|$ and reaches approximately $\pm 54^\circ$ for pure transverse compressive stress (see Fig. 8).

The real failure envelope is not symmetric to any vertical line. This is clearly illustrated by the fracture curve in Fig. 24 and cannot be modeled by conventional global failure criteria. Besides, these criteria cannot calculate the fracture angle nor do they explain the effects observed and explained above. However, the understanding of these effects is crucial for the development of reasonable failure criteria. Of special interest is in this context the analysis of the fracture angle under pure transverse compression σ_2^c . Fracture occurs on a plane inclined by approximately $\pm 54^\circ$ to the action plane of σ_2^c . A simple sketch of the Mohr circle shows what stresses act on this fracture plane (Fig. 25). This shall be derived in detail:

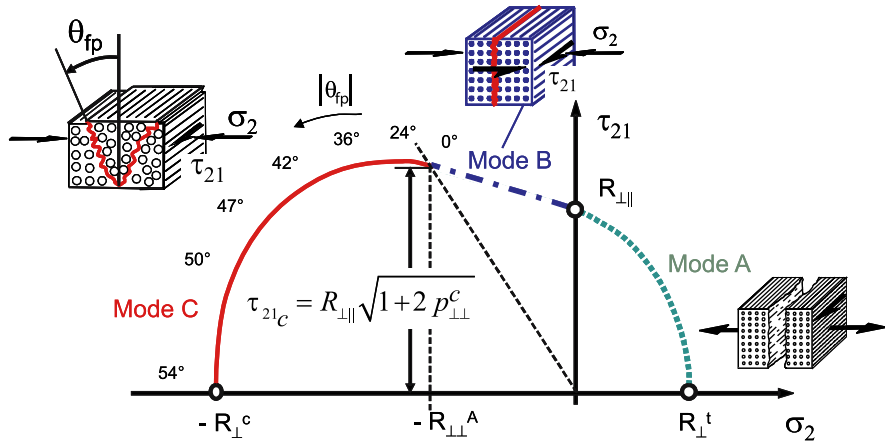


Fig. 24. Fracture curve (σ_2, τ_{21})

On the action plane of σ_2^c ($\theta = 0^\circ$) pure transverse compression ($\sigma_n^c = \sigma_2^c, \tau_{nt} = 0$) is acting. On this plane no fracture can occur. On a perpendicular plane ($\theta = 90^\circ$) there is no stress at all. On all other planes with $0^\circ < \theta < 90^\circ$ combinations of a transverse compressive stress $\sigma_n^c(\theta)$ and a transverse shear stress $\tau_{nt}(\theta)$ are acting. Under $\theta = 45^\circ$ the maximum shear stress $\tau_{nt \max} = \tau_{nt}(45^\circ)$ is reached. It has the same value as $\sigma_n^c(45^\circ)$ acting on the same plane and the magnitude is just half that of σ_2 . Under 54° – on the fracture plane – the shear stress $\tau_{nt}(54^\circ)$ is just slightly smaller than $\tau_{nt \max}$. However, the transverse compressive stress $\sigma_{nt}(54^\circ)$ which impedes fracture is considerably smaller than the corresponding value un-

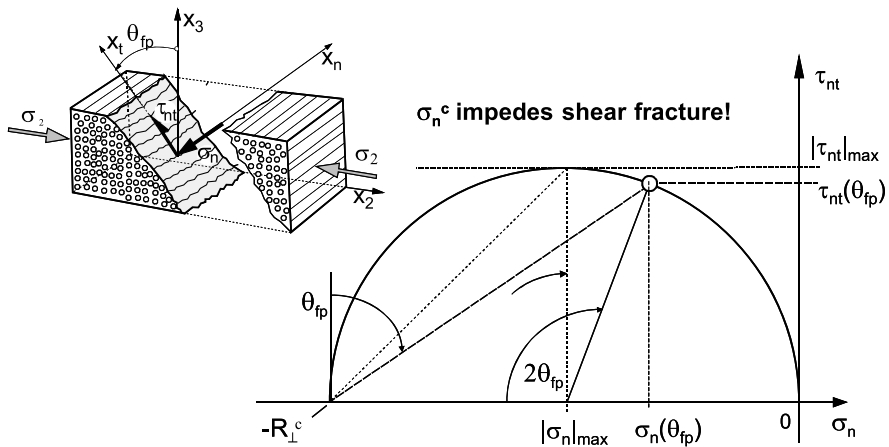


Fig. 25. Fracture under uniaxial compressive stress σ_2^c

der 45° . This fact explains why the fracture angle is greater than $\pm 45^\circ$. This is in accordance with the observation that higher shear stresses can be sustained in the presence of moderate transverse compression.

The analysis of the fracture behavior which will be presented here, works with the stresses on the action plane and not with the lamina stresses $\sigma_2, \sigma_3, \tau_{23}, \tau_{31}, \tau_{21}$. This is a fundamental fact and leads to the approach to formulate fracture criteria using the stresses of the action plane. These fracture criteria will be presented and explained in the next sections. Before this, the fracture hypotheses those criteria are based on, are discussed. Besides, the basic strengths and some inclination parameters needed for calibration are presented.

4.2.2 Different IFF-fracture modes

The different kinds of IFF described above for the (σ_2, τ_{21}) -fracture curve lead to the differentiation of three IFF-fracture modes, namely Mode A, Mode B and Mode C defined as follows:

- *Mode A*: Transverse tensile stressing σ_\perp^t or longitudinal shear stressing τ_{\parallel} cause – acting either alone or in combination – fracture. In the case of a 2D-state of stress with $\sigma_1, \sigma_2, \tau_{21}$ the cracks run in thickness direction and thus in the common action plane of the lamina stresses σ_2 and τ_{21} . The fracture surfaces are separated from each other due to the tensile stressing. This leads from a macroscopic point of view to a degradation of both the Young's modulus E_\perp and the shear modulus G_{\parallel} .
- *Mode B*: Fracture is caused by longitudinal shear stressing τ_{\parallel} . This fracture occurs on the action plane of the external shear stress τ_{21} . In contrast to Mode A, the transverse normal stressing σ_\perp^c which acts on the fracture plane simultaneously with τ_{\parallel} is a compressive stressing! Thus the crack does not open and the fracture surfaces are pressed on each other¹⁷. Consequently the degradation of stiffness due to $\text{IFF}^{\text{Mode B}}$ is much less significant than that due to $\text{IFF}^{\text{Mode A}}$. An $\text{IFF}^{\text{Mode B}}$ occurs as long as the ratio of the compressive stress at fracture and the transverse compressive strength $|\sigma_{\perp\text{fr}}^c/R_\perp^c|$ is smaller than roughly 0.4.
- *Mode C*: If the ratio of the compressive normal stressing at fracture and the transverse compressive strength $|\sigma_{\perp\text{fr}}^c/R_\perp^c|$ exceeds roughly 0.4, the action plane of the external shear stress τ_{21} is no longer the fracture plane. Instead fracture occurs on a plane inclined by an angle $|\theta_{\text{fp}}| \neq 0^\circ$ to the action plane of σ_2 and τ_{21} . The fracture angle $|\theta_{\text{fp}}|$ increases in the case of a plane state of stress $(\sigma_1, \sigma_2, \tau_{21})$ from 0° at the threshold

¹⁷ Thermal tensile stresses in the matrix might lead to a separation of the fracture surfaces nonetheless.

between Mode B and Mode C to roughly $|54^\circ|$ for pure transverse compression ($\tau_{21} = 0$). $\text{IFF}^{\text{Mode C}}$ implies the risk of delamination between the broken layer and adjacent layers.

In a more general 3D state of stress a forth fracture mode can occur:

- *Mode A**: On the fracture plan acts a combination of σ_\perp^t , $\tau_{\perp\perp}$ and $\tau_{\perp\parallel}$.

4.2.3 Fracture hypotheses

4.2.3.1 Mohr's fracture hypothesis

Fiber fracture (FF) is – in the sense as it used here – defined as the simultaneous breaking of thousands of filaments. FF of a UD-lamina is regarded as final failure of the affected lamina. Inter fiber fracture (IFF) on the other hand is defined as a macroscopic crack which runs parallel to the fibers and separates an isolated UD-layer into two pieces. Usually, such a macroscopic separation is preceded by micro-mechanical damage of the matrix or the fiber/matrix-interface, respectively.

Fiber reinforced composites (FRP) used in lightweight construction usually show brittle fracture behavior concerning both FF and IFF. This means that fracture occurs suddenly on a certain fracture plane without any major plastic deformation. This characteristic material behavior is especially distinctive for σ_\perp^t - and $\tau_{\perp\perp}$ -stressing. In both cases brittle fracture occurs on the plane with the highest tensile stress (compare Fig. 26). Paul [Paul 1961] called materials with such a behavior “intrinsically brittle”. The compressive strength of such materials (here: R_\perp^c) is much higher than (usually twice the value of) the tensile strength (here: R_\perp^t). Uniaxial compression leads to shearing on a plane which is inclined to the direction of the compressive stressing (compare Fig. 26). This fracture is caused by the transverse shear stressing (here: $\tau_{\perp\perp}$) acting on the inclined fracture plane.

The described brittle fracture in FRP-structures has been known for decades now. Nevertheless, most commercial Finite-Element-programs still work with global strength criteria like that of Tsai/Wu [Tsai 1992], which are in principle all based on the von Mises yielding criterion. Those global strength criteria can only be regarded as pure interpolating formulae. They are not based on a failure hypothesis and thus do not consider the true material behavior. All stresses are put into one formula not regarding whether the single stress causes FF or IFF.

Obviously, yielding criteria are not adequate for FRP-failure analysis. Because of the brittle material behavior of FRP, failure analysis should instead be based on the ideas of Mohr [Mohr 1900] and Coulomb

[Coulomb 1776]. **Mohr's fracture hypothesis** for brittle materials is the following:

The fracture limit of a material is determined by the stresses on the fracture plane.

The cited original work refers to brittle isotropic material (for instance cast iron).

4.2.3.2 Puck's fracture hypotheses

Most failure conditions in use are pure mathematical interpolation functions with no physical basis. Puck, however, based his fracture criteria on a reasonable understanding of the brittle fracture, formulated in his fracture hypotheses. He works with the stresses σ_n , τ_{nt} and τ_{nl} which are acting on a common fiber parallel action plane of a UD-lamina. The two shear stresses τ_{nt} and τ_{nl} can be combined to one resulting shear stress $\tau_{n\psi}$ (see (Eq. 4) and Fig. 18).

Puck's fracture hypotheses are the following:

1. Inter Fiber Fracture on a plane parallel to the fibers is caused by the stresses σ_n and $\tau_{n\psi}$ acting on the fracture plane.
2. If σ_n is a tensile stress it promotes fracture together with the shear stress $\tau_{n\psi}$ or even alone for $\tau_{n\psi} = 0$.

In contrast to that σ_n impedes fracture if it is a compressive stress by raising the fracture resistance of the fracture plane against shear fracture with increasing compressive stress σ_n .

Experimental experience has shown, that transverse shear stressing $\tau_{\perp\perp}$ causes a fracture not in the action plane of $\tau_{\perp\perp}$ but in the plane of the tensile principal stress which has the same magnitude as $\tau_{\perp\perp}$. Therefore, a rule has been formulated by Puck for the case of combined stresses σ_2 , σ_3 , τ_{23} or σ_{II} , σ_{III} respectively:

If the UD-lamina is just stressed in the plane of transverse isotropy (only stresses σ_2 , σ_3 , τ_{23}) fracture occurs either as tensile fracture due to σ_n as the highest normal stress or as shear fracture due to τ_{nt} – impeded by a transverse compressive stress σ_n . Which of the two kinds occurs depends on the ratios of the stresses σ_2 , σ_3 , τ_{23} .

This additional rule might not be valid for composites with an unusually small ratio between transverse compressive and transverse tensile strength $R_{\perp}^c/R_{\perp}^t < 2$. Experimental results for thermoplastic FRP (TP-FRP) like PEEK (Polyetheretherketon) show however, that for those thermoplastic materials the rule is valid just as for thermoset FRP¹⁸ [Kuhnel 2008].

¹⁸ These investigations show, too, that for PEEK the ratio R_{\perp}^c/R_{\perp}^t is larger than 2,5.

If there is a UD-material with an extraordinary low ratio R_{\perp}^c/R_{\perp}^t it is expected that the rule just mentioned is not fulfilled. $\tau_{\perp\perp}$ -stressing would instead lead to a mixed mode fracture of combined σ_{\perp}^t -stressing and $\tau_{\perp\perp}$ -stressing.

4.2.4 Fracture resistance of the action plane

In almost all failure criteria the used mathematical functions are calibrated by using the maximum sustainable stresses for uniaxial tensile or compressive stresses and pure shear stresses. The absolute values of these stresses are given by the so called “strengths” R . For stress based fracture criteria of UD-composites the so called basic strengths

$$R_{\parallel}^t, R_{\parallel}^c, R_{\perp}^t, R_{\perp}^c, R_{\perp\perp}, R_{\perp\parallel}$$

are used for calibration. All these are given as positive values, also the compressive strengths. This is a source of misunderstanding and mistakes, because in fracture criteria sustainable stresses have to be used. As compressive stresses have a negative sign, the corresponding maximum sustainable uniaxial stresses are for a UD-composite “ $-R_{\perp}^c$ ” and “ $-R_{\parallel}^c$ ”.

The basic strengths correspond to the fracture limit under pure σ_{\parallel} , σ_{\perp} , $\tau_{\perp\perp}$ or $\tau_{\perp\parallel}$ stressing, respectively. These fracture limits are measured without giving any attention to the kind of failure (failure by yielding, brittle fracture, crushing etc.). Thus, $R_{\perp\perp}$ is defined as the transverse shear stressing $\tau_{\perp\perp}$ leading to failure in the absence of all other stresses. However, experimental experience shows that in this case in brittle material fracture takes place on a plane inclined by 45° to the action plane of the applied $\tau_{\perp\perp}$ (compare Fig. 26). On this plane pure transverse tension σ_{\perp}^t is acting. This is not considered when conventional failure criteria are used. The shear strength $R_{\perp\perp}$ is calculated by dividing the applied shear load by the area it has been applied on.

In the same way as $R_{\perp\perp}$, the transverse compressive strength R_{\perp}^c corresponds to σ_{\perp}^c stressing leading to failure in the absence of all other stresses. However, it has been proved that by no means fracture occurs on the action plane of the σ_{\perp}^c -stressing but on a plane inclined by some $\pm 54^\circ$ (see above). On this plane transverse shear stressing $\tau_{\perp\perp}$ is dominant and responsible for IFF. But this experience is also not considered when the transverse compressive strength R_{\perp}^c has to be determined. R_{\perp}^c is also found by dividing the applied transverse compressive failure load by the area of the cross-section of the specimen.

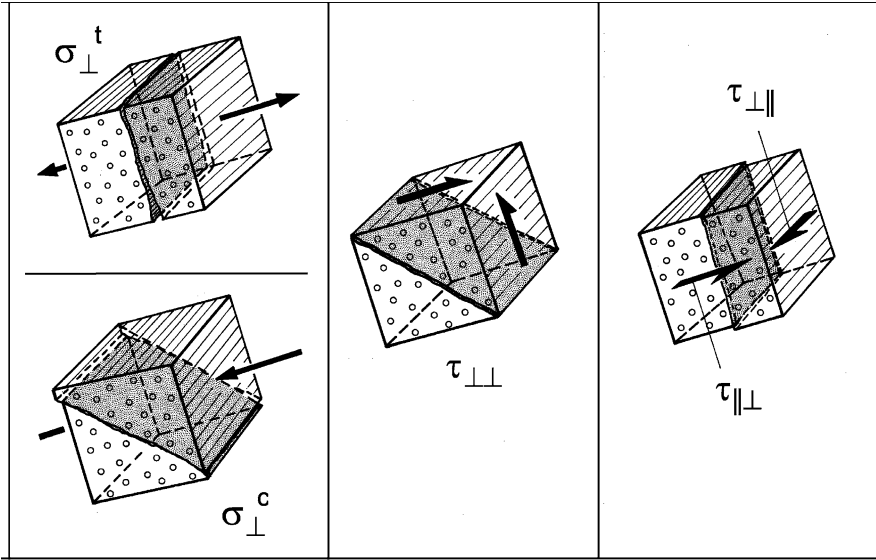


Fig. 26. Stressings of the UD-lamina causing IFF and corresponding fracture planes

As long as a failure criterion is formulated with stresses defined in the natural coordinate system of the layer (x_1, x_2, x_3) the basic strengths are the usual calibration parameters. Puck's IFF-criteria, however, are formulated with the stresses of the action plane ($\sigma_n, \tau_{nt}, \tau_{n1}$). Consequently, the corresponding fracture resistances of the action plane (defined as R^A in order to distinguish them from the basic strengths R) are needed.

Instead of employing the standard form of a failure condition

$$F(\sigma_1, \sigma_2, \sigma_3, \tau_{23}, \tau_{31}, \tau_{21}, R_{||}^t, R_{||}^c, R_{\perp}^t, R_{\perp}^c, R_{\perp\perp}, R_{\perp||}) = 1 \quad (\text{Eq. 22})$$

a IFF-fracture condition is formulated in the form

$$F(\sigma_n(\theta_{fp}), \tau_{nt}(\theta_{fp}), \tau_{n1}(\theta_{fp}), R_{\perp}^t, R_{\perp\perp}^A, R_{\perp||}^A) = 1. \quad (\text{Eq. 23})$$

Looking on (Eq. 23) it is important to remember that the stresses $\sigma_n(\theta)$, $\tau_{nt}(\theta)$, $\tau_{n1}(\theta)$ are the three stresses which in the most general case are acting simultaneously on one and the same action plane¹⁹. The action plane which is inclined by $\theta = \theta_{fp}$ is the fracture plane because on this action plane the risk of fracture is the highest one.

¹⁹ That $\sigma_n, \tau_{nt}, \tau_{n1}$ have the same action plane can be seen from the index "n" of all three stresses.

If all three stresses σ_n , τ_{nt} , τ_{nl} act simultaneously on an action plane, they represent a combined stressing consisting of a σ_{\perp} -stressing, a $\tau_{\perp\perp}$ -stressing and a $\tau_{\perp\parallel}$ -stressing.

In order to answer the question whether a certain combination of σ_n , τ_{nt} , τ_{nl} can be sustained by a fiber parallel action plane a fracture criterion has to be formulated mathematically. On the one hand it should contain the stresses σ_n , τ_{nt} , τ_{nl} acting simultaneously on a common action plane. On the other hand a fracture criterion of this kind can only be calibrated by experimental values for the sustainable stress of the action plane, when a σ_{\perp} -stressing is acting alone, when a $\tau_{\perp\perp}$ -stressing is acting alone and when a $\tau_{\perp\parallel}$ -stressing is acting alone. This means that fracture tests have to be performed with uniaxial σ_{\perp} , pure $\tau_{\perp\perp}$ and pure $\tau_{\perp\parallel}$.

If in such a test with – for instance – a single tensile stressing σ_{\perp}^t the fracture would occur in the action plane of the applied stressing this would be the sustainable tensile stressing of the action plane. Puck has introduced the following expression:

- “*Fracture resistance of the action plane*” and the corresponding symbol R^A .

The definition of R^A is the following:

A fracture resistance of the action plane is the resistance (expressed in the dimension of a stress) by which an action plane resists its own fracture caused by a single stressing (σ_{\perp} or $\tau_{\perp\perp}$ or $\tau_{\perp\parallel}$) acting in the action plane under consideration.

This definition shows how important it is for the fracture experiments to check whether or not the applied σ_{\perp} - or $\tau_{\perp\perp}$ - or $\tau_{\perp\parallel}$ -stressing really leads to a fracture in the action plane of the applied stress.

Some of the fracture resistances of the action plane used in (Eq. 23) are identical to the basic strengths as will be shown in the following. However, it is important to understand that the underlying question is different. The question is for instance

“To which value σ_{\perp}^t has to be increased in order to provoke failure **on its** action plane?”

and not

“To which value σ_{\perp}^t has to be increased in order to provoke fracture (on any plane)?”

There are three single fracture resistances to be differentiated:

R_{\perp}^A = Resistance of the action plane against its fracture due to transverse tensile stressing σ_{\perp}^t acting in that plane.

$R_{\perp\perp}^A$ = Resistance of the action plane against its fracture due to transverse shear stressing $\tau_{\perp\perp}$ acting in that plane.

$R_{\perp\parallel}^A$ = Resistance of the action plane against its fracture due to longitudinal shear stressing $\tau_{\perp\parallel}$ acting in that plane.

In the following some examples will be given to illustrate the meaning of action plane fracture resistances. The first example is a pure longitudinal shear stressing $\tau_{\perp\parallel}$ caused by $\tau_{21} \neq 0$ in the absence of all other stresses. This will obviously occur in a test with a pure longitudinal shear stressing realized by applying – for instance – a pure shear stress τ_{21} in absence of all other stresses. In this case a shear stress $\tau_{n1} = \tau_{21} \cdot \cos\theta$ is acting on a plane inclined by the angle θ to the x_2 -plane on which τ_{21} is acting. Obviously, for all angles $\theta \neq 0^\circ$ the shear stress τ_{n1} is smaller than τ_{21} . Fracture must therefore occur on the action plane of τ_{21} ($\theta_{fp} = 0^\circ$) and therefore

$$R_{\perp\parallel}^A = R_{\perp\parallel} \quad (\text{Eq. 24})$$

This means that the action plane fracture resistance $R_{\perp\parallel}^A$ is identical to the longitudinal shear strength $R_{\perp\parallel}$.

Transverse tension – for instance σ_2^t – normally leads in the absence of other stresses to fracture in its action plane, too, and therefore:

$$R_{\perp}^A = R_{\perp}^t \quad (\text{Eq. 25})$$

This, however, is not as evident as in the case of pure longitudinal shear. In the case of transverse tension σ_2^t there is a combination of transverse tension ($\sigma_{\perp}^t = \sigma_2 \cos^2\theta$) and transverse shear ($\tau_{\perp\perp} = -0.5 \sigma_2 \sin 2\theta$) on planes $\theta \neq 0$. If the resistance of the action plane against $\tau_{\perp\perp}$ shear fracture would be considerably smaller than that against transverse tension a different fracture angle $\theta_{fp} \neq 0^\circ$ would occur.

The third relevant fracture resistance $R_{\perp\perp}^A$ cannot as easily be determined as $R_{\perp\parallel}$ and R_{\perp}^t . When applying a pure τ_{23} stress to a unidirectional layer in the absence of any other stress there are three planes on which just one stressing is acting:

- $\theta = 0^\circ$: action plane of τ_{23} ($\tau_{\perp\perp}$ -stressing)
- $\theta = 90^\circ$: action plane of τ_{32} ($\tau_{\perp\perp}$ -stressing)
- $\theta = 45^\circ$: action plane of the principal tensile stress (σ_{\perp}^t -stressing) resulting from τ_{23} and being of same magnitude as τ_{23} and τ_{32} .

According to Puck's hypotheses fracture occurs on the plane with the highest stress exposure. Fracture tests on UD-specimens loaded by $\tau_{\perp\perp}$ show fracture under $\theta_{fp} = 45^\circ$. This leads to the clear conclusion that the fracture resistance R_{\perp}^{At} against transverse tension is smaller than the fracture resistance $R_{\perp\perp}^A$ against transverse shear. In other words: With a transverse shear test not $R_{\perp\perp}^A$ but instead the resistance against transverse tension R_{\perp}^{At} is measured.

In fact there is no way to measure $R_{\perp\perp}^A$ for intrinsically brittle fiber reinforced plastics directly. However, the unidirectional compression test offers an indirect way for the determination of $R_{\perp\perp}^A$ as long as the hypothesis for pure transverse stressing (compare chapter "Fracture hypotheses") is valid. If just σ_2^c is applied, a fracture angle of $\theta_{fp} \approx \pm 54^\circ$ results. On this fracture plane a combination of transverse shear $\tau_{\perp\perp}$ and transverse compression σ_{\perp}^c is acting. According to fracture hypothesis 2, a transverse compressive stress adds an additional fracture resistance to the "intrinsic" fracture resistance $R_{\perp\perp}^A$. This additional fracture resistance can be calculated by the used mathematical fracture condition. In this way the test result can be corrected in order to find $R_{\perp\perp}^A$. Thus, the calculated value of $R_{\perp\perp}^A$ depends on the fracture model used. Therefore this $R_{\perp\perp}^A$ is perhaps not the "real" value of the material property $R_{\perp\perp}^A$ but it can be used for the fracture model by which it has been calculated. At least it is guaranteed that by using this same fracture model in a fracture analysis for the special case of uniaxial compression the result will be $(\sigma_2)_{fr} = -R_{\perp}^c$ with R_{\perp}^c being the real transverse compressive strength.

The example of longitudinal shear is well suited to explain again the difference between a fracture resistance (of the action plane) and a conventional basic strength. The stress τ_{21} is acting on the x_2 -plane parallel to the fibers and the corresponding shear stress τ_{12} of the same magnitude is acting on the x_1 -plane. This shear stress on the x_1 -plane is correctly addressed as τ_{12} . However, there is just one strength parameter $R_{\perp\parallel}$ and it does not contain the information about the fracture plane. This could be either the x_2 - or the x_1 -plane or even another plane. The corresponding fracture resistances of the two planes under consideration differ, however, considerably. Namely, the fracture resistance ($R_{\perp\parallel}^A$) of the x_2 -plane – parallel to the fibers – is much smaller than the fracture resistance $R_{\parallel\perp}^A$ of the x_1 -plane perpendicular to the fibers. This phenomenon can easily be understood: On the x_2 -plane the stressing $\tau_{\perp\parallel}$ provokes Inter Fiber Fracture. The fracture plane runs parallel to the fibers whereas a fracture on the x_1 -plane would be a Fiber Fracture (shear off of the fibers)!

Obviously it makes no sense to talk about a resistance of the action plane against fracture due to transverse compressive stressing σ_{\perp}^c because a compressive stress cannot produce a fracture in its own action plane. Summing up this, there are three action plane fracture resistances to be differentiated:

R_{\perp}^{At} = Resistance of the action plane against its fracture due to transverse tensile stressing σ_{\perp}^t acting in that plane. For structural UD-material under normal temperature and humidity conditions it can be expected that $R_{\perp}^{At} = R_{\perp}^t$ is valid,

$R_{\perp\perp}^A$ = Resistance of the action plane against its fracture due to transverse shear stressing $\tau_{\perp\perp}$ acting in that plane. Attention has to be paid to the fact that $R_{\perp\perp}^A \neq R_{\perp\perp}$,

$R_{\perp\parallel}^A$ = Resistance of the action plane against its fracture due to longitudinal shear stressing $\tau_{\perp\parallel}$ acting in that plane. For elementary reasons $R_{\perp\parallel}^A = R_{\perp\parallel}$.

Experience has shown that most mechanical engineers are not familiar with the difference between “strength” and “action plane fracture resistance”. It could be helpful to realize the different underlying question. Dealing with strengths the underlying question is

“To which value can a certain stressing (for instance uniaxial stressing σ_{\perp}^t) be increased until failure occurs somewhere (and somehow) in the evenly stressed volume of the test specimen?”

Dealing with action plane fracture resistances the underlying question is:

“To which value can a certain stressing be increased until a fracture occurs on the action plane in which the evenly applied stressing is acting?”

4.2.5 Visualization of the stress/strength problem

Preliminary remark:

The content of the following chapter is not required to be read by somebody who is interested in the application only of the algorithms of Puck’s laminate failure analysis. However, it is strongly recommended to have a look on the astonishing possibilities of the visualization because they present a much better understanding of the results of the mathematical treatment of the physical problems which is explained in the subsequent chapters. But the reader being in a hurry may continue with the chapter “Universal 3-D-formulation of the action plane related IFF-criteria”.

4.2.5.1 Mohr's Circles and Fracture Envelopes

Within a failure analysis independently of the kind of material the engineer has to complete two tasks: First the stresses of the material caused by the loads have to be calculated and in a second step these stresses have to be compared to the failure limit. If the material fails by brittle fracture, Mohr's circles are helpful for the first task and Mohr's envelope for the second one.

Because of the fact that Puck's IFF hypotheses are based on the ideas of Mohr [Mohr 1900] and Coulomb [Coulomb 1776] one can partially use these classical solutions. However, it must be recognized that the approaches of Mohr and Coulomb are valid only for macroscopically isotropic materials. In the isotropic case fracture due to an arbitrary three dimensional state of stress can be treated as a 2D-problem. Any stress combination leading to fracture can be visualized by means of the well known Mohr's circle and Mohr's envelope.

The reason for this opportunity of simplification is the isotropy and the validity of Mohr's fracture hypothesis for brittle fracture. Any 3D-stress combination $(\sigma_1, \sigma_2, \sigma_3, \tau_{23}, \tau_{31}, \tau_{21})$ ²⁰ – to use the coordinates which are established for the UD-lamina (compare Fig. 16) – can be transformed to an equivalent $(\sigma_a, \sigma_b, \sigma_c)$ stress state without any shear stresses on the action planes of $\sigma_a, \sigma_b, \sigma_c$ where σ_a, σ_b and σ_c are the so called principal stresses. If $\sigma_b > \sigma_a$ by $\sigma_b < \sigma_a$ being the intermediate principal stress, fracture depends according to Mohr only on the major and minor principal stresses σ_b and σ_c (Fig. 27). In the (σ, τ) -diagram Fig. 27 points on the circumference of a circle with the coordinates σ and τ present the stresses σ and τ on section planes through the material, the normal of which is perpendicular to one of the three axes a, b or c, that means perpendicular to one of the three principal stresses. It can be shown theoretically that the stresses σ and τ of all other section planes are given by points located in the hatched areas of Fig. 27.

Therefore the highest shear and normal stresses occurring in the material under the given stresses depend only on the two extreme principal stresses. In Fig. 27 σ_b and σ_c are chosen as the extreme principal stresses for demonstration. However, depending on the load case it could be any other pair of the three principal stresses $\sigma_a, \sigma_b, \sigma_c$ too. The axes a, b, c of the Cartesian coordinate system in which the acting stress combination can be presented for the isotropic material *changes its spatial orientation* depending on the actual stress state $(\sigma_1, \sigma_2, \sigma_3, \tau_{23}, \tau_{31}, \tau_{21})$. That means that gen-

²⁰ The additional corresponding shear stresses follow from $\tau_{23}=\tau_{32}, \tau_{31}=\tau_{13}, \tau_{21}=\tau_{12}$.

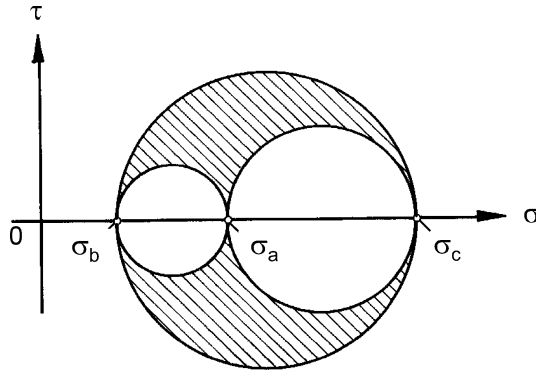


Fig. 27. System of the three Mohr-circles for isotropic material

erally the directions a, b, c in which the principal stresses σ_a , σ_b , σ_c are acting do not coincide with any of the chosen axes x_1 , x_2 , x_3 of the original reference coordinate system for the actual stress combination $(\sigma_1, \sigma_2, \sigma_3, \tau_{23}, \tau_{31}, \tau_{21})$, see Fig. 28.

If there is isotropy there is no difficulty in working with a coordinate system with axes a, b, c of the principal stresses σ_a , σ_b , σ_c which for different states of stress has a different spatial orientation and there is also no problem to work with an unlimited number of coordinate systems for the axes of the principal stresses. However, obviously such versatility does not exist for transversely-isotropic materials like the UD-lamina where the fixed direction of the fibers prevents such a procedure. When dealing with transversely-isotropic material a change of the direction of coordinate axes

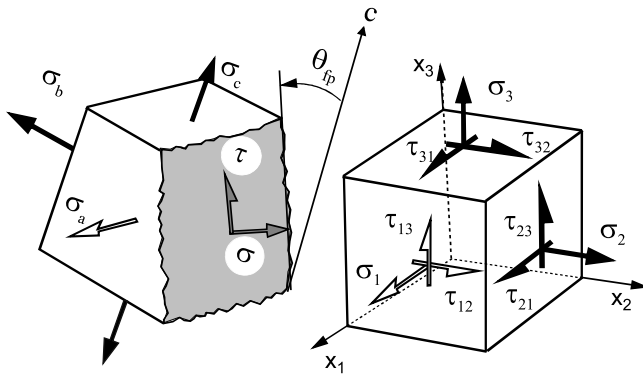


Fig. 28. The stresses σ and τ given by the coordinates of a point on the largest circle in Fig. 27 are acting on a potential fracture plane which is parallel to σ_a . The direction of σ and τ is perpendicular to σ_a

is at least possible in the plane of transverse isotropy which is perpendicular to the fixed axis parallel to the fibers.

4.2.5.2 Mohr's circle and Mohr's envelop for a transversely-isotropic UD-lamina under plane ($\sigma_2, \sigma_3, \tau_{23}$)-stress

In a UD-lamina the stresses $\sigma_2, \sigma_3, \tau_{23}$ which are acting on action planes being parallel to the fixed fiber direction x_1 are the only stresses to which Mohr's circle can be applied effectively. Transverse isotropy allows to switch over from the (x_2, x_3)-coordinate system to a (x_n, x_t)-coordinate system.

In order to get familiar with the derivation and application of Mohr's circle, a plane ($\sigma_2, \sigma_3, \tau_{23}$) stress state will be investigated now. The stresses acting on the plane which is inclined by an angle θ to the x_3 -axis (compare Fig. 33) can be determined by (Eq. 1) and (Eq. 2). Using the well known theorems for "sin" and "cos" (Eq. 1) and (Eq. 2) gives the form

$$\sigma_n(\theta) = \frac{1}{2}(\sigma_2 + \sigma_3) + \frac{1}{2}(\sigma_2 - \sigma_3) \cdot \cos 2\theta + \tau_{23} \cdot \sin 2\theta \quad (\text{Eq. 26})$$

$$\tau_{nt}(\theta) = -\frac{1}{2}(\sigma_2 - \sigma_3) \cdot \sin 2\theta + \tau_{23} \cdot \cos 2\theta \quad (\text{Eq. 27})$$

These equations look already like the mathematical description of a circle using the angle 2θ as a parameter. This can be confirmed in the following way: Rearrangement of terms, squaring of (Eq. 26) and adding up of the squared form of (Eq. 27) finally leads to the following expression:

$$\left[\sigma_n(\theta) - \frac{1}{2}(\sigma_2 + \sigma_3) \right]^2 + [\tau_{nt}(\theta)]^2 = \left[\frac{1}{2}(\sigma_2 - \sigma_3) \right]^2 + \tau_{23}^2 \quad (\text{Eq. 28})$$

(Eq. 28) confirms the very welcome opportunity for the visualization of stress transformation because (Eq. 28) is the mathematical description of a circle with the center on the σ_n -axis at $0.5(\sigma_2 + \sigma_3)$ and the radius

$\sqrt{\left[\frac{1}{2}(\sigma_2 - \sigma_3) \right]^2 + \tau_{23}^2}$. This circle is illustrated in Fig. 29.

Figure 29 presents a graphical procedure by which the stresses σ_{II} and σ_{III} can be determined if σ_2, σ_3 and τ_{23} are known.

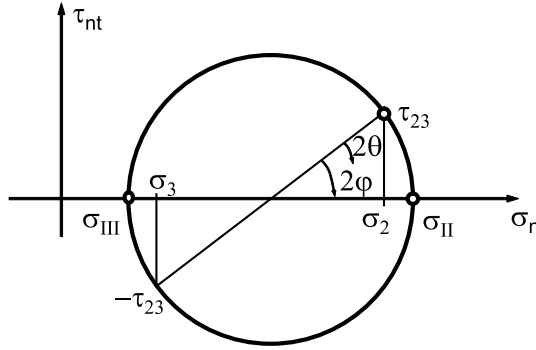


Fig. 29. Mohr circle for $\{\sigma_2, \sigma_3, \tau_{23}\}$

On planes characterized by the angles φ and $(\varphi+90^\circ)$ there is no shear stress τ_{nt} . The corresponding normal stresses $\sigma_n(\varphi)$ and $\sigma_n(\varphi+90^\circ)$ are designated by σ_{II} and σ_{III} and are called “extreme normal stresses of the transversely-isotropic plane”. In general they are not real principal stresses. This is explained later.

It is important to realize that for instance an angle φ in the real material with a mathematically positive sense of rotation corresponds to an angle of 2φ with a mathematically negative sense of rotation in the Mohr-circle!

The “extreme normal stresses σ_{II} and σ_{III} of the transversely isotropic plane” and the angle φ (compare Fig. 29) can also very easily be found in the usual analytical way by setting $\tau_{nt} = 0$ in (Eq. 27). It is

$$2\varphi = \arctan \frac{2\tau_{23}}{\sigma_2 - \sigma_3} \quad (\text{Eq. 29})$$

and with (Eq. 26)

$$\sigma_{II} = \frac{1}{2}(\sigma_2 + \sigma_3) + \frac{1}{2}(\sigma_2 - \sigma_3)\cos 2\varphi + \tau_{23} \sin 2\varphi \quad (\text{Eq. 30})$$

$$\sigma_{III} = \frac{1}{2}(\sigma_2 + \sigma_3) - \frac{1}{2}(\sigma_2 - \sigma_3)\cos 2\varphi - \tau_{23} \sin 2\varphi. \quad (\text{Eq. 31})$$

With known extreme normal stresses σ_{II} and σ_{III} the stresses $\sigma_n(\Theta)$ and $\tau_n(\Theta)$ on planes inclined to the direction of σ_{II} by the angle Θ can be calcu-

lated with (Eq. 32) and (Eq. 33). These equations correspond to (Eq. 26) and (Eq. 27).

$$\sigma_n(\Theta) = \frac{1}{2}(\sigma_{II} + \sigma_{III}) + \frac{1}{2}(\sigma_{II} - \sigma_{III})\cos 2\Theta \quad (\text{Eq. 32})$$

$$\tau_{nt}(\Theta) = -\frac{1}{2}(\sigma_{II} - \sigma_{III})\sin 2\Theta \quad (\text{Eq. 33})$$

Mohr's circle as shown in Fig. 30 is based on (Eq. 32) and (Eq. 33). The coordinates σ_n and τ_n of a point P at a radian distance of 2Θ from σ_{II} are the stresses acting on a plane inclined by Θ to the action plane of σ_{II} (compare Fig. 30). The centre of the circle has a distance of $0.5(\sigma_{II} + \sigma_{III}) = 0.5(\sigma_2 + \sigma_3)$ from the point of origin. The radius of the circle is $0.5(\sigma_{II} - \sigma_{III})$. The term $(\sigma_{II} - \sigma_{III})$ can be negative or positive. To make sure that the graphical construction is in line with (Eq. 32) and (Eq. 33) (positive radius), the sense of rotation and the starting point of the Θ -measurement has to be adapted in a way that $\sigma_n(\Theta)$ and $\tau_n(\Theta)$ are correct by means of magnitude and algebraic sign, see sketch on the bottom of Fig. 30.

All Mohr's circles for arbitrary states of stress have their centers on the σ_n - axis. Each point on the circumference of such a circle with coordinates σ_n and τ_{nt} belongs to a certain section through the material with an angle Θ (in reality). The stress vector belonging to such a section has its starting point in the origin of the (σ_n, τ_{nt}) -coordinate system and its tip touches the point $(\sigma_n(\Theta), \tau_{nt}(\Theta))$ on the circumference of Mohr's circle.

No vector tip belonging to a vector representing a sustainable state of stress can exceed a certain fracture limit of the material. Therefore Mohr

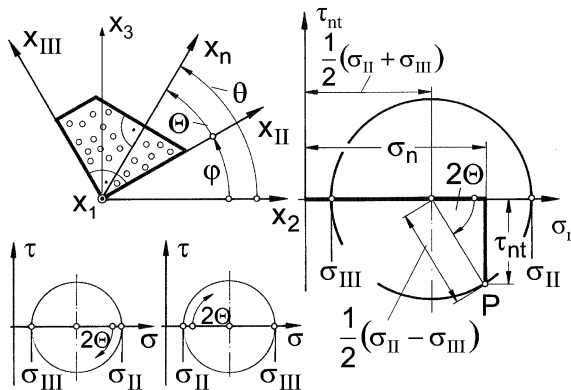


Fig. 30. Mohr circle and derivation of stresses on inclined planes

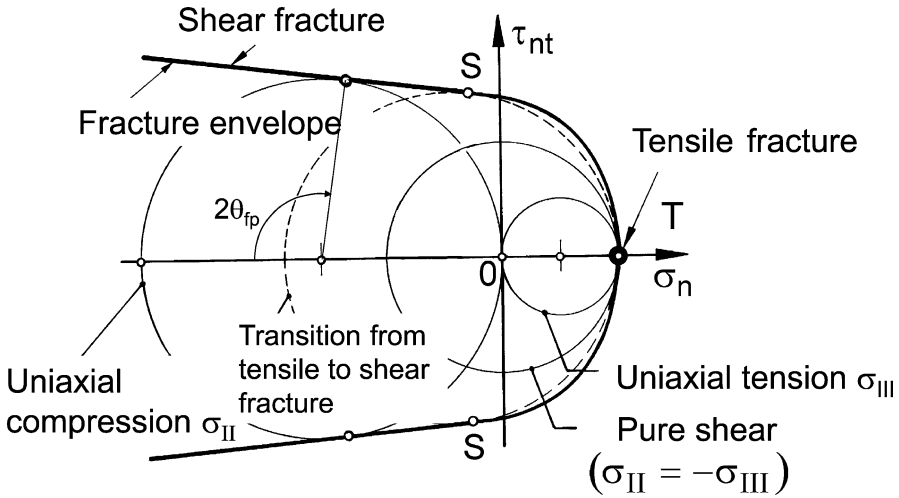


Fig. 31. Mohr's circles for special stress states and Mohr's fracture envelope

has not only provided the helpful visualization of stresses acting on inclined action planes by Mohr's circle but he has also tried to draw a fracture limit of the material as a curve in the (σ_n, τ_{nt}) -diagram. This is called "Mohr's envelope", see Fig. 31. It envelops all sustainable stress combinations. Obviously no Mohr's circle for sustainable stress can exceed this envelope; it can at the most touch it.

It is important to realize that if the contact point of a Mohr's circle with the Mohr-envelope is found, not only the combined stresses σ_n and τ_{nt} on the fracture plane but as well the fracture angle θ_{fp} can be found in the diagram, see for instance Fig. 31.

For a UD-lamina the fracture envelope is chosen by Puck as a parabola in the area of $\sigma_n < 0$ and an ellipse in the area of $\sigma_n > 0$. At $\sigma_n = 0$ the curve might have a sharp bend or – more mathematically spoken – a discontinuity in terms of gradient.

According to the fracture hypotheses discussed in detail in the chapter "Fracture hypotheses", there is (as far as IFF is concerned) either tensile fracture or shear fracture in a UD-lamina stressed by $(\sigma_2, \sigma_3, \tau_{23}, 0, 0)$. Consequently, on the fracture plane there is either a $\sigma_n > 0$ (pure σ_{\perp}^I) stressing or a combination of $\sigma_n < 0$ and τ_{nt} ($(\sigma_{\perp}^c, \tau_{\perp\perp})$ -stressing). A combined $(\sigma_{\perp}^I, \tau_{\perp\perp})$ -stressing or a pure $\tau_{\perp\perp}$ -stressing on the fracture plane are both not possible according to the additional "rule" given with the two fracture hypotheses (compare chapter "Fracture hypotheses").

Under these conditions, all Mohr circles describing states of stress which lead to tensile fracture touch the fracture envelope at the same point,

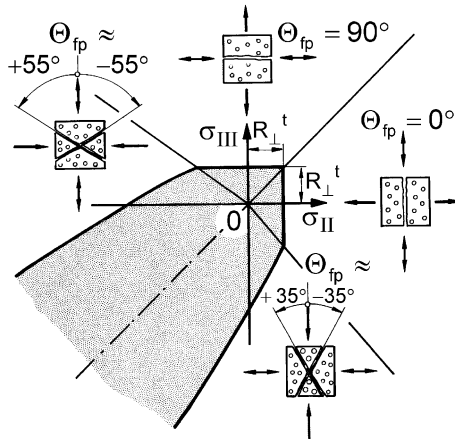


Fig. 32. $(\sigma_{II}, \sigma_{III})$ fracture curves resulting from Mohr's fracture envelope

namely $T(R_{\perp}^t, 0)$ (compare Fig. 31). In a $(\sigma_{II}, \sigma_{III})$ -diagram the corresponding fracture curve for tensile fracture consists of two straight lines, running at a distance of R_{\perp}^t parallel to the σ_{II} - and σ_{III} -axes (compare Fig. 32). This corresponds to Paul's [Paul 1961] findings for intrinsically brittle materials. In the first quadrant of the $(\sigma_{II}, \sigma_{III})$ -diagram tensile fracture occurs as a consequence of σ_{II} ($\theta_{fp} = 0^\circ$) – in the case of $\sigma_{II} > \sigma_{III}$ – or as a consequence of σ_{III} ($\theta_{fp} \pm 90^\circ$) in the case of $\sigma_{III} > \sigma_{II}$. For the straight fracture lines $\sigma_{II} = R_{\perp}^t$ and $\sigma_{III} = R_{\perp}^t$ Paul introduced the term “tensile cut offs”. In the 2nd and 4th quadrant, either tensile or shear fracture can occur. What fracture occurs depends on the ratio σ_{II}/σ_{III} . In the 3rd quadrant, where both σ_{II} and σ_{III} are compressive stresses fracture is always a shear fracture. However, the fracture plane is not the plane with the highest shear stressing ($\theta_{fp} = \pm 45^\circ$ with $\tau_{nt} = 0.5|(\sigma_{II} - \sigma_{III})|$; in Mohr's circle straight above and below the centre point at $\pm 2\theta_{fp} = \pm 90^\circ$). Instead, the fracture angle deviates by $\approx \pm 5^\circ$ to $\pm 10^\circ$ from the plane with the highest shear stress. This becomes understandable when regarding the normal stress σ_n^c acting simultaneously to τ_{nt} . This compressive normal stress is reduced considerably when the angle deviates a bit from $\pm 45^\circ$, whereas the shear stress τ_{nt} stays nearly the same (compare Fig. 25). Knowing that compressive normal stress impedes shear fracture, this explains why the observed angle of shear fracture is not $\pm 45^\circ$ but somewhat larger. This has been experimentally confirmed with uniaxial compression tests, see Fig. 8.

Figure 31 shows that the fracture envelope and the Mohr's circles have no points of contact between the points $T(R_{\perp}^t, 0)$ and S (point of transition

from tensile fracture to shear fracture). The dashed circle in Fig. 31 marks the “circle of transition” from tensile to shear fracture. For this special $(\sigma_{II}, \sigma_{III})$ -compression/tension stress combination there can either occur a shear fracture or a tensile fracture. Also the circle for pure transverse shear shows contact only in T, that means $R_{\perp\perp} = R_{\perp}^I$ is to be expected.

The course of the fracture envelope between the points T and S does not seem to be relevant for the states of stress treated so far. There are no contact points on it. It is a so called “dead branch” of the fracture envelope. However, from the following paragraph it will become clear, that the course of the (σ_n, τ_{nt}) fracture curve between T and S has an influence on the fracture envelope for 3D-stressings $(\sigma_n, \tau_{nt}, \tau_{n1})$, the so called Master Fracture Body (MFB). Such a 3D-stressing is present as soon as there is longitudinal shear $\tau_{\varpi 1}$, that means τ_{21} and/or τ_{31} too.

4.2.5.3 From Mohr’s circle to Puck’s cosine-shaped cylinder

The idea of Mohr’s circles and Mohr’s envelope is used now as the basis for a corresponding procedure for transversely-isotropic materials with the most general 3D-state of stress. Figure 33 shows all stresses and their correct designation of a UD-lamina. The stress σ_1 leads to a fiber parallel stressing σ_{\parallel} , whereas both the stress σ_2 and the stress σ_3 cause a transverse stressing σ_{\perp} . The stress $\tau_{23} = \tau_{32}$ leads to a transverse shear stressing $\tau_{\perp\perp}$ and τ_{21} and τ_{31} both lead to a longitudinal shear stressing $\tau_{\perp\parallel}$. That means that obviously all three fracture resistances R_{\perp}^{At} , $R_{\perp\perp}^A$, $R_{\perp\parallel}^A$ of the fiber parallel action plane will now generally influence the IFF-process.

In order to get to visualization also of the most general stress situation one must try not to use more than three variables. For this reason one should combine as much stresses as possible in “resulting” stresses. The

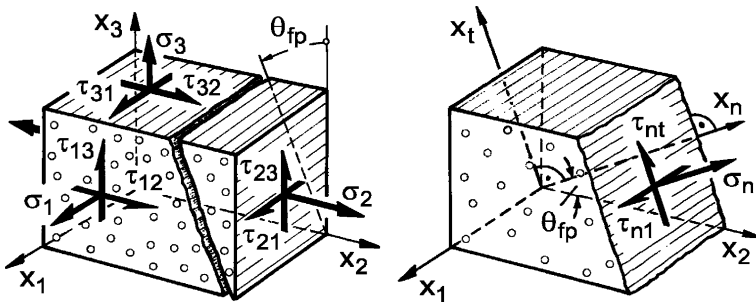


Fig. 33. Stresses of the UD-lamina and stresses on a possible (IFF)-fracture plane which is parallel to the fibers

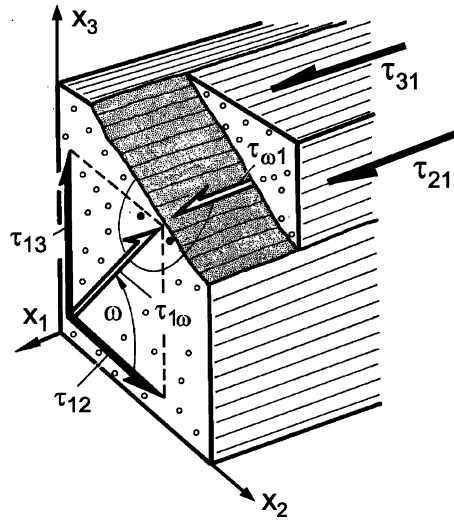


Fig. 34. Uniting τ_{12} and τ_{13} to $\tau_{1\omega}$ and τ_{21} and τ_{31} to $\tau_{\omega 1}$

longitudinal shear stresses τ_{12} and τ_{13} and their corresponding stresses τ_{21} and τ_{31} are quite special in this respect. Figure 34 shows that τ_{12} and τ_{13} are in fact components of only one longitudinal shear stress $\tau_{1\omega}$. The two components are $\tau_{12} = \tau_{1\omega} \cos \omega$ and $\tau_{13} = \tau_{1\omega} \sin \omega$. Adequate equations can also be written with the corresponding stresses τ_{21} , τ_{31} and $\tau_{\omega 1}$ (this is the stress provoking IFF in its fiber parallel action plane). Implicitly the fact that the longitudinal shear stresses can easily be united in one stress means: there does exist only one relevant longitudinal shear stress and this is $\tau_{\omega 1}$. As long as only $\tau_{\omega 1}$ acts in the absence of any other stress, IFF will occur in the plane in which the resulting longitudinal shear stress $\tau_{\omega 1}$ is acting as soon as $\tau_{\omega 1} = R_{\perp\parallel}$ is reached. The fracture plane is orientated perpendicular to the direction of $\tau_{1\omega}$ as shown in Fig. 34.

It is important to note that the stresses σ_{II} and σ_{III} are only true principal stresses like σ_b and σ_c respectively, if there is no longitudinal shear $\tau_{\omega 1}$. In this special case σ_I , σ_{II} , σ_{III} are real principal stresses. As soon as $\tau_{\omega 1} \neq 0$, there is longitudinal shear on the action plane of σ_{II} and/or σ_{III} . The action plane of “true” principal stresses is however free of any shear stresses.

Obviously the combined action by which the stresses σ_{II} , σ_{III} and $\tau_{\omega 1}$ cause an IFF will depend on the direction of the shear stress $\tau_{\omega 1}$ compared to the directions of the normal stresses σ_{II} and σ_{III} . But due to the transverse isotropy of the UD-lamina (with respect to the x_1 -axis) not the absolute

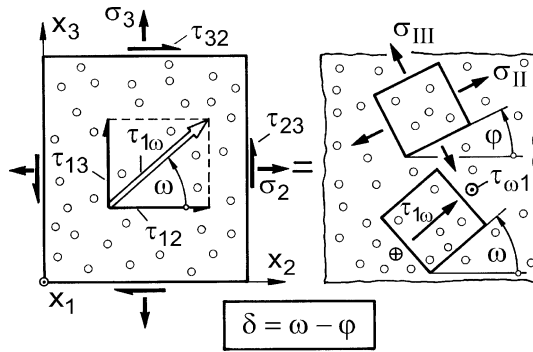


Fig. 35. Combining σ_2 , σ_3 , τ_{23} to σ_{II} and σ_{III} and τ_{12} and τ_{13} to $\tau_{1\varpi}$; definition of angle δ

values of the angles ϖ and ϕ are relevant for the risk of fracture. Instead, the difference δ between ϖ and ϕ is relevant (see Fig. 35):

$$\delta = \omega - \phi. \quad (\text{Eq. 34})$$

Because of the meaning of ω and ϕ (see Fig. 35 and (Eq. 29)) δ can be written as:

$$\delta = \arctan \frac{\tau_{31}}{\tau_{21}} - \frac{1}{2} \arctan \frac{2\tau_{23}}{\sigma_2 - \sigma_3}. \quad (\text{Eq. 35})$$

Longitudinal shear stress $\tau_{\varpi 1}$ cannot be eliminated like a transverse shear stress τ_{23} by the introduction of stresses like σ_{II} and σ_{III} . Thus, in the general case fracture has to be calculated for a $(\sigma_1, \sigma_{II}, \sigma_{III}, 0, \tau_{\varpi 1})$ state of stress.

For the moment it is assumed that just as in the case of isotropic material (with σ_a being the intermediate principal stress) the fiber parallel stress σ_1 has no influence on the fracture angle Θ_{fp} and no influence on the magnitude of the fracture stresses σ_{II} , σ_{III} , $\tau_{\varpi 1}$ at IFF – this is at least correct as long as σ_1 is considerably smaller than $\approx 50\%$ of the fiber fracture strength $|R_{||}|$.

In the particular case that the longitudinal shear $\tau_{\varpi 1}$ acts alone ($\sigma_{II} = \sigma_{III} = 0$), fracture occurs in the action plane of $\tau_{\varpi 1}$ which is turned by the angle difference $\delta = \varpi - \phi$ with respect to the action plane of σ_{II} (compare Fig. 35). In a further special case, $\tau_{\varpi 1}$ acts on the fracture plane of the tensile fracture provoked by $(\sigma_{II}, \sigma_{III})$ alone. In this case, the longitudinal shear simply “helps” provoking fracture without changing the fracture angle. The

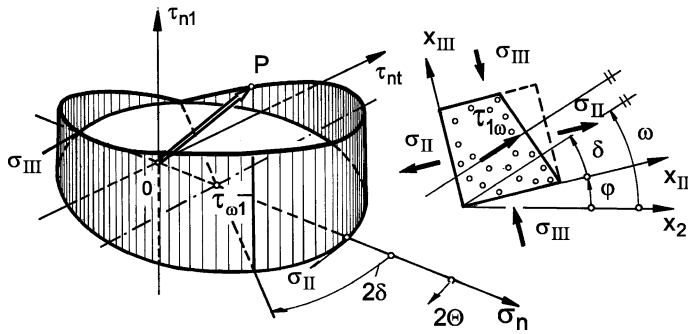


Fig. 36. Mohr's circle with longitudinal shear τ_{n1} representation for UD-lamina

common presence of σ_{II} , σ_{III} and $\tau_{\omega 1}$ leads to a combined $(\sigma_{\perp}^t, 0, \tau_{\perp\parallel})$ mode of fracture, that means a Mode A-fracture.

The tensile fracture occurs on the action plane of σ_{II} or that of σ_{III} (depending on which of both stresses is larger). If, however, the action plane of $\tau_{\omega 1}$ is neither equal to that of a tensile σ_{II} nor that of a tensile σ_{III} , fracture will sometimes occur on a plane which is not the action plane of any of the 3 stresses σ_{II} , σ_{III} , $\tau_{\omega 1}$. On the actual fracture plane there will then be a $(\sigma_{\perp}^t, \tau_{\perp\perp}, \tau_{\perp\parallel})$ stress combination, called a Mode A*-fracture. This is a major difference to the fracture behavior of brittle isotropic material, where a comparable stressing (a combination of a tensile stress σ^t and a shear stress τ) on the fracture plane is not possible.

It seems necessary to have a closer look on the stress distribution. In general, a $(\sigma_{II}, \sigma_{III}, \tau_{\omega 1})$ stress state leads to a stressing $\sigma_n(\theta)$, $\tau_{nt}(\theta)$, $\tau_{n1}(\theta)$ on all planes (parallel to the fiber direction). The maximum of τ_{n1} with the magnitude of $\tau_{n1} = \tau_{\omega 1}$ occurs on a plane inclined by the angle δ to the action plane of σ_{II} , see Fig. 36. On planes inclined by $\pm 90^\circ$ to the plane of $\tau_{n1} = \tau_{\omega 1}$ the longitudinal shear τ_{n1} is zero. In between these extreme inclinations of the fiber parallel action plane τ_{n1} follows a cosine function, compare (Eq. 3).

A rotation of the fiber parallel action plane by $\pm 90^\circ$ (in the real material) corresponds to a rotation of $\pm 180^\circ$ in the Mohr's circle. This leads to an illustration of the state of stress as a Mohr's circle with a "cosine-half-wave" on top of the Mohr's circle. The amplitude of the cosine-function is $\tau_{n1} = \tau_{\omega 1}$ (compare Fig. 36). The maximum of τ_{n1} is – with respect to the σ_{II} -axis – rotated by the angle δ in reality and 2δ in the Mohr's circle respectively.

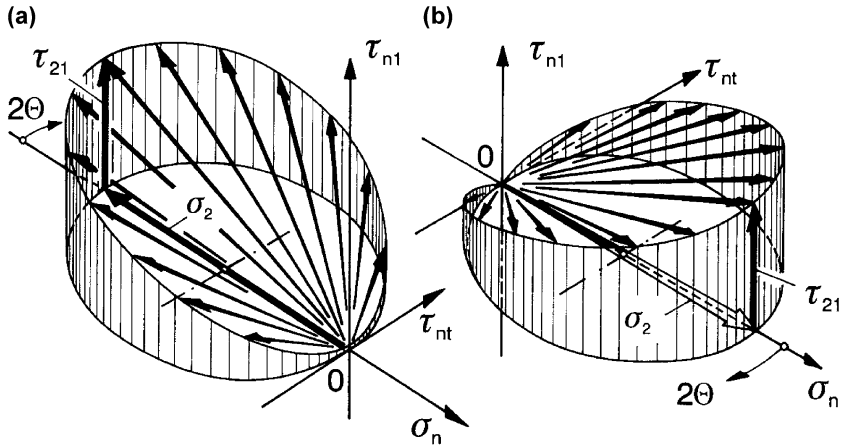


Fig. 37. Spatial vector fan for combined (σ_2, τ_{21}) -stressings: a) for $\sigma_2 < 0$; b) for $\sigma_2 > 0$

In addition to (Eq. 32) and (Eq. 33) there is now an additional equation for the longitudinal shear τ_{n1} in dependence of the angle Θ :

$$\tau_{n1}(\Theta) = \tau_{\omega 1} \cos(\Theta - \delta) = \sqrt{\tau_{21}^2 + \tau_{31}^2} \cos(\Theta - \delta) \quad (\text{Eq. 36})$$

A stress vector $(\sigma_n(\Theta), \tau_{nt}(\Theta), \tau_{n1}(\Theta))$ in Fig. 36 reaches from the center of origin to a point P on the cosine-half-wave. The infinite number of tips of all stress vectors (acting on planes $-90^\circ \leq (\Theta - \delta) \leq +90^\circ$) of a given $(\sigma_2, \sigma_3, \tau_{23}, \tau_{31}, \tau_{21})$ state of stress form together the cosine-half-wave in Fig. 36. All these vectors form a spatial “vector fan”, special examples of which are shown in Fig. 37.

The fracture limit for all stress vectors is now no longer an enveloping fracture limit curve in the (σ_n, τ_{nt}) -plane, but a surface in the $(\sigma_n, \tau_{nt}, \tau_{n1})$ -space. This fracture envelope comprises all cosine-half-waves and corresponding stress vectors which do not lead to fracture. In order to differentiate this fracture envelope from other well known envelopes for instance in the $(\sigma_1, \sigma_2, \tau_{21})$ -space, the envelope in the $(\sigma_n, \tau_{nt}, \tau_{n1})$ -space is called Master Fracture Body (MFB) (compare Fig. 38).

The visualization of the stress state on any fiber parallel action plane by the cosine-half-waves and the visualization of the $(\sigma_n, \tau_{nt}, \tau_{n1})$ -fracture limit by the Master Fracture Body (MFB) are very helpful both for the interpretation of the results of a fracture analysis of special stress states and quite generally for a deeper understanding of the background and the results of Puck’s criteria.

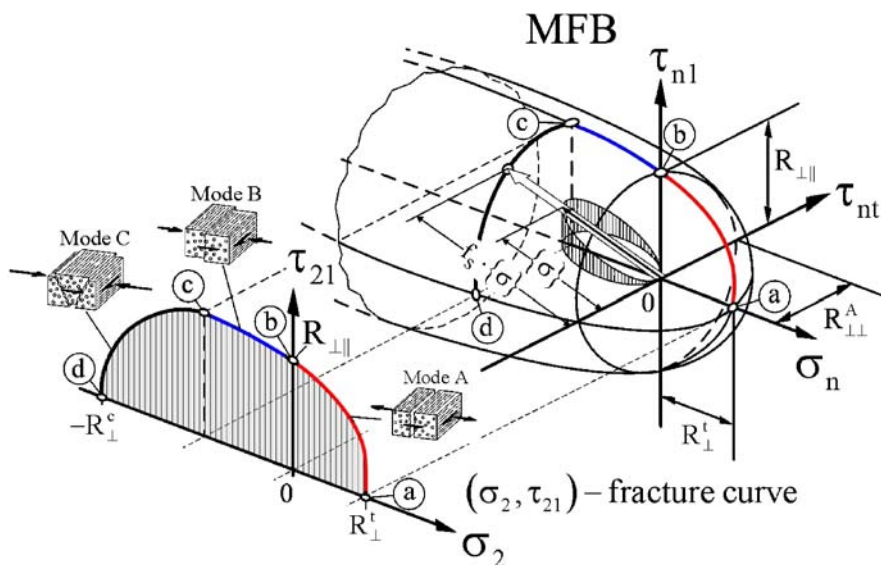


Fig. 38. IFF-Master Fracture Body [Lutz 2006]

It helps for instance to understand that on the surface of the MFB at certain places “dead areas” appear [Ritt 1999]. One of these dead areas contains the “dead branch” between the points S and T in Fig. 31. Stress points $(\sigma_n, \tau_{nt}, \tau_{n1})$ in “dead areas” symbolize $(\sigma_n, \tau_{nt}, \tau_{n1})$ -stresses *on the fracture plane* which never occur (The cosine half wave is unable to get in contact with these parts of the surface of the MFB).

All steps of the application of Puck's action plane fracture criteria can be visualized from Fig. 38. In order to answer for instance the question “what stress combinations are sustainable?” for a given (σ_2, τ_{21}) -stress combination, one steps into the $(\sigma_n, \tau_{nt}, \tau_{n1})$ -stress space where the Master Fracture Body (MFB) is given. Here, one has to find the point on the MFB-surface where the cosine shaped stress line touches the MFB.

What the algorithm of the fracture analysis really performs is the following procedure: Every $(\sigma_n, \tau_{nt}, \tau_{n1})$ stress vector on any inclined section is elongated (stretched) in its original direction by the so called stretch factor $f_s = (f_E)^{-1}$ the way that the tip of the vector just gets in contact with the MFB-surface. The $(\sigma_n, \tau_{nt}, \tau_{n1})$ -vector which needs the minimal stretch factor f_{smin} is the one which in reality leads to IFF. For (σ_2, τ_{21}) -combinations Puck has found an analytical solution. For the general $(\sigma_1, \sigma_2, \sigma_3, \tau_{23}, \tau_{31}, \tau_{21})$ -stress combinations fast numerical search procedures have been developed. In Fig. 38 the cosine line in the tensile region of σ_n has a contact

point on the line “ $\tau_{nt} = 0$ ”, which means $\theta_{fp} = 0^\circ$. In the compressive region the contact point can be in an area where all 3 stresses σ_n , τ_{nt} , τ_{nl} exist. This means that $\theta_{fp} \neq 0^\circ$ is possible. It is interesting to see in Fig. 38 how the fracture curve on the (σ_2, τ_{21}) -plane is represented in the MFB. Surprisingly the stress σ_n on the fracture surface is constant ($\sigma_n = -R_{\perp\perp}^A$) in the whole area of oblique fractures ($\theta_{fp} \neq 0^\circ$), see part (c) to (d) of the corresponding fracture curves.

4.2.6 Universal 3-D-formulation of the action plane related IFF-criteria

4.2.6.1 Preliminary remarks

The action plane related IFF-criteria are valid for arbitrary combinations of the stresses σ_1 , σ_2 , σ_3 , τ_{23} , τ_{31} , τ_{21} . The influence stresses parallel to the fibers (σ_1) have on IFF is assumed to be negligible as long as σ_1 is much smaller than the fiber parallel strength R_{\parallel} . Thus, that influence is neglected in a first approach and will be discussed later (compare chapter “Influence of stresses σ_1 acting parallel to the fibers on IFF”).

Puck’s approach is based on the hypothesis that the stresses acting on a fracture surface provoke fracture, this was first proposed by Hashin [Hashin1980]. Consequently, Puck’s criteria are formulated with the stresses $\sigma_n(\theta)$, $\tau_{nt}(\theta)$, $\tau_{nl}(\theta)$ (compare Fig. 18) which can easily be calculated from the stresses σ_2 , σ_3 , τ_{23} , τ_{31} , τ_{21} (see (Eq. 1), (Eq. 2), (Eq. 3)).

The stresses $\sigma_n(\theta)$, $\tau_{nt}(\theta)$, $\tau_{nl}(\theta)$ depend on the angle θ of the plane under consideration or in other words of their action plane. The same is true for the risk of fracture. On a plane with $\theta = \theta_1$ the risk of fracture might be higher than on a plane $\theta = \theta_2$. Eventually, when the lamina stresses are increased to the fracture limit the lamina will suffer IFF on a fracture plane $\theta = \theta_{fp}$. On this plane the risk of fracture is highest and here the stresses $\sigma_n(\theta)$, $\tau_{nt}(\theta)$, $\tau_{nl}(\theta)$ reach first the fracture limit.

A measure for the likelihood of fracture is the stress exposure $f_E(\theta)$ on the action plane. In fact, the plane with the highest stress exposure will be the fracture plane ($f_E(\theta) = [f_E(\theta)]_{\max} = f_E|_{\theta=\theta_{fp}}$). If the stresses of the UD-lamina (σ_2 , σ_3 , τ_{23} , τ_{31} , τ_{21}) are multiplied by the smallest stretch factor $f_{Smin} = 1/[f_E(\theta)]_{\max}$ the lamina will suffer IFF exclusively on that fracture plane. All other planes remain intact.

For the general 3D-state of stress, the fracture plane has to be found numerically. That means that the stresses $\sigma_n(\theta)$, $\tau_{nt}(\theta)$, $\tau_{nl}(\theta)$ need to be

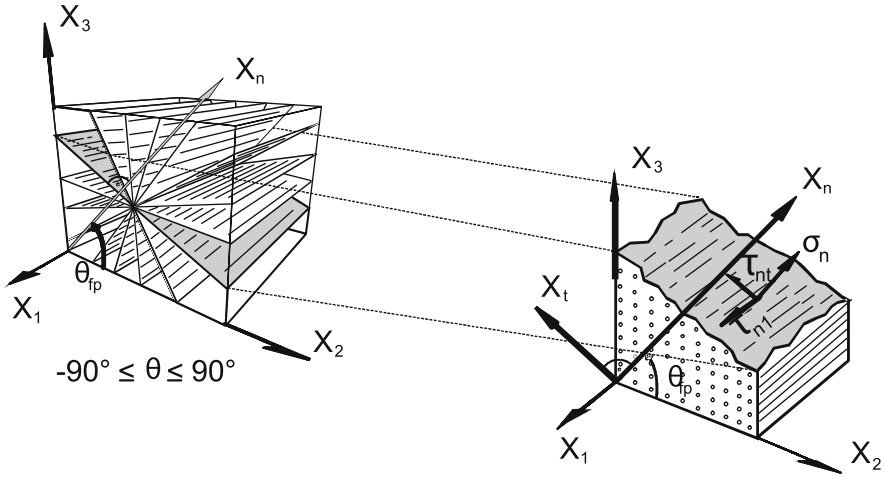


Fig. 39. Search for the fracture plane

calculated for all planes with angles $-90^\circ \leq \theta \leq 90^\circ$ and that for all these angles the stress exposure $f_E(\theta)$ needs to be calculated, see Fig. 39. This is done by inserting the stresses into an IFF-criterion formulated with the stresses of the action plane $\sigma_n(\theta)$, $\tau_{nt}(\theta)$, $\tau_{nl}(\theta)$. The procedure is usually done in 1° -steps leading to 180 calculations. With modern computers that is no problem. Nevertheless, it makes sense to reduce the numerical effort as far as possible.

Figure 40 illustrates the course of the angle dependent stress exposure $f_E(\theta)$ as a function of the angle θ of the action plane for a selected state of stress ($\sigma_1 = \sigma_2 = \sigma_3 = \tau_{21} = 0$; $\tau_{23} = \tau_{31}$). As a result of the fracture analysis one gets a fracture angle $\theta_{fp} = 58^\circ$ and a stress exposure $f_E = 0.5$. This corresponds to the global maximum of the bold curve in Fig. 40. If the stresses are multiplied by the stretch factor $f_S = 1/f_E = 2$, for $\theta = 58^\circ$ $f_E = 1$ is reached in this case. The thin curve in Fig. 40 illustrates the curve $f_E(\theta)$ resulting from multiplying the stresses by $(f_S(\theta_{fp}) = 1/f_E(\theta_{fp}))$.

Originally in 1993, Puck proposed the following IFF-condition for compressive stress σ_n^c :

$$\left(\frac{\tau_{nt}(\theta_{fp})}{R_{\perp\perp}^A - p_{\perp\perp}^c \cdot \sigma_n(\theta_{fp})} \right)^2 + \left(\frac{\tau_{nl}(\theta_{fp})}{R_{\perp\parallel}^A - p_{\perp\parallel}^c \cdot \sigma_n(\theta_{fp})} \right)^2 = 1, \text{ for } \sigma_n < 0 \quad (\text{Eq. 37})$$

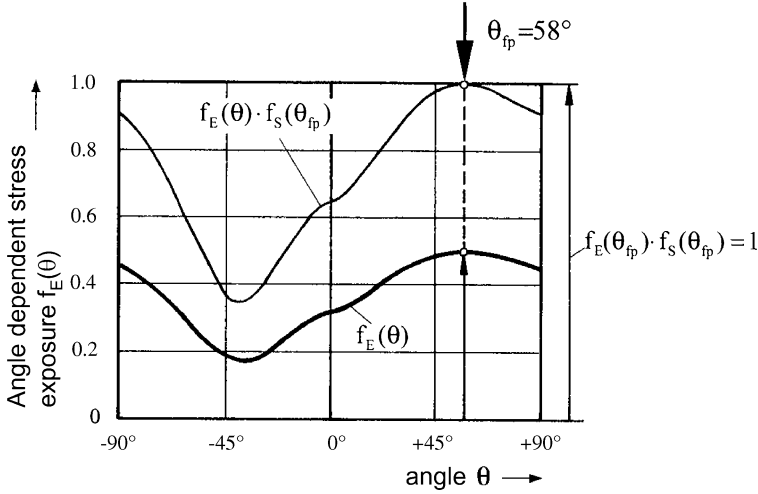


Fig. 40. Stress exposure $f_E(\theta)$ for a τ_{23}/τ_{31} -combination

With the inclination of the (σ_n, τ_{nt}) - and (σ_n, τ_{nl}) -curves at the point $\sigma_n = 0$:

$$-p_{\perp\perp}^c = \left[\frac{\partial \tau_{nt}}{\partial \sigma_n} \right]_{\sigma_n=0} \quad (\text{Eq. 38})$$

$$-p_{\perp\parallel}^c = \left[\frac{\partial \tau_{nl}}{\partial \sigma_n} \right]_{\sigma_n=0} \quad (\text{Eq. 39})$$

Here, the classical quadratic additive approach was chosen for the interaction of the two shear stresses τ_{nt} and τ_{nl} . The two denominators fulfill Puck's second hypothesis stating that a compressive stress σ_n^c (a stress with a negative value) adds an additional fracture resistance $-p_{\perp\perp}^c \sigma_n(\theta_{fp})$ to $R_{\perp\perp}^A$ and $-p_{\perp\parallel}^c \sigma_n(\theta_{fp})$ to $R_{\perp\parallel}^A$, respectively.

At this point one should recall the correct meaning of this statement: It does not mean that adding an additional compressive stress σ_2^c reduces the IFF-stress exposure $f_E = [f_E(\theta)]_{\max}^{21}$! It does only mean that the stress exposure on the action plane $f_E(\theta)$ under consideration decreases, if $|\sigma_n^c|$ on this plane grows. This implies that on other planes – with a different angle

²¹ Even though that might be true in some cases.

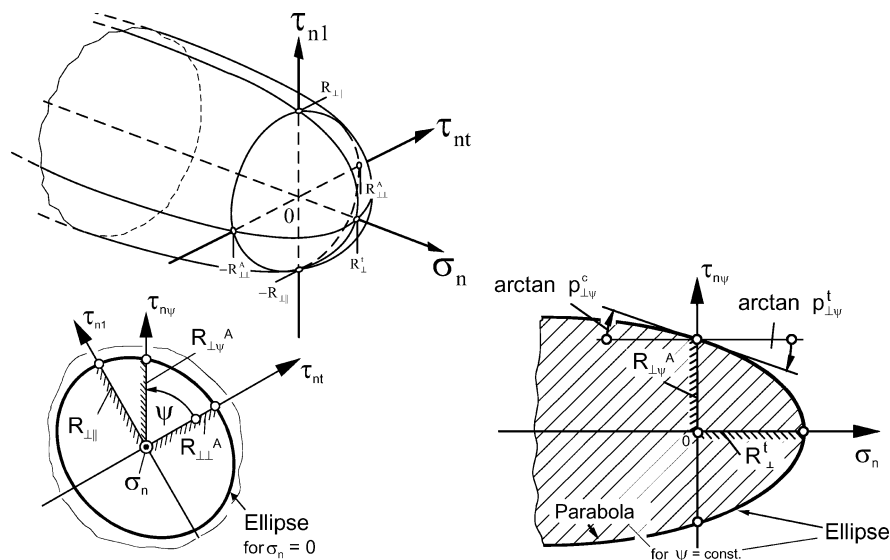


Fig. 41. Master Fracture Body in the $(\sigma_n, \tau_{nt}, \tau_{n1})$ -space

θ – where the same state of stress leads to different stresses $\sigma_n(\theta)$, $\tau_{nt}(\theta)$, $\tau_{n1}(\theta)$ the stress exposure might increase.

Another important aspect is the difference between a conventional fracture body written in $\sigma_2, \sigma_3, \tau_{23}, \tau_{31}, \tau_{21}$ (and σ_1 , if fiber fracture is covered, too) on the one hand and the Master Fracture Body (MFB) describing which stress-combinations $(\sigma_n, \tau_{nt}, \tau_{n1})$ lead to fracture on their action plane.

Again, the difference can well be illustrated regarding the simple example of plane stress ($\sigma_3 = \tau_{23} = 0$). Figure 24 shows the fracture curve for the (σ_2, τ_{21}) -stress combination. The curve is closed indicating that any stress ratio σ_2/τ_{21} leads to fracture, if the magnitude of the stresses is sufficiently high. Figure 41 shows schematically the corresponding Master Fracture Body (MFB) in the $(\sigma_n, \tau_{nt}, \tau_{n1})$ -space. Additionally, a cross section as described by (Eq. 37) and an arbitrary longitudinal section of the (MFB) are shown.

Comparing the fracture curve in the (σ_2, τ_{21}) -diagram and the longitudinal section of the MFB $((\sigma_n, \tau_{n\psi})$ -diagram) several misunderstandings and misinterpretations are possible as long as the subject has not been fully understood. First thing to recognize is that any longitudinal section of the MFB has no intersection with the σ_n -axis in the area of $\sigma_n < 0$. At first glance that seems to be in contrast both to common sense and the (σ_2, τ_{21}) -fracture curve: Does transverse compression not lead to fracture?

Of course, it does! But not on the action plane of the transverse compressive stress σ_2 ! A single transverse compressive stress does never ever provoke fracture on its action plane. That is, why the MFB is open to the negative σ_n -axis. For pure transverse compression σ_2^c fracture does occur on a plane inclined by $\pm 54^\circ$. That means, that first the stresses $\sigma_n(\theta = \pm 54^\circ)$ and $\tau_{nt}(\theta = \pm 54^\circ)$ have to be calculated. In the case of pure (σ_2, τ_{21}) -loading (Eq. 1) simplifies to

$$\sigma_n = \sigma_2 \cdot \cos^2 \theta, \text{ for } \sigma_3 = \tau_{23} = 0 \quad (\text{Eq. 40})$$

$$\tau_{nt} = -\sigma_2 \cdot \sin \theta \cos \theta, \text{ for } \sigma_3 = \tau_{23} = 0 \quad (\text{Eq. 41})$$

$$\tau_{n1} = \tau_{21} \cdot \cos \theta, \text{ for } \tau_{31} = 0 \quad (\text{Eq. 42})$$

For pure transverse compression the longitudinal shear stress τ_{21} and consequently τ_{n1} are zero. Thus on the fracture plane $\theta_{fp} = \pm 54^\circ$ just σ_n and τ_{nt} are acting. The magnitude of these stresses can be calculated with (Eq. 40) to (Eq. 42) and is also illustrated in Fig. 25.

This simple example might help to understand the procedure the concept of action plane related fracture criteria implies. The criteria are formulated with the stresses of the action plane. For all possible action planes with inclination angles θ between -90° and $+90^\circ$ the stress exposure $f_E(\theta)$ is calculated and the plane with the highest stress exposure determined. This plane is the fracture plane (compare Fig. 39 and Fig. 40).

The fracture condition (Eq. 37) mirrors well the mechanics and the material behavior. However, it is not very well suited for the numerical search of the fracture plane as explained below.

If a state of stress $\sigma_n(\theta)$, $\tau_{nt}(\theta)$, $\tau_{n1}(\theta)$ does not lead to fracture on the plane examined, the expression on the left hand side of (Eq. 37) is smaller than “1”. Fracture will occur on this plane if all three stresses are multiplied by the reciprocal value of the stress exposure $[1/f_E(\theta)]$, the so called stretch factor f_s . This magnification factor leading to the value “1” on the left hand side of (Eq. 37) is unknown at first and must be calculated. However, if f_s is introduced as a factor for σ_n , τ_{nt} , τ_{n1} in (Eq. 37), a 4th grade equation for f_E results. This equation cannot easily be solved. Thus, (Eq. 37) seems to be unsuitable for the calculation of $f_E(\theta)$.

Geometrically (Eq. 37) describes a fracture body with elliptical cross sections for $\sigma_n^c = \text{const.}$ (compare Fig. 41). Of course the fracture body can also mathematically be described by its longitudinal sections, the so called

contour lines. By this means the numerical effort for the search of the fracture plane can considerably be reduced. The simple reason for that is the following:

The direction of the stress vector does not change when it is stretched by the stretch factor f_s . This means that the ratios between the three stresses $\sigma_n(\theta):\tau_{nt}(\theta):\tau_{nl}(\theta)$ remain constant. Geometrically, the extension of the stress vector takes place within a longitudinal section characterized by the ratio $\tau_{nl}(\theta)/\tau_{nt}(\theta) = \tan\psi$ (Fig. 41). This means, that $f_E(\theta)$ can relative easily be calculated, if the fracture body is mathematically defined by its longitudinal sections.

In the following the mathematical derivation of the fracture condition is given. Here, of course, a distinction of the cases transverse tension ($\sigma_n > 0$) and transverse compression ($\sigma_n < 0$) is necessary.

4.2.6.2 Fracture condition for tensile stress σ_n

The longitudinal section of the MFB characterized by $\tau_{nt} = 0$ ($\psi = 90^\circ$) is well known from experimental experience. This special section is the same as the (σ_2, τ_{21}) -fracture curve. Fracture occurs on the common action plane of σ_2 and τ_{21} , thus $\sigma_n(\theta_{fp}) = \sigma_2$ and $\tau_{nl}(\theta_{fp}) = \tau_{21}$. In the region of tensile stress σ_n on the fracture plane this fracture curve can well be fitted with an elliptical function having a slightly negative inclination at $\sigma_n = 0$, $\tau_{nl} = R_{\perp\parallel}$ and hitting the σ_n -axis perpendicularly at $\sigma_n = R_{\perp}^t$, $\tau_{nl} = 0$.

Puck assumes that all other longitudinal sections ($\psi = \text{const.}$) can be described with similar curves. The resultant shear stress for such a section is derived from the two stresses $\tau_{nt}(\theta)$ and $\tau_{nl}(\theta)$ with common action plane (compare Fig. 18):

$$\tau_{n\psi}(\theta) = \sqrt{\tau_{nt}^2(\theta) + \tau_{nl}^2(\theta)} \quad (\text{Eq. 43})$$

Now, the problem can be treated as 2-dimensional with the two stresses $\sigma_n(\theta)$ (in the following abbreviated with σ_n) and $\tau_{n\psi}(\theta)$ (abbreviated with $\tau_{n\psi}$) similar to that of the classical fracture envelope of Otto Mohr, compare Fig. 31. Defining the fracture resistance of the action plane against a resultant shear stress $\tau_{n\psi}$ as $R_{\perp\psi}^A$ (see Fig. 41), the fracture condition formulated as an elliptic equation results to be:

$$\left(\frac{\tau_{n\psi}}{R_{\perp\psi}^A} \right)^2 + c_1 \cdot \frac{\sigma_n}{R_{\perp}^{At}} + c_2 \cdot \frac{\sigma_n^2}{(R_{\perp}^{At})^2} = 1, \text{ for } \sigma_n \geq 0 \quad (\text{Eq. 44})$$

The constants c_1 and c_2 can be determined by boundary conditions: For $\tau_{n\psi} = 0$ the expression $\sigma_n = R_{\perp}^{At}$ must result. This leads to

$$c_1 + c_2 = 1 \quad (\text{Eq. 45})$$

At the intersection with the $\tau_{n\psi}$ -axis the fracture curve takes the value $R_{\perp\psi}^A$ and the inclination shall be by definition

$$\left(\frac{\partial \tau_{n\psi}}{\partial \sigma_n} \right)_{\sigma_n=0} = -p_{\perp\psi}^t \quad (\text{Eq. 46})$$

Implicit differentiation of (Eq. 44) at the point $\sigma_n = 0$, $\tau_{n\psi} = R_{\perp\psi}^A$ gives:

$$\frac{2}{R_{\perp\psi}^A} \cdot \left(\frac{\partial \tau_{n\psi}}{\partial \sigma_n} \right)_{\sigma_n=0} + \frac{c_1}{R_{\perp}^{At}} = 0 \quad (\text{Eq. 47})$$

That leads eventually to the fracture condition:

$$\left(\frac{\tau_{n\psi}}{R_{\perp\psi}^A} \right)^2 + 2 \cdot \frac{p_{\perp\psi}^t \cdot \sigma_n}{R_{\perp\psi}^A} + \left(1 - 2 \cdot \frac{p_{\perp\psi}^t \cdot R_{\perp}^{At}}{R_{\perp\psi}^A} \right) \cdot \frac{\sigma_n^2}{(R_{\perp}^{At})^2} = 1, \quad (\text{Eq. 48})$$

for $\sigma_n \geq 0$

4.2.6.3 Fracture condition for compressive stress σ_n

In principle several mathematical functions might be adequate to model the Master Fracture Body in the zone of negative σ_n .

Up to a stress magnitude $|\sigma_2^c| \approx 0,4R_{\perp}^c$ (This is the region of $\theta_{fp} = 0$) the experimentally determined (σ_2, τ_{21}) -fracture curve can well be modeled by a parabola. The mentioned experimental experience and the fact that Otto Mohr himself has assumed that the increase in sustainable shear stress caused by a superimposed compressive stress σ_n would grow less than linearly with σ_n led Puck to a general parabolic approach for $\sigma_n < 0$. A suitable parabola can be formulated as follows:

$$\left(\frac{\tau_{n\psi}}{R_{\perp\psi}^A} \right)^2 + c \cdot \sigma_n = 1, \text{ for } \sigma_n < 0 \quad (\text{Eq. 49})$$

Here, the inclination at $\sigma_n = 0$ shall be by definition:

$$\left(\frac{\partial \tau_{n\psi}}{\partial \sigma_n} \right)_{\sigma_n=0} = -p_{\perp\psi}^c \quad (\text{Eq. 50})$$

Differentiation of (Eq. 49) at $\sigma_n = 0$, $\tau_{n\psi} = 0$ gives with (Eq. 50):

$$c = \frac{2 \cdot p_{\perp\psi}^c}{R_{\perp\psi}^A} \quad (\text{Eq. 51})$$

All this leads finally to the following fracture condition for compressive stress σ_n on the fracture plane:

$$\left(\frac{\tau_{n\psi}}{R_{\perp\psi}^A} \right)^2 + 2 \cdot \frac{p_{\perp\psi}^c}{R_{\perp\psi}^A} \cdot \sigma_n = 1, \text{ for } \sigma_n < 0 \quad (\text{Eq. 52})$$

In (Eq. 48) and (Eq. 52) there are still the fracture resistances $R_{\perp\psi}^A$ and the inclination parameters $p_{\perp\psi}$ as unknown parameters. Consequently, the next paragraphs deal with the definition of reasonable values for these parameters.

4.2.6.4 Description of the cross section of the MFB at $\sigma_n = 0$, determination of $R_{\perp\psi}^A$

Figure 41 is helpful for the interpretation of the parameter $R_{\perp\psi}^A$. In fact, the fracture resistance $R_{\perp\psi}^A$ is – at the point $\sigma_n = 0$ – the distance from the point of origin to the surface of the MFB under the angle ψ . This angle ψ characterizes the longitudinal section and depends on the ratio of τ_{nt} and τ_{n1} . For $\psi = 0^\circ$ ($\tau_{n\psi} = \tau_{n0^\circ} = \tau_{nt}$, $\tau_{n1} = 0$) the fracture resistance is $R_{\perp\perp}^A$ and for $\psi = 90^\circ$ ($\tau_{n\psi} = \tau_{n90^\circ} = \tau_{n1}$, $\tau_{nt} = 0$) it is $R_{\perp\parallel}^A$.

Considerations based on micro-mechanics suggest that these two fracture resistances ($R_{\perp\perp}^A$ and $R_{\perp\parallel}^A$) are not equal but of very similar magnitude. Thus, the classical elliptic approach for intermediate values $R_{\perp\psi}^A$ seems to be appropriate:

$$\left(\frac{\tau_{n\psi 0}}{R_{\perp\psi}^A} \right)^2 = \left(\frac{\tau_{nt 0}}{R_{\perp\perp}^A} \right)^2 + \left(\frac{\tau_{n1 0}}{R_{\perp\parallel}^A} \right)^2 = 1 \quad (\text{Eq. 53})$$

Here, the additional index “0” indicates that all stresses are taken at $\sigma_n = 0$. With the correlations $\tau_{nt0} = \tau_{n\psi 0} \cos \psi$ and $\tau_{n10} = \tau_{n\psi 0} \sin \psi$ (Eq. 53) leads to:

$$\left(\frac{1}{R_{\perp\psi}^A} \right)^2 = \left(\frac{\cos \psi}{R_{\perp\perp}^A} \right)^2 + \left(\frac{\sin \psi}{R_{\perp\parallel}^A} \right)^2 = 1 \quad (\text{Eq. 54})$$

However, the normal stress σ_n has no influence on ψ . For all values of σ_n the following correlations are valid:

$$\cos \psi = \frac{\tau_{nt}}{\tau_{n\psi}} \quad (\text{Eq. 55})$$

and

$$\sin \psi = \frac{\tau_{n1}}{\tau_{n\psi}} \quad (\text{Eq. 56})$$

Thus, (Eq. 53) is generally valid for all σ_n :

$$\left(\frac{\tau_{n\psi}}{R_{\perp\psi}^A} \right)^2 = \left(\frac{\tau_{nt}}{R_{\perp\perp}^A} \right)^2 + \left(\frac{\tau_{n1}}{R_{\perp\parallel}^A} \right)^2 \quad (\text{Eq. 57})$$

With (Eq. 57) the Master Fracture Body is defined by a transverse section ($\sigma_n = 0$) and an infinite number of longitudinal sections $\psi = \text{const.}$ ((Eq. 48) and (Eq. 52)). The only parameter left to be defined is the inclination of the longitudinal sections at $\sigma_n = 0$ (compare Fig. 41). Guidelines concerning the choice of values for the inclination parameters can be found in the next paragraphs.

In the case $\tau_{nt} = \tau_{n1} = 0$ it does not matter which value is taken for $p_{\perp\psi}^t / R_{\perp\psi}^A$ since this coefficient can be (in the special case of no shear stress) eliminated from (Eq. 48). The fracture condition of the action plane for negative σ_n (Eq. 52) is not defined for $\tau_{nt} = \tau_{n1} = 0$, because there is no fracture on a plane with pure transverse compression. In this case fracture takes place on another action plane.

4.2.6.5 Rearrangement of the fracture condition for searching the fracture plane

To use the action plane related fracture condition

$$F(\sigma_n(\theta_{fp}), \tau_{nt}(\theta_{fp}), \tau_{n1}(\theta_{fp})) = 1 \quad (\text{Eq. 58})$$

first the fracture angle θ_{fp} needs to be determined. The fracture plane (and with this the fracture angle θ_{fp}) is characterized as the action plane with the maximum “local” stress exposure: $f_E(\theta_{fp}) = [f_E(\theta)]_{\max}$ with $-90^\circ \leq \theta \leq 90^\circ$. It is better to use the stress exposure and not the reciprocal stretch factor $f_s = 1/f_E(\theta)$ for the numerical search of the fracture plane, because on planes being free of stress, $[1/f_E(\theta)]$ equals “ ∞ ” whereas $f_E(\theta)$ equals “0” which poses no numerical problems.

Assuming that the stresses $\tau_{n\psi}(\theta)$ and $\sigma_n(\theta)$ in (Eq. 48) and (Eq. 52) do not yet cause fracture, they must be multiplied by f_s or divided by $f_E(\theta)$ in order to lead to fracture (on this very plane) and to fulfill the fracture condition. Keeping this in mind, it is obvious that the fracture conditions (Eq. 48) and (Eq. 52) lead to quadratic equations for $f_E(\theta)$, because the stresses occur just in the first and second order in the fracture conditions. The solution of these quadratic equations can be explicitly determined, see (Eq. 12). The resulting expression for $f_E(\theta)$ is homogeneous of first grade concerning the stresses. This means that the stress exposure $f_E(\theta)$ grows linearly with the stresses. Thus the stress exposure is a direct measure of the risk of fracture.

In Fig. 42 all equations needed for the described numerical search of the fracture plane are summarized.

$$f_E(\theta) = \sqrt{\left[\left(\frac{1}{R_{\perp}^t} - \frac{p_{\perp\psi}^t}{R_{\perp\psi}^A} \right) \cdot \sigma_n(\theta) \right]^2 + \left(\frac{\tau_{nt}(\theta)}{R_{\perp\perp}^A} \right)^2 + \left(\frac{\tau_{n1}(\theta)}{R_{\perp\parallel}} \right)^2} + \frac{p_{\perp\psi}^t}{R_{\perp\psi}^A} \sigma_n(\theta)$$

for $\sigma_n \geq 0$

$$f_E(\theta) = \sqrt{\left(\frac{\tau_{nt}(\theta)}{R_{\perp\perp}^A} \right)^2 + \left(\frac{\tau_{n1}(\theta)}{R_{\perp\parallel}} \right)^2 + \left(\frac{p_{\perp\psi}^c}{R_{\perp\psi}^A} \sigma_n(\theta) \right)^2} + \frac{p_{\perp\psi}^c}{R_{\perp\psi}^A} \sigma_n(\theta)$$

for $\sigma_n < 0$

$$\frac{p_{\perp\psi}^{t,c}}{R_{\perp\psi}^A} = \frac{p_{\perp\perp}^{t,c}}{R_{\perp\perp}^A} \cdot \cos^2 \psi + \frac{p_{\perp\parallel}^{t,c}}{R_{\perp\parallel}^A} \cdot \sin^2 \psi \quad \cos^2 \psi = \frac{\tau_{nt}^2}{\tau_{nt}^2 + \tau_{n1}^2}$$

$$R_{\perp\perp}^A = \frac{R_{\perp}^c}{2 \cdot (1 + p_{\perp\perp}^c)} \quad \sin^2 \psi = \frac{\tau_{n1}^2}{\tau_{nt}^2 + \tau_{n1}^2}$$

Fig. 42. Equations needed for the numerical search of the fracture plane

4.2.6.6 Choice of inclination parameters $p_{\perp\psi}^t$ and $p_{\perp\psi}^c$

The parameters $p_{\perp\parallel}^t$ and $p_{\perp\parallel}^c$ ($\psi = 90^\circ$) can be deduced from the (σ_2, τ_{21}) -fracture curve (compare Fig. 24). This is possible due to the fact, that the fracture angle θ_{fp} is zero for both $\sigma_2 > 0$ and $\sigma_2 < 0$. Thus, the stresses on the fracture plane are $\sigma_n = \sigma_2$ and $\tau_{n1} = \tau_{21}$.

Those – experimentally determined – values for the parameters $p_{\perp\parallel}^t$ and $p_{\perp\parallel}^c$ usually lie between 0.25 and 0.35 (Table 1). Quite often experimental results are best fit to (Eq. 48) and (Eq. 52) respectively, if $p_{\perp\parallel}^t$ is chosen slightly higher than $p_{\perp\parallel}^c$. Generally speaking, values between 0.2 and 0.35 lead to reasonable fracture curves (Puck et al. 2002). Table 1 shows typical values for unidirectional layers with thermosetting matrix. They represent mean values resulting from two major experimental projects [Cuntze et al. 1997; Kopp2000].

Corresponding validated data for $p_{\perp\perp}^c$ and $p_{\perp\perp}^t$ ($\psi = 0^\circ$) do not exist, because the (τ_{nt}, σ_n) -fracture curve is experimentally non-accessible in the region $\sigma_n \approx 0$ [Puck 1996, Ritt 1999]. However, $p_{\perp\perp}^c$ can indirectly be drawn from transverse compression fracture tests recording the fracture angle θ_{fp} . Here the following equation holds:

$$p_{\perp\perp}^c = \frac{1}{2 \cdot \cos^2 \theta_{fp}} - 1 \quad (\text{Eq. 65})$$

As stated before, for both GFRP and CFRP one obtains – under uniaxial transverse compression – fracture angles slightly above 50° from experiments. In this case values greater than $p_{\perp\perp}^c = 0.21$ result from (Eq. 65). However, it should be recognized that the measurement of fracture angles is very difficult and that results scatter considerably [Cuntze et al. 1997; Kopp2000]. Moreover, (Eq. 65) is very sensitive even to marginal changes of the fracture angle θ_{fp} under pure transverse compression. Thus, it cannot be recommended to use (Eq. 65) for fitting $p_{\perp\perp}^c$ and it must be accepted for the moment that no experiments are available for the validated determination of $p_{\perp\perp}^c$ and $p_{\perp\perp}^t$.

At first glance it seems logical to choose $p_{\perp\perp}^t$ and $p_{\perp\perp}^c$ identical to $p_{\perp\parallel}^t$ and $p_{\perp\parallel}^c$, respectively, because both $\tau_{\perp\parallel}$ and $\tau_{\perp\perp}$ are shear stressings in a plane parallel to the fibers. In fact, this approach is reasonable. However, from a micro-mechanical point of view $\tau_{\perp\parallel}$ - and $\tau_{\perp\perp}$ -stressings lead to different stress distributions in the matrix. In the first case the shear stressing is oriented parallel to the fibers, in the latter case it is transverse. This has consequences for the micro-cracking preceding IFF, too. Consequently the values for $R_{\perp\parallel}$ and $R_{\perp\perp}^A$ are slightly different for both cases. Likewise, for $p_{\perp\parallel}^c$ and $p_{\perp\perp}^c$ similar but not necessarily equal values can be expected. The

same is valid for $p_{\perp\parallel}^t$ and $p_{\perp\perp}^t$. However, there is no reason for $p_{\perp\parallel}^c = p_{\perp\perp}^t$ since in the corresponding longitudinal cut through the master fracture body σ_n changes its fracture mode from impeding IFF-formation ($\sigma_n < 0$) to promoting IFF-formation ($\sigma_n > 0$).

Evaluating all available information it is hereby recommended to use the set of parameters given in Table 1.

Table 1. Inclination parameters for typical FRP [Cuntze et al. 1997; Kopp 2000; Puck et al. 2002]

$\varphi = 60^\circ$	$p_{\perp\parallel}^t$ [–]	$p_{\perp\parallel}^c$ [–]	$p_{\perp\perp}^t$ [–]	$p_{\perp\perp}^c$ [–]
GFRP/ Epoxy	0.3	0.25	0.20 to 0.25	0.20 to 0.25
CFRP/ Epoxy	0.35	0.3	0.25 to 0.30	0.25 to 0.30

In order to keep the MFB at all points continuously differentiable an interpolation is necessary for all longitudinal sections $\psi \neq 0^\circ$ and $\psi \neq 90^\circ$. This is done as follows:

$$\frac{P_{\perp\psi}^{t,c}}{R_{\perp\psi}^A} = \frac{P_{\perp\perp}^{t,c}}{R_{\perp\perp}^A} \cdot \cos^2 \psi + \frac{P_{\perp\parallel}^{t,c}}{R_{\perp\parallel}^A} \cdot \sin^2 \psi \quad (\text{Eq. 66})$$

with

$$\cos^2 \psi = \frac{\tau_{nt}^2}{\tau_{nt}^2 + \tau_{n\parallel}^2} \quad (\text{Eq. 67})$$

$$\sin^2 \psi = 1 - \cos^2 \psi \quad (\text{Eq. 68})$$

4.2.6.7 Limits of validity of the recommended inclination parameters

There is one last factor of relevance with regard to the choice of the inclination parameters $p_{\perp\perp}^t$ and $p_{\perp\perp}^c$. This is due to the fracture mechanism of brittle materials subjected to a pure τ_{23} -stress (Fig. 44).

Intrinsically brittle materials subjected to a pure τ_{23} -stress always fail due to the principal normal stress $\sigma_n = \sigma_{\parallel}$ occurring on a fracture plane which is inclined towards the direction of the τ_{23} -stress by $\theta_{fp} = 45^\circ$ [Paul 1961].

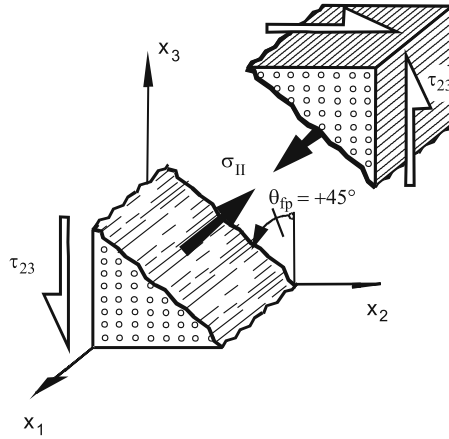


Fig. 44. Fracture due to pure τ_{23} -stress

The fracture criterion will only predict this behavior and not a 'mixed mode fracture' due to simultaneously acting τ_{nt} - and σ_n^t -stresses, if the following condition is complied [Cuntze et al. 1997]:

$$p_{\perp}^t \leq \frac{R_{\perp}^A}{R_{\perp}^t} - \frac{R_{\perp}^t}{R_{\perp}^A} \quad (\text{Eq. 69})$$

This has also been shown by numerical studies [Ritt 1999]. In case of $p_{\perp}^c = p_{\perp}^t = p_{\perp}$ – as proposed above – and applying the equation in Fig. 42 to replace R_{\perp}^A one gets

$$p_{\perp} \leq \frac{\sqrt{(r+4)^2 + 2 \cdot (r^2 - 4) \cdot (r+2)} - (r+4)}{2 \cdot (r+2)} \quad (\text{Eq. 70})$$

with $r = R_{\perp}^c/R_{\perp}^t$.

In accordance with Table 1 usually $p_{\perp} = 0.25$ is chosen for GFRP and $p_{\perp} = 0.3$ for CFRP. Under terms of (Eq. 70) this does not cause any problems for CFRP as long as $R_{\perp}^c/R_{\perp}^t \geq 3$ holds, which is a valid assumption for most CFRP having a thermosetting matrix. As long as $R_{\perp}^c/R_{\perp}^t \geq 2.8$ holds, $p_{\perp} = 0.25$ is applicable. For most but not for all GFRP having a thermosetting matrix this ratio will not be undercut. For the remaining exceptional cases it makes sense to determine the value of p_{\perp} according to (Eq. 70). However, in accordance with Table 1 no values lower than $p_{\perp} = 0.2$ (corresponding to $R_{\perp}^c/R_{\perp}^t = 2.65$) should be used since otherwise unrealistic transverse compression fracture angles θ_{fp}^c would be calculated from (Eq. 65).

If in case of $R_{\perp}^c/R_{\perp}^t < 2.65$ the lower limit $p_{\perp\perp} = 0.2$ is chosen one has to accept that the calculation procedure incorporating (Eq. 48) and (Eq. 52) will not lead to a fracture angle of $\theta_{fp} = 45^\circ$ for a pure τ_{23} -stress. In other words the fracture criterion will indicate a ‘mixed mode fracture’ due to simultaneously acting shear stress τ_{nt} - and **tensile** σ_n -stress.

However, all FRP known to the author have a ratio of $R_{\perp}^c/R_{\perp}^t > 2.65$. This applies according to latest measurements to carbon fiber reinforced PEEK ($R_{\perp}^c = 270 \text{ N/mm}^2$; $R_{\perp}^t = 90 \text{ N/mm}^2$) and glass fiber reinforced Polyamid12 ($R_{\perp}^c = 141 \text{ N/mm}^2$; $R_{\perp}^t = 42 \text{ N/mm}^2$), too.

But – on the other hand – it can be expected that for a material with an unusually low ratio R_{\perp}^c/R_{\perp}^t a mixed mode fracture and the corresponding fracture angle $\theta_{fp} \neq 45^\circ$ resulting from Puck’s fracture criteria will really occur.

4.2.7 Analytical 2-D-formulation for plane states of stress

In thin laminates there are often no considerable stresses present in thickness direction. In this case a 2D stress and strength analysis is sufficient and no numerical search of the fracture plane is required. The equations for the stresses on the action plane σ_n , τ_{nt} and τ_{n1} (compare (Eq. 1), (Eq. 2), (Eq. 3)) simplify to:

$$\sigma_n(\theta) = \sigma_2 \cdot \cos^2 \theta \quad (\text{Eq. 40})$$

$$\tau_{nt}(\theta) = -\sigma_2 \cdot \sin \theta \cdot \cos \theta \quad (\text{Eq. 41})$$

$$\tau_{n1}(\theta) = \tau_{21} \cdot \cos \theta \quad (\text{Eq. 42})$$

This case has been discussed before and used for the explanation of the different IFF fracture modes (compare chapter “Different IFF-fracture modes” and Fig. 19). Figure 45 illustrates again the (σ_2, τ_{21}) -fracture curve and the correspondent lines on the surface of the Master Fracture Body (MFB).

For deriving the analytical 2D-formulation of the IFF-criterion a separate inspection of the three IFF-Modes is useful.

If σ_2 is a tensile stress, the fracture occurs on the plane perpendicular to the x_2 -axis ($\theta_{fp} = 0^\circ$) and the fracture mode is Mode A. The stresses on the fracture plane are identical to the stresses σ_2 , τ_{21} of the UD-lamina: $\sigma_n = \sigma_2$, $\tau_{nt} = 0$ and $\tau_{n1} = \tau_{21}$. The IFF-criterion for $\sigma_n \geq 0$ (Mode A, compare Fig. 42) can therefore be written with the stresses σ_2 and τ_{21} :

$$f_{E,IFF} = \sqrt{\left[\left(\frac{1}{R_{\perp}'} - \frac{p'_{\perp\parallel}}{R_{\perp\parallel}'} \right) \cdot \sigma_2 \right]^2 + \left(\frac{\tau_{21}}{R_{\perp\parallel}'} \right)^2} + \frac{p'_{\perp\parallel}}{R_{\perp\parallel}'} \sigma_2, \text{ for } \sigma_2 \geq 0 \quad (\text{Eq. 71})$$

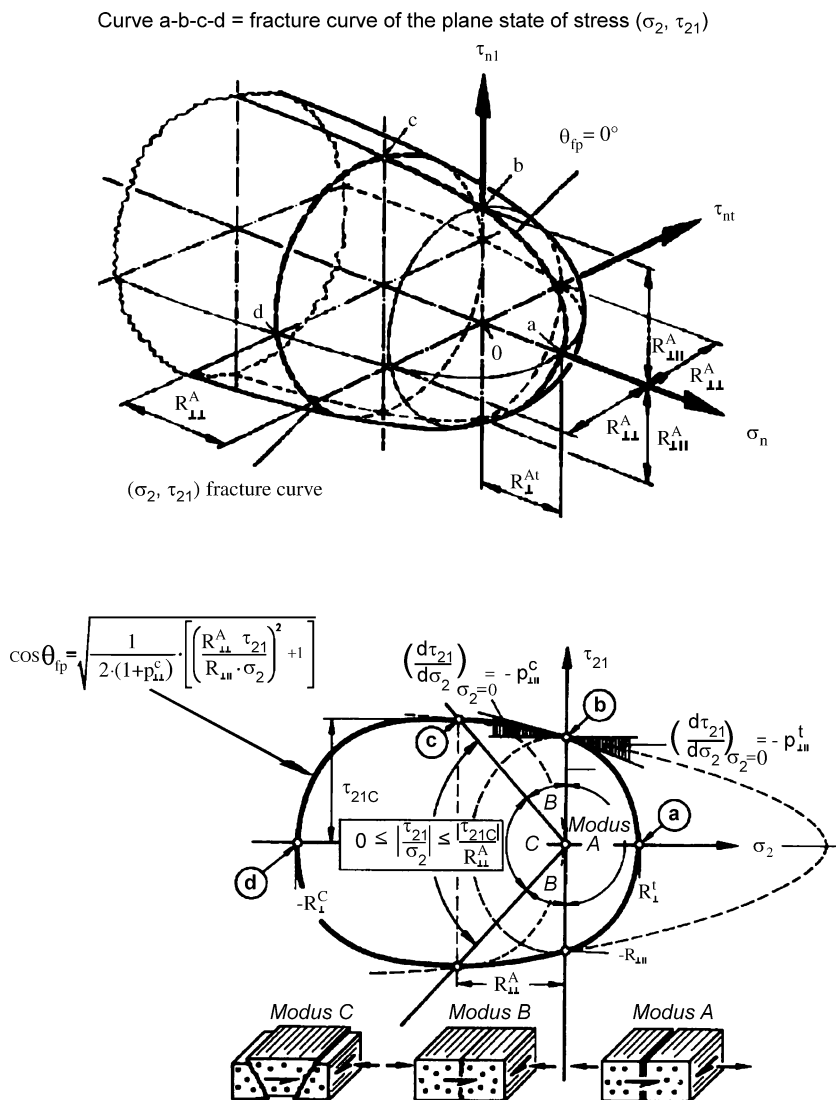


Fig. 45. (σ_2, τ_{21}) -fracture curve and its derivation from the Master-Fracture-Body

For $\sigma_n < 0$ the IFF-criterion in Fig. 42 has the general form

$$f_{E,IFF}(\theta) = \sqrt{\left(\frac{\tau_{nt}(\theta_{fp})}{R_{\perp\perp}^A} \right)^2 + \left(\frac{\tau_{nl}(\theta_{fp})}{R_{\perp\parallel}} \right)^2 + \left(\frac{p_{\perp\psi}^c}{R_{\perp\psi}^A} \sigma_n(\theta_{fp}) \right)^2} + \frac{p_{\perp\psi}^c}{R_{\perp\psi}^A} \sigma_n(\theta_{fp}), \text{ for } \sigma_n < 0$$

(Eq. 72)

The angle θ_{fp} of the fracture plane is unknown in first place. However, as long as the ratio of the transverse stress at fracture and the transverse compressive strength $|\sigma_2/R_{\perp}^c|$ does not exceed a critical value of roughly 0.4 the fracture angle equals zero ($\theta_{fp} = 0$) just as for transverse tensile stress. The fracture mode is Mode B and the fracture condition (Eq. 72) can also be written with the stresses σ_2 and τ_{21} . In this case the transverse shear stress is zero ($\tau_{nt} = 0$), the inclination parameter $p_{\perp\psi}^c = p_{\perp\parallel}^c$ and the shear strength of the action plane $R_{\perp\psi}^A = R_{\perp\parallel}$ (compare Fig. 41).

$$f_{E,IFF} = \sqrt{\left(\frac{\tau_{21}}{R_{\perp\parallel}}\right)^2 + \left(\frac{p_{\perp\parallel}^c}{R_{\perp\parallel}}\sigma_2\right)^2} + \frac{p_{\perp\parallel}^c}{R_{\perp\parallel}}\sigma_2, \sigma_2 < 0 \wedge \left|\frac{\sigma_2}{\tau_{21}}\right| \leq \left|\frac{R_{\perp\parallel}^A}{\tau_{21,c}}\right| \quad (\text{Eq. 73})$$

The fact that the transverse compressive strength R_{\perp}^c does not occur in (Eq. 73) reflects that $\text{IFF}^{\text{Mode B}}$ is a pure shear fracture on the action plane of τ_{21} . This shear fracture is impeded by the compressive stress σ_2^c acting simultaneously to τ_{21} on the fracture plane. Higher shear stress τ_{21} can be sustained in the presence of a compressive stress σ_2^c . This means that the fracture resistance of the action plane ($\theta = 0^\circ$) is increased by increasing $|\sigma_2^c|$.

If $|\sigma_2^c|$ exceeds a critical value, the fracture resistance of the plane with $\theta = 0^\circ$ is no longer the lowest of all action planes. Consequently, fracture takes place on a different plane with $\theta \neq 0^\circ$. The critical value for $|\sigma_2^c|$ is $R_{\perp\perp}^A$, the fracture resistance of the action plane against transverse shear stressing. The point $|\sigma_2^c| = R_{\perp\perp}^A$ marks the transition point to Mode C. The shear stress reached at this point is $\tau_{21,c}$. Thus the point

$$\sigma_2 = -R_{\perp\perp}^A; \tau_{21,c} = R_{\perp\parallel} \cdot \sqrt{1 + 2p_{\perp\perp}^c} \quad (\text{Eq. 74})$$

marks on the fracture curve the transition from Mode B to Mode C. This will be explained in more detail in the following.

To find an analytical solution in σ_2 and τ_{21} for the fracture condition in Mode C is much more difficult than to formulate the (σ_2, τ_{21}) -fracture conditions for Mode A and Mode B. In a first step the extremum problem $d(f_E)/d\theta = 0$ has to be solved. How the problem has been tackled by Puck can be found in [Puck 1996, Puck and Schürmann 1998].

For mathematical simplification Puck coupled the two (usually independent) parameters $p_{\perp\parallel}^c$ and $p_{\perp\perp}^c$ in the following way:

$$\frac{p_{\perp\perp}^c}{R_{\perp\perp}^A} = \frac{p_{\perp\parallel}^c}{R_{\perp\parallel}} \quad (\text{Eq. 75})$$

Constraining the free choice of parameters by this means does not considerably change the results of fracture analysis nor does it lead to contradictions or a confinement of the physical basis of Puck's criteria [Puck 1996].

As a provisional result he found a surprising correlation of the fracture angle θ_{fp} and the normal stress $[\sigma_n(\theta_{fp})]_{fr}$ at fracture [Puck 1996, Puck and Schürmann 1998]

$$[\sigma_n(\theta_{fp})]_{fr} = (\sigma_2)_{fr} \cdot \cos^2 \theta_{fp} = -R_{\perp\perp}^A \quad (\text{Eq. 76})$$

That means that for the entire range of (σ_2, τ_{21}) -combinations which cause fracture by Mode C the stress $[\sigma_n(\theta_{fp})]_{fr}$ on the fracture plane is constant and can be calculated from $[\sigma_n(\theta_{fp})]_{fr} = -R_{\perp\perp}^A = -R_{\perp\perp}^c / [2(1 + p_{\perp\perp}^c)] \approx -0.4 R_{\perp\perp}^c$. That means that all fracture points $(\sigma_2, \tau_{21})_{fr}$ on the Master Fracture Body are located on the boundary of a cross section of the MFB. This is the curve (c) \rightarrow (d) in Fig. 45.

With these results the analytical solution in (σ_2, τ_{21}) for the fracture criterion of Mode C is

$$f_{E,IFF} = \left[\left(\frac{\tau_{21}}{2(1 + p_{\perp\perp}^c) R_{\perp\parallel}} \right)^2 + \left(\frac{\sigma_2}{R_{\perp\perp}^c} \right)^2 \right] \frac{R_{\perp\perp}^c}{-\sigma_2}, \quad (\text{Eq. 77})$$

$$\text{for } \sigma_2 < 0 \wedge \left| \frac{\sigma_2}{\tau_{21}} \right| \geq \left| \frac{R_{\perp\perp}^A}{\tau_{21,c}} \right|$$

Using (Eq. 77) in order to formulate $\cos^2 \theta_{fp} = -R_{\perp\perp}^A / (\sigma_2)_{fr}$ the following relationship for the fracture angle θ_{fp} is found

$$\cos \theta_{fp} = \sqrt{\frac{1}{2 \cdot (1 + p_{\perp\perp}^c)} \cdot \left[\left(\frac{R_{\perp\perp}^A \cdot \tau_{21}}{R_{\perp\parallel} \cdot \sigma_2} \right)^2 + 1 \right]} \quad (\text{Eq. 78})$$

This relation is very useful. For instance it allows to calculate the fracture angle without having calculated the fracture stress $(\sigma_2)_{fr}$ first. It depends only on the ratio of τ_{21}/σ_2 . Further it demonstrates that θ_{fp} does not change if $R_{\perp\perp}^A$ and $R_{\perp\parallel}$ are decreased by the same factor for instance by a weakening factor η_{w1} which will be dealt with in the next Section.

4.3 Extensions to the IFF-criteria

The following two chapters are in main parts identical to the corresponding chapters of the annex to VDI 2014 Part 3 [VDI 2006]. These chapters of the VDI 2014 have been written by Alfred Puck and Günther Lutz and the use of this work is authorized by VDI.

4.3.1 Inclusion of stresses not acting on the fracture plane in the action-plane-related inter-fiber fracture criteria

The action-plane-related strength criteria for inter-fiber fracture (IFF) – Fig. 42 and also (Eq. 71), (Eq. 73) and (Eq. 77) – are based on Mohr’s hypothesis. According to this, only the stresses $\sigma_n(\theta_{fp})$, $\tau_{nt}(\theta_{fp})$ and $\tau_{nl}(\theta_{fp})$ acting on the parallel-to-fiber *fracture plane* (angle of inclination θ_{fp}) are of decisive importance for fracture stresses at IFF. All parallel-to-fiber section planes are in principle potential fracture planes for IFF. Their angles of inclination θ (definition of θ in Fig. 18) vary between $\theta = -90^\circ$ and $\theta = +90^\circ$, where the section planes with $\theta = -90^\circ$ and $\theta = +90^\circ$ are identical. The fracture plane which is to be expected is determined by finding the section plane with the highest stress exposure $f_E(\theta)_{\max}$ dependent on the angle of intersection (The stress exposure is defined in Fig. 21 and Fig. 22). The search for the angle of the fracture plane was analytically anticipated when equations (Eq. 71), (Eq. 73) and (Eq. 77) were set up. If the equations of Fig. 42 are used, the section plane with the highest IFF stress exposure $f_E(\theta_{\max}) = f_E(\theta_{fp})$ must be found by a numerical search of the intersection-angle range from $\theta = -90^\circ$ to $\theta = +90^\circ$.

If the fracture plane has been identified in this way, the stresses (σ_2 , σ_3 , τ_{23} , τ_{31} , τ_{21})_{fr} when the IFF occurs may be obtained by dividing the components of the given stress (σ_2 , σ_3 , τ_{23} , τ_{31} , τ_{21}) by the stress exposure $f_E(\theta_{fp})$ present on the fracture plane. This therefore means that it does not matter whether the stresses $\sigma_n(\theta)$, $\tau_{nl}(\theta)$, $\tau_{nt}(\theta)$ acting on other sections with angles $\theta \neq \theta_{fp}$ bring about relatively high or low IFF stress exposures. On account of the gradual development of an IFF due to progressive formation of micro cracks and for probabilistic reasons, it is, however, to be expected that there are stress states where the Mohr approach gives results which in dimensioning calculations would tend to be on the non-conservative side. This problem will be the subject of chapter 4.3.1.2.

According to Mohr’s hypothesis, even the parallel-to-fiber stress σ_1 does not have any influence on the IFF since it does not act on a parallel-to-fiber section plane and thus does not act on a potential fracture plane for IFF.

Micromechanical aspects do mean that even in this case a correction will be needed. Chapter 4.3.1.1 will deal with a correction of this kind.

4.3.1.1 Inclusion of a parallel-to-fiber stress σ_1 in the action-plane IFF conditions

Physical considerations

According to Mohr's hypothesis, the stress σ_1 does not have any influence on the IFF due to the fact that the action plane of σ_1 is perpendicular to the plane which is acted on by the stresses σ_n , τ_{n1} and τ_{nt} which are of decisive importance to the IFF. However, a series of effects appear to make it necessary to include a σ_1 term in the IFF criteria which reduces 'IFF strength' somewhat [Puck 1996]. The most essential effect may be the following one. FF is taken to mean the fracture of a very large number of elementary fibers which in turn causes a lamina to loose some of its load-bearing capacity in the fiber direction over a 'macro-region'. Statistical laws, however, state that in the event of tensile stress σ_1 some elementary fibers will already have ruptured before the FF limit of the UD lamina at $|\sigma_1| = R_{||}^t$ has been reached. In the case of compressive stress σ_1 it is possible that individual bundles of fibers could already start kinking before total fracture occurs when $|\sigma_1| = R_{||}^c$. Occasional 'micro fiber fractures' cause local damage in the UD lamina which takes the form of debonding at fiber matrix interfaces and of micro-fractures in the matrix material. They weaken the fiber matrix cohesion and thus also reduce its resistance to IFF.

Analytical treatment

In order to include in IFF analysis the weakening effect resulting from σ_1 in a way which is appropriate to the physical circumstances, the action-plane-fracture resistances R_{\perp}^t , $R_{\perp\perp}^A$, $R_{\perp\parallel}$ are multiplied by a degradation factor η_{w1} (w = weakening, $1 \hat{=}$ weakening due to σ_1). A factor of this kind can be used not only in the tensile range but also in the compressive range of σ_1 . For the sake of simplicity it is assumed that the 'weakening factor' η_{w1} has the same numerical value for all three action plane-fracture resistances R_{\perp}^t , $R_{\perp\perp}^A$, $R_{\perp\parallel}$. This assumption has the effect that the inclination of the fracture plane given by the fracture plane angle θ_{fp} and the IFF fracture mode connected with it are not affected by the weakening which is now solely dependent on σ_1 , since σ_1 does not depend on θ . **Searching the fracture angle can be carried out in the same way as before neglecting an influence of σ_1 .**

Reducing the fracture resistances results in an increased stress exposure factor. Therefore the stress exposure factor f_{E_1} when taking into account the influence of σ_1 becomes:

$$f_{E_1} = \frac{f_{E_0}}{\eta_{w1}} \quad (\text{Eq. 79})$$

As in [Puck 1996, Puck and Schürmann 2002] the weakening which increases progressively with σ_1 is described by a fracture curve in the form of a segment of an ellipse, Fig. 46. Previously η_{w1} had always to be calculated iteratively but now a closed solution has been found. The section of the ellipse starts at “ $s \cdot R_{||}$ ” and ends at the FF-limit namely at $|\sigma_1| = R_{||}$. Here, at the FF-limit the weakening factor η_{w1} reaches its minimum “ m ”. Both parameters “ s ” and “ m ” can be chosen independently between 0 and 1 resulting in an excellent adaptability to experiments, especially as the parameter pairs s and m can be set differently in the tension area and in the compression area of σ_1 (see Fig. 46).

Under the given assumptions the following formula for the weakening factor η_{w1} has been derived:

$$\eta_{w1} = \frac{c \left(a \sqrt{c^2(a^2 - s^2) + 1} + s \right)}{(ca)^2 + 1} \quad (\text{Eq. 80})$$

$$\text{with } c = \frac{f_{E_0}}{f_E(\text{FF})} \text{ and } a = \frac{1-s}{\sqrt{1-m^2}}.$$

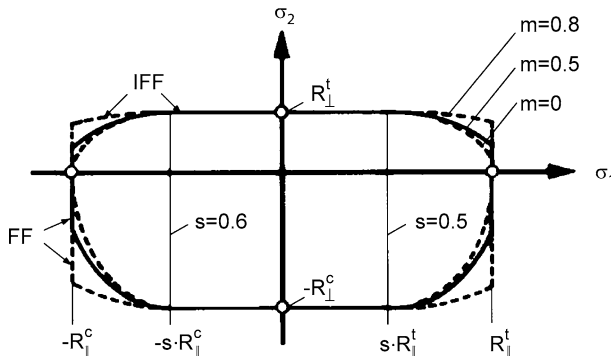


Fig. 46. Form of a (σ_1, σ_2) -fracture curve with influence of σ_1 on the IFF expressed as a function of parameters s and m

$f_E(\text{FF})$ is the FF-stress exposure factor, which is calculated by using the FF-condition $|\sigma_1| = R_{\parallel}$ given in (Eq. 14). The stress exposure factor f_{E_0} is the IFF exposure without an influence of σ_1 (The subscript 0 indicates that $\sigma_1 = 0$). If weakening due to (m+p) effects is not taken into account, then what should be used for f_{E_0} are the stress exposure values f_E calculated with the aid of (Eq. 71), (Eq. 73) and (Eq. 77) or the fracture criteria from Fig. 42 with measured basic strengths and with the guide values given in Table 1, chapter 4.2.6.6 for the inclination parameters. When (m+p) effects are included, what should be used for f_{E_0} is the value of $f_{E_{m+p}}$ according to (Eq. 88) and using the corrected basic strengths $R_{\perp \text{ cor}}^t$, $R_{\perp \text{ cor}}^c$, $R_{\parallel \text{ cor}}$, and the corrected parameter $p_{\perp \parallel \text{ cor}}^c$.

The range of validity of the weakening factor η_{w1} is given by

$$\frac{1}{s} \geq \frac{f_{E_0}}{f_E(\text{FF})} \geq m \quad (\text{Eq. 81})$$

Beyond this region there is either no damage or no IFF occurs before the FF-limit is reached. In the later case it makes no sense to talk about an IFF-stress exposure factor. Instead, there is just a FF-stress exposure factor. This is because FF usually results in an extensive destruction of the fiber-matrix-composite. Thus there is no such thing as an independent IFF anymore.

So far there are no reliable experimentally determined values for the parameters s and m available [Kaiser Kuhnel Obst 2004]. Thus assumed values must be chosen. It is recommended to use $s = 0.5$ and $m = 0.5$ both at $\sigma_1 > 0$ and at $\sigma_1 < 0$. With these values η_{w1} becomes

$$\eta_{w1} = \frac{c \left(\sqrt{c^2 + 12} + 3 \right)}{2(c^2 + 3)} \quad \text{for } 2 \geq c \geq 0.5. \quad (\text{Eq. 82})$$

In principle, one might doubt whether the weakening by η_{w1} could influence the fracture angle θ_{fp} . Thus, the question whether there is such an influence or not is discussed in the following. For doing so, the expression for η_{w1} documented in (Eq. 80) needs to be examined further. Based on the assumption that IFF will occur on the action plane with a maximum of the stress exposure f_{E_1} (including weakening by σ_1), roots of $d(f_{E_1}(\theta))/d\theta$ have to be examined:

$$f_{E_1}(\theta) = \frac{f_{E_0}(\theta)}{\eta_{w1}} = f_{E_0}(\theta) \frac{(ac)^2 + 1}{c \left(a \sqrt{c^2 (a^2 - s) + 1} + s \right)} \quad (\text{Eq. 83})$$

with $c = \frac{f_{E_0}(\theta)}{f_{E(\text{FF})}}$

Here, $f_{E(\text{FF})}$ does not depend of θ and is therefore not of interest for the search for an extremum.

$$\frac{d(f_{E_1}(\theta))}{d\theta} = \frac{d}{dc}(f_{E_1}(c)) \frac{dc}{d\theta} = \frac{d}{dc}(f_{E_1}(c)) \frac{df_{E_0}}{d\theta} = 0 \quad (\text{Eq. 84})$$

This means, that the stress exposure f_{E_1} including the weakening effect of σ_1 has an extremum at the same point as the stress exposure f_{E_0} calculated without weakening by σ_1 . Now the question left to be answered is whether there are further extrema, namely a solution for

$$\frac{d}{dc}(f_{E_1}(c)) = 0. \quad (\text{Eq. 85})$$

The result for (Eq. 85) is

$$c^2 = -\frac{1}{a}. \quad (\text{Eq. 86})$$

This means, that there is no real solution. There are no further extrema of the stress exposure apart from those which are valid for the stress exposure without weakening by σ_1 , too.

4.3.1.2 Inclusion of stresses $\sigma_n(\theta), \tau_{nt}(\theta), \tau_{nl}(\theta)$ which act on parallel-to-fiber planes but not on the fracture plane

Physical fundamentals

The effects which are examined will first be presented by taking the example of a (σ_2, τ_{31}) -stress combination, where σ_2 is to be a tensile stress. According to Mohr's hypothesis, with (σ_2, τ_{31}) -combinations of this kind there either occurs a σ_{\perp} -tensile fracture on the action plane of σ_2 – in other words, at $\theta_{fp} = 0^\circ$ when $\sigma_2 = R_{\perp}^I$ – or a $\tau_{\perp\parallel}$ -shear fracture on the action plane of τ_{31} – in other words, at $\theta_{fp} = \pm 90^\circ$ and this when $\tau_{31} = R_{\perp\parallel}$. Which fracture actually does occur depends on where the (σ_2, τ_{31}) -stress state vector intersects the fracture curve which, according to Mohr's hypothesis, consists of the two straight lines $\sigma_2 = R_{\perp}^I$ and $\tau_{31} = R_{\perp\parallel}$ (fracture curve for (σ_2, τ_{31}) , see Fig. 47). If we had a uniaxial σ_2 -stress state, then a stress $\sigma_n(\theta) = \sigma_2 \cos^2 \theta$ and $\tau_{nt}(\theta) = -\sigma_2 \sin \theta \cos \theta$ would act on the sections adjacent to the fracture plane at angles of inclination $\theta \neq 0^\circ$.

We will now consider a (σ_2, τ_{31}) -vector which meets the straight line $\sigma_2 = R_{\perp}^I$ close to its intersection with the straight line $\tau_{31} = R_{\perp\parallel}$. In this case

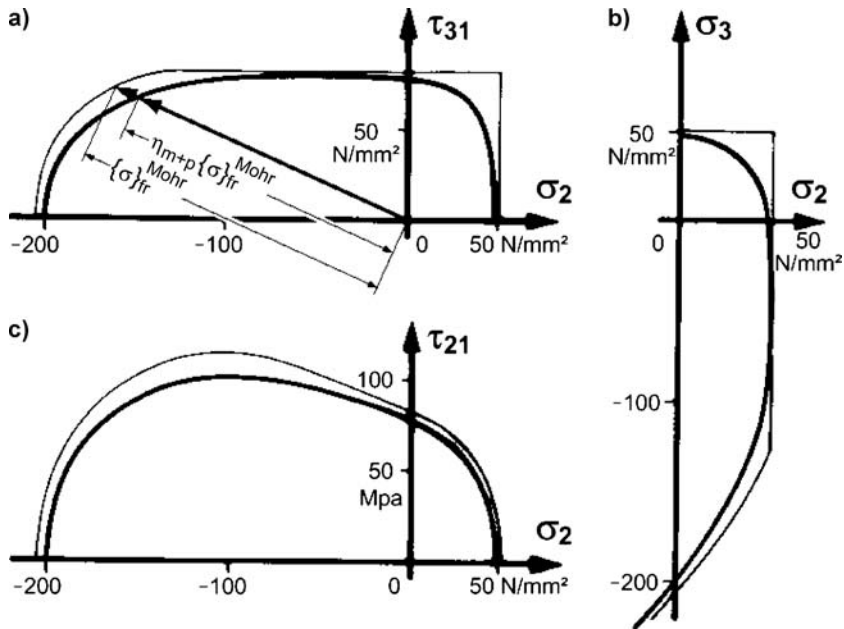


Fig. 47. Fracture curves for three stress combinations: (a) (σ_2, τ_{31}) , (b) (σ_2, τ_{31}) and (c) (σ_2, τ_{21}) . The thin lines represent the starting curves for η_{m+p} -correction, calculated using the equations given in Fig. 42 with corrected basic strength values and corrected parameter $p_{\perp\parallel}^c$ according to (Eq. 91): $R_{\perp}^t = 48.57 \text{ N/mm}^2$, $R_{\perp}^c = 204.82 \text{ N/mm}^2$, $R_{\perp\parallel}^c = 82.16 \text{ N/mm}^2$, $p_{\perp\parallel}^t = 0.35$, $p_{\perp\parallel}^c = 0.45$, $p_{\perp\perp}^t = p_{\perp\perp}^c = 0.275$. The thick lines represent the result curves of an η_{m+p} -correction according to (Eq. 87), (Eq. 88), (Eq. 89) and (Eq. 90).

the angle of the fracture plane according to Mohr will clearly also be $\theta_{fp} = 0^\circ$. But if stresses σ_2 and τ_{31} are present simultaneously, in addition to $\sigma_n(\theta)$ and $\tau_{nt}(\theta)$ a transverse/longitudinal shear stress $\tau_{n1}(\theta) = \tau_{31} \cdot \sin\theta$ will occur on sections at an angle $\theta \neq 0^\circ$. With this, as $\theta = -90^\circ$ and $\theta = +90^\circ$ is approached and provided $\tau_{31}/R_{\perp\parallel}$ is only a little less than σ_2/R_{\perp}^t , there follows an IFF stress exposure $f_E(\theta)$ which is almost as high as that on the action plane at $\theta_{fp} = 0^\circ$ (see standardized stress exposure $f_E'(\theta)$ in Fig. 48). For the combination of σ_2 with τ_{31} which we are considering, the IFF stress exposure over the whole range between $\theta = -90^\circ$ and $\theta = +90^\circ$ will not be much lower than on the action plane itself.

Micromechanical studies show that an IFF does not simply happen suddenly for no particular reason. Once the IFF stress exposure f_E' (standardized to $f_{E_{\max}} = 1$) exceeds a threshold value of about $f_E' \approx 0.5$, instances of

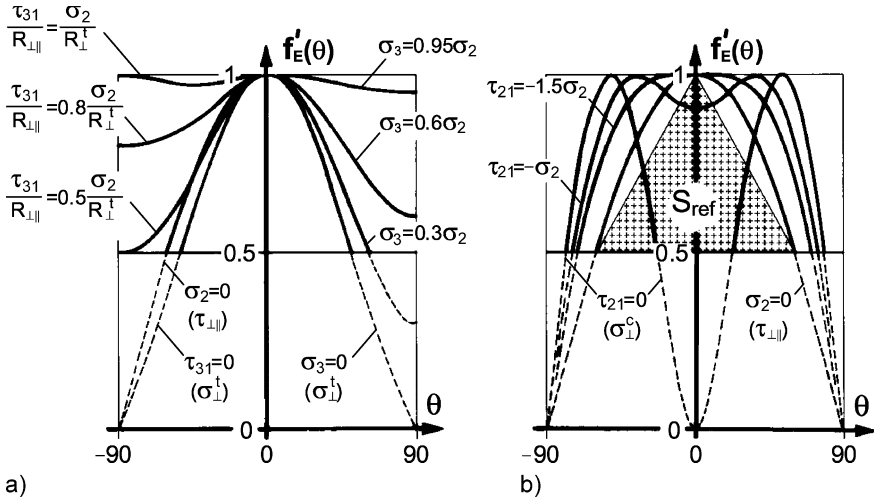


Fig. 48. Standardized stress exposure curves $f'_E(\theta)$ (parameters from Fig. 47); a) Left-hand side of diagram for different (σ_2, τ_{31}) -stress combinations; right-hand side for (σ_2, σ_3) -stress combinations. The complete $f'_E(\theta)$ -curves for (σ_2, τ_{31}) - and (σ_2, σ_3) -stress combinations are symmetrical to the f'_E axis at $\theta = 0^\circ$. b) For different (σ_2, τ_{21}) -stress combinations. The triangular area marked in the figure gives an impression of the magnitude of the reference sum S_{ref}

micro-damage to the fiber/matrix composite will already occur which increase progressively as stress increases. In the case of transverse/longitudinal shear stressing $\tau_{\perp\parallel}$, these are the familiar 45° micro cracks (hackles) which are stopped at fibers and cause often tiny delaminations there (see Fig. 49). It is only when micro-fractures have exceeded a certain magnitude that the IFF will suddenly occur.

In the case of the (σ_2, τ_{31}) -combination under consideration here, not only micro-fractures resulting from σ_2 but also those resulting from τ_{31} develop simultaneously – the case is different with a uniaxial σ_2 stress. The latter type of micro-fractures due to τ_{31} further weakens the fiber/matrix composite as compared with the situation with uniaxial σ_2 -stress. The micro-fractures have a weakening effect on *all sections* with inclination angles between $\theta = -90^\circ$ and $\theta = +90^\circ$. *They also reduce the transverse tensile strength* which in the end is still available on the fracture plane when IFF happens at $\theta_{fp} = 0^\circ$. It is therefore to be expected that σ_2 in combination with a relatively high τ_{31} stress will not reach at IFF that fracture stress which is obtained in the uniaxial transverse tension test with $\sigma_2 = R_{\perp}^t$.

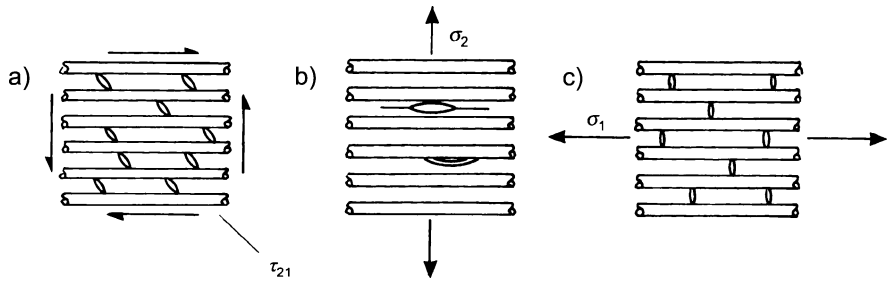


Fig. 49. Occurrence of matrix cracks [Puck 1992]; a) τ_{21} shear stress leads to cracks under 45° (so called hackles) which are stopped at the fibers and are cause of parallel to fiber mini delaminations. b) With σ_2 tensile stress cracks are particularly encouraged where there are flaws and can spread along the fibers without hindrance. c) σ_1 stress results in cracks occurring at the tip of broken individual fibers and running transverse with respect to the fiber until stopped at adjacent fibers.

As a further example let us examine a biaxial (σ_2 , σ_3)-transverse tensile stress. In this case a tensile fracture occurs at $\theta_{fp} = 0^\circ$ if $\sigma_2 > \sigma_3$ or at $\theta_{fp} = \pm 90^\circ$ if $\sigma_3 > \sigma_2$. If $\sigma_2 = \sigma_3 = \sigma$ were the case, the same stress would prevail at all sections at any angle θ due to the relation $\sigma(\theta) = \sigma_2 \cdot \cos^2 \theta + \sigma_3 \cdot \sin^2 \theta = \sigma$ and thus the intersection-angle-dependent stress exposure $f_E(\theta)$ would be equally high on every section plane with θ between -90° and $+90^\circ$. In this special individual case Mohr's hypothesis predicts that IFF will occur simultaneously on all section planes with angles of θ between -90° and $+90^\circ$. At what angle fracture will actually take place in a biaxial transverse tension test with two stresses of equal magnitude depends on contingencies, e. g. on the distribution of flaws.

We will now pass on to a (σ_2 , σ_3)-combination where $\sigma_3 = 0.95 \cdot \sigma_2$. In this case the stress exposure $f_E(\theta)$ is nearly the same in all sections with angles θ between -90° and $+90^\circ$ (see again the standardized stress exposures $f'_E(\theta)$ in Fig. 48). For this reason a more massive instance of micro-damage is to be expected before the IFF occurs than would be the case with uniaxial transverse tensile stress.

A real fiber/matrix composite in addition always contains flaws – for example, in the form of curing cracks, flat air entrapments, or local imperfections in the bonding between fiber and matrix which often cover only a part of the circumference of the fibers. Flaws of this kind have a 'sense of direction'. For example, a curing crack will have an especially strength-reducing effect when a tensile stress σ_n perpendicular to the crack plane occurs. In the case under consideration, in which σ_3 is only 5% less than

σ_2 , the stress exposure $f_E(\theta)$ is theoretically at its maximum at $\theta_{ip} = 0^\circ$. There is nevertheless a high probability that with a different angle of inclination θ of the section plane, a particularly serious flaw will trigger the IFF despite the somewhat lower theoretical stress exposure $f_E(\theta)$ found there. This is a probabilistic effect. It makes prediction of the angle of the fracture plane uncertain and causes the fracture stresses at IFF to be somewhat lower than those calculated on the basis of Mohr's hypothesis.

In both examples there is a mixture of the effects of microdamage and of probabilistic effects; they cannot be treated separately. Generalizing, these examples permit us to arrive at the following conclusion. ***It is to be expected that the effects of microdamage and probabilistics reduce the magnitude of fracture stresses when the IFF occurs will rise the more parallel-to-fiber sections at different angles θ there are for which relatively high values of the stress exposure factor $f_E(\theta)$ can be calculated –*** or, to put it another way, the 'rounder' the 'stress exposure curve' $f_E(\theta)$ will be. A clear picture of which situation of this kind exists with the stress state to be investigated can be obtained by examining the entire stress exposure curve $f_E'(\theta)$ calculated using Mohr's equations of Fig. 42 (see standardized stress exposures in Fig. 48). The stress combination $\sigma_2 = \sigma_3 > 0$ has been recognized as being an extreme case where at any section the value for $f_E'(\theta)$ is equally high.

Analytical treatment

Micromechanical failure analyses and mathematical methods from probabilistics cannot be used in component design. A calculation method will therefore be presented below whereby it is possible, with minimal effort, to estimate the effects of **micro-damage** and **probabilistics** (in abbreviated form: (m+p) effects) with the aid of a phenomenological approach on physical foundations and which is applicable in engineering practice. This method will be referred to as η_{m+p} **correction**. It is a slightly modified form of the approach which appears in [Puck 1996]. The η_{m+p} -correction is based on the following assumptions:

The fracture plane at IFF appears at the angle of intersection θ_{ip} for which, according to Mohr's hypothesis the maximum stress exposure $f_E(\theta)_{\max} = f_E(\theta_{ip})$ is calculated from the fracture criteria in Fig. 42.

The fracture stresses at IFF are obtained by correcting the fracture stresses calculated from $f_E(\theta_{ip})$ by Mohr's hypothesis to lower stresses using a correction factor of $\eta_{m+p} < 1$. (Correspondingly, the IFF stress exposures calculated by Mohr are corrected to higher values by dividing the Mohr stress exposures by η_{m+p}).

Expressed formally (see also Fig. 47a):

$$\{\sigma\}_{m+p} = \{\sigma\}_{fr}^{Mohr} \cdot \eta_{m+p} = \frac{\{\sigma\}}{f_E(\theta_{fp})} \cdot \eta_{m+p} = \frac{\{\sigma\}}{f_{E_{m+p}}} \quad (\text{Eq. 87})$$

$$f_{E_{m+p}} = \frac{f_E(\theta_{fp})}{\eta_{m+p}}. \quad (\text{Eq. 88})$$

- $\{\sigma\}_{m+p}$ = fracture stress vector taking (m+p) effects into account,
- $\{\sigma\}_{fr}^{Mohr}$ = fracture stress vector without taking (m+p) effects into account,
- $\{\sigma\}$ = vector of the effective stress state,
- η_{m+p} = correction factor of the fracture stresses for taking (m+p) effects into account,
- $f_{E_{m+p}}$ = stress exposure of the fracture plane taking (m+p) effects into account,
- $f_E(\theta_{fp})$ = stress exposure of the fracture plane without taking (m+p)-effects into account.

As will be explained later, $\{\sigma\}_{fr}^{Mohr}$ and $f_E(\theta_{fp})$ have to be calculated by using corrected strengths $R_{\perp cor}^t$, $R_{\perp cor}^c$, $R_{\parallel cor}$. The reason for this is the following. Experimentally determined strengths values are “real” values. This means that effects of micro-damage and probabilistics have already influenced these values. The analytical procedure of the η_{m+p} -correction should therefore not a second time degrade these values. In other words: When operating the η_{m+p} -procedure and applying the η_{m+p} -correction to the case of uniaxial transverse tension, to the case of uniaxial transverse compression and to pure longitudinal shear the results should be the experimental values for R_{\perp}^t , R_{\perp}^c and R_{\parallel} . This is achieved in the following way:

Before starting a fracture analysis with η_{m+p} -correction the experimentally determined values R_{\perp}^t , R_{\perp}^c and R_{\parallel} are divided by η_{m+p} belonging to uniaxial tensile stressing, uniaxial compressive stressing and pure longitudinal shear stressing respectively. The appropriate factors η_{m+p} for correcting R_{\perp}^t , R_{\perp}^c and R_{\parallel} are calculated from (Eq. 89) and (Eq. 90) by using the corrected strengths $R_{\perp cor}^t$, $R_{\perp cor}^c$ and $R_{\parallel cor}$. These are not known at the beginning. This is no problem as far as $R_{\perp cor}^c$ and $R_{\parallel cor}$ are concerned, because when normalizing f_E to f_E' the chosen values for these strengths are cancelled from the equation. This is different for uniaxial tension, where f_E is dependent on $R_{\perp cor}^t$ and $R_{\perp cor}^A$. In this case a few iterations are necessary.

Later on, perhaps also the sustainable strengths for uniaxial σ_{\perp}^t and σ_{\perp}^c or pure τ_{\parallel} are calculated in the course of a general fracture analysis including

(m+p) effects. This is done now automatically by multiplying the corrected strengths $R_{\perp \text{ cor}}^t$, $R_{\perp \text{ cor}}^c$ and $R_{\perp\parallel \text{ cor}}$ with just those η_{m+p} by which R_{\perp}^t , R_{\perp}^c and $R_{\perp\parallel}$ had been divided before. Therefore, the results of these η_{m+p} -corrections are just the experimentally determined strengths R_{\perp}^t , R_{\perp}^c and $R_{\perp\parallel}$.

The dependence of the (m+p) correction factor η_{m+p} on the “roundness” of the standardized stress exposure curve $f_E'(\theta)$ can be quantified by means of the following evaluation of the stress exposure curve $f_E'(\theta)$ with the aid of a “summation” formula. In the fracture analysis of a general three-dimensional stress state, during the necessary numerical search for the fracture plane angle the intersection-angle-dependent IFF stress exposure $f_E(\theta)$ from $\theta = -90^\circ$ to $\theta = +90^\circ$ is calculated with the aid of the fracture criteria in Fig. 42 in small angular increments $\Delta\theta$ (in most cases with $\Delta\theta = 1^\circ$). The result is a large number of $f_E(\theta)$ -values which represent points of the stress exposure curve $f_E(\theta)$. To ensure that all possible stress states are treated alike, the stress exposure curves are standardized in such a way that at point $\theta = \theta_{fp}$ the stress exposure factor has a value of 1. The standardized stress exposure curve $f_E'(\theta)$ is then valid for just that magnitude of the stresses which according to the fracture criteria in Fig. 42 would produce fracture and this is true for any kind of stress combination.

It follows from the foregoing that section planes with $f_E'(\theta)$ -values close to 1 are of much greater importance than those with $f_E'(\theta)$ values which are considerably smaller. For this reason, as already occurs in [Puck 1996], standardized $f_E'(\theta)$ values below a threshold $f_{E\text{thr}}' = 0.5$ are not taken into consideration. On the basis of equation (10.5) in [Puck 1996], the following sum is obtained with the standardized $f_E'(\theta)$ values:

$$S \approx \sum_{-90^\circ}^{+89^\circ} \left(f_E'(\theta) - f_{E\text{thr}}' \right) \cdot \Delta\theta, \text{ only for } f_E'(\theta) \geq f_{E\text{thr}}'. \quad (\text{Eq. 89})$$

(The limits -90° and $+89^\circ$ apply to the angular increment $\Delta\theta = 1^\circ$ which was used).

This summing (with a zero line shifted by $f_{E\text{thr}}'$) results in high $f_E'(\theta)$ values being weighted considerably more heavily than low values – for example, a value $f_E'(\theta) = 0.9$ is weighted four times higher than a value $f_E'(\theta) = 0.6$. For the extreme case which we mentioned of $\sigma_2 = \sigma_3 > 0$, when $f_E'(\theta) = 0.5$ the maximum S value of $S_{\text{max}} = (1 - 0.5) \cdot 180^\circ = 90^\circ$ is obtained.

If the summation formula (Eq. 89) is applied to the standardized stress exposure curves $f_E'(\theta)$ for the basic stressings, uniaxial transverse tension σ_{\perp}^t , uniaxial transverse compression σ_{\perp}^c and pure transverse/longitudinal shear $\tau_{\perp\parallel}$ (see Fig. 17), we obtain values for the corresponding sums S_{\perp}^t ,

S_{\perp}^c , $S_{\perp\parallel}$ which will lie between 30° and 40° . $S_{\perp\parallel} = 39.24^\circ$ is a material-independent fixed value while S_{\perp}^c depends on the inclination parameter $p_{\perp\perp}^c$ and has a value of approximately $S_{\perp}^c \approx 36^\circ$. For S_{\perp}^t we find material dependent values with $S_{\perp}^t \approx 33^\circ$.

Taking the value S which corresponds to a given stress state and slightly modifying equation (10.6) in [Puck 1996], we obtain the following for the (m+p)-correction factor:

$$\eta_{m+p} = 1 - \Delta_{\max} \frac{S - S_{\text{ref}}}{S_{\max} - S_{\text{ref}}} \quad (\text{Eq. 90})$$

for $\Delta_{\max} \leq 0.25$ with $S_{\max} = 90^\circ$ and $S_{\text{ref}} = 30^\circ$.

It is necessary to introduce a reference value S_{ref} in order to obtain a reasonable sensitivity of η_{m+p} to the differences in the S values occurring with different stress states. Experience shows that there is no S value of any stress state which is less than the value $S_{\text{ref}} = 30^\circ$. The variable Δ_{\max} is the relative difference between the fracture stress vector calculated according to Mohr and that corrected by η_{m+p} when $\sigma_2 = \sigma_3 > 0$. Values for Δ_{\max} should lie between 0.15 and 0.25. Selection of a value for Δ_{\max} results in a 'calibration' of the η_{m+p} -correction factor.

Applications

In common practice of the design and dimensioning of fiber composite components, fracture criteria are used for calculating the IFF stress exposure (and FF stress exposure) at some locations of the component which are regarded as critical. In what follows, however, entire fracture curves for IFF will be presented. Fracture curves of this kind reveal in which stress states η_{m+p} -correction is important and in which it is not. In Fig. 47a it can be seen that with the (σ_2, τ_{31}) -combinations, η_{m+p} -correction is very important in the first quadrant. With the (σ_2, σ_3) -combinations (Fig. 47b), a very noticeable influence also occurs in the first quadrant of the (σ_2, σ_3) -fracture curve. In the case where $\sigma_2 = \sigma_3$, this yields the utilized "calibration value" $\Delta_{\max} = 0.25$ used with η_{m+p} -correction. In the fourth (and second) quadrants, on the other hand – that is, where $\sigma_2 > 0$ and $\sigma_3 < 0$ – only a relatively minor effect of the η_{m+p} -correction is found. At $\sigma_3 = -\sigma_2$ the fracture stress at IFF calculated with η_{m+p} is even a little higher than that calculated on the basis of Mohr's hypothesis ($\sigma_2 = -\sigma_3 = R_{\perp}^t$). This results from the fact that for the pure transverse/transverse shearing stressing $\tau_{\perp\perp}$ which is here present the corresponding sum has the value $S_{\perp\perp} = 31.45^\circ$, and this is somewhat less than $S_{\perp}^t = 32.45^\circ$ for uniaxial transverse tension stressing σ_{\perp}^t .

To date there has been a lack of credible experimental results for (σ_2, τ_{31}) - and (σ_2, σ_3) -stress combinations.

The situation is entirely different for the (σ_2, τ_{21}) -stress combinations shown in Fig. 47c. The (σ_2, τ_{21}) -fracture curve is the only one which has adequate experimental backing not only for CFRP but also for GFRP [Cuntze et al. 1997]. An outstandingly good mathematical model is obtained with equations (Eq. 71), (Eq. 73) and (Eq. 77) or the fracture criteria in Fig. 42 using inclination parameters from Table 1, chapter 4.2.6.6. Before proceeding further, it is important to bear in mind the fact that the effects of η_{m+p} -effects on IFF strength are basically already included in experimentally determined fracture stresses, as also in the test results from which the modeled (σ_2, τ_{21}) -fracture curve (thick line in Fig. 47c) is obtained. If one wished to generate mathematically a (σ_2, τ_{21}) -fracture curve which involved use of η_{m+p} -correction, then the experimentally obtained (σ_2, τ_{21}) -fracture curve which was modeled using the measured basic strengths R_{\perp}^t , R_{\perp}^c , R_{\parallel} and inclination parameters from Table 1 is not the *starting curve* for the η_{m+p} -correction procedure but represents rather the *result curve*.

If it is exclusively plane $(\sigma_1, \sigma_2, \tau_{21})$ -stress states which have to be investigated, then the question of the unknown starting curve for an η_{m+p} -correction is irrelevant since the mathematically modeled, experimentally determined (σ_2, τ_{21}) -fracture curve is being used directly for fracture analysis. On the other hand, use of η_{m+p} -correction is advisable in those cases where it is necessary, during dimensioning of FRP components, to also analyze load application zones in which spatial stresses σ_3 , τ_{32} , τ_{31} of a similar magnitude to σ_2 and τ_{21} occur. To ensure that absolutely consistent calculation results are obtained here, it is, of course, necessary that the same parameters be used uniformly in the fracture criteria in Fig. 42 for all stress states which occur – in other words, even for the $(\sigma_1, \sigma_2, \tau_{21})$ -stress states prevailing in undisturbed areas. For this reason the parameters must be known which are appropriate for the (σ_2, τ_{21}) -starting curve which is itself as yet unknown.

Since in the case of the (σ_2, τ_{21}) -stress combinations the *result curve* is known and the starting curve is required, an inversion of the η_{m+p} -correction, as it were, is now necessary. The corrected basic strengths $R_{\perp}^t{}_{cor}$, $R_{\perp}^c{}_{cor}$, $R_{\parallel}{}_{cor}$ for the starting curve are obtained by ‘inverting’ the η_{m+p} -correction: the measured values R_{\perp}^t , R_{\perp}^c , R_{\parallel} are not multiplied but are instead now divided by the η_{m+p} -value which is associated with the corresponding basic stressing. (Comment: These corrected basic strengths of course apply not only to the (σ_2, τ_{21}) -stress state but of course also to any stress state.) Since the sum values S_{\perp}^t , S_{\perp}^c , S_{\parallel} of the basic stressings are

only a little higher than the reference value $S_{\text{ref}} = 30^\circ$, the correction they need remains less than 5%. In the range of high compressive stress values $|\sigma_2|$ with at the same time high values of τ_{21} , sum values up to around $S \approx 60^\circ$ are however reached in the vicinity of the transition point between Mode B ($\theta_{\text{fp}} = 0^\circ$) and Mode C ($\theta_{\text{fp}} \neq 0^\circ$) (see Fig. 24). This results in $\eta_{\text{m+p}}$ -corrections up to approximately 12%, see Fig. 48b and Fig. 47c.

The required starting curve of the (σ_2, τ_{21}) -stress combination cannot be obtained as a whole from the known result curve simply by inverting the $\eta_{\text{m+p}}$ -correction. The reason for this lies in the complex nature of the $\eta_{\text{m+p}}$ -correction which is only to be carried out numerically on a point by point basis and which makes impossible a closed mathematical formulation of the required starting curve. What is needed, however, is a (σ_2, τ_{21}) starting curve formulated using the equations in Fig. 42, since only these equations happen to be available for the fracture analysis of general three-dimensional stress states. For this reason, an acceptable approximated starting curve which is described using the equations in Fig. 42 must be found by selecting suitable parameters. What acceptable means is that when a $\eta_{\text{m+p}}$ -correction of this starting curve has been carried out correctly, a (σ_2, τ_{21}) -fracture curve is obtained as the result which will deviate only to an acceptable extent from the known modeled experimental (σ_2, τ_{21}) -fracture curve.

By iterative selection of different inclination parameters $p_{\perp\parallel}^{\text{c cor}}$ for the (σ_2, τ_{21}) -starting curve and reviewing to what extent the required acceptance is thereby achieved, the following result is obtained. If a corrected inclination parameter $p_{\perp\parallel}^{\text{c cor}} = 0.45$ is chosen for the required starting curve of the $\eta_{\text{m+p}}$ correction when the calibration value $\Delta_{\text{max}} = 0.25$ is used, what is obtained as the result of a correctly performed $\eta_{\text{m+p}}$ -correction is a (σ_2, τ_{21}) -fracture curve which comes very close to the experimental curve modeled in the usual way using the equations in Fig. 42. (Modeling of the experimental curve was carried out using the basic strengths for CFRP $R_{\perp}^{\text{t}} = 48 \text{ N/mm}^2$, $R_{\perp}^{\text{c}} = 200 \text{ N/mm}^2$, $R_{\perp\parallel} = 79 \text{ N/mm}^2$ [Soden et al. 1998] and the inclination parameters $p_{\perp\parallel}^{\text{t}} = 0.35$, $p_{\perp\parallel}^{\text{c}} = 0.30$, $p_{\perp\perp}^{\text{t}} = p_{\perp\perp}^{\text{c}} = 0.275$ according to [Puck Kopp Knops 2002]).

If, in response to one's own experimental results, one wishes to use a value different from the value $\Delta_{\text{max}} = 0.25$ used in the example and also, within the permitted limits [Puck Kopp Knops 2002], to diverge from the guideline value $p_{\perp\parallel}^{\text{c}} = 0.3$ given in Table 1, you can proceed iteratively as described above to obtain a corrected parameter $p_{\perp\parallel}^{\text{c cor}}$ provided you have a computer program which can display (σ_2, τ_{21}) -fracture curves. If this is

not the case, the following extrapolation formula may be used within a restricted range of $p_{\perp\parallel}^c$ and Δ_{\max} :

$$\frac{p_{\perp\parallel\text{cor}}^c}{p_{\perp\parallel}^c} = 1 + 0.6 \cdot \frac{\Delta_{\max}}{p_{\perp\parallel}^c} \quad (\text{Eq. 91})$$

for $0.15 \leq \Delta_{\max} \leq 0.25$ and $0.25 \leq p_{\perp\parallel}^c \leq 0.35$.

Comment

It has been shown that depending on whether you work with or without η_{m+p} -correction, you will have to analyze the stress exposure curve $f_E(\theta)$ by using different inclination parameters $p_{\perp\parallel\text{cor}}^c$ or $p_{\perp\parallel}^c$ respectively which may differ according to (Eq. 91) by a factor of up to 1.6. If shear stresses τ_{21} and/or τ_{31} occur in the stress state under investigation, by calculating with and without η_{m+p} -correction you will therefore obtain angles of the fracture plane θ_{fp} which differ somewhat. In the case of (σ_2, τ_{31}) -stress combinations the differences are from 1° to 5° . With (σ_2, τ_{21}) -stress combinations similar differences are found, provided the angles of the fracture plane $|\theta_{fp}| \geq 30^\circ$. Considerably greater differences occur in the vicinity of the transition point from mode B to mode C (see Fig. 24). But here any statements about the angle of the fracture plane which actually occurs will be tainted with a high degree of uncertainty anyway: this is due to the probabilistic effects which occur and which can be expected due to the flat course of the standardized stress exposure curve. This has been shown in experiments as well [Kopp 2000]. All in all, these deviations are not problematic in the fracture analysis.

4.3.2 Calculation of the stretch factor f_S^L of the load-determined stresses when residual stresses are present

4.3.2.1 Basic considerations

In the following the procedure to be used when calculating the stretch factor f_S^L of the (changing) load-determined lamina stresses $\sigma_1^L, \sigma_2^L, \tau_{21}^L$ when (constant) residual stresses $\sigma_1^r, \sigma_2^r, \tau_{21}^r$ are simultaneously present will be explained for the case of a $(\sigma_1, \sigma_2, \tau_{21})$ stress state. This procedure is based on Puck's action-plane fracture criteria for IFF and takes into consideration the weakening influence of the parallel-to-fiber stress σ_1 . The formulae required for the procedure are given.

The fracture conditions are the starting point for IFF when there is no influence from σ_1 . These are (see equations (Eq. 71), (Eq. 73) and (Eq. 77)):

IFF mode A

$$f_{E_0} = \sqrt{\left[\left(\frac{1}{R_{\perp}'} - \frac{p_{\perp\parallel}'}{R_{\perp\parallel}'}\right) \cdot \sigma_2\right]^2 + \left(\frac{\tau_{21}}{R_{\perp\parallel}}\right)^2} + \frac{p_{\perp\parallel}'}{R_{\perp\parallel}} \sigma_2 = 1, \text{ for } \sigma_2 \geq 0 \quad (\text{Eq. 71})$$

IFF mode B

$$f_{E_0} = \sqrt{\left(\frac{\tau_{21}}{R_{\perp\parallel}}\right)^2 + \left(\frac{p_{\perp\parallel}^c}{R_{\perp\parallel}}\right)^2} + \frac{p_{\perp\parallel}^c}{R_{\perp\parallel}} \sigma_2 = 1, \sigma_2 < 0 \wedge \left|\frac{\sigma_2}{\tau_{21}}\right| \leq \left|\frac{R_{\perp\perp}^A}{\tau_{21c}}\right| \quad (\text{Eq. 73})$$

IFF mode C

$$f_{E_0} = \frac{\tau_{21}^2}{4(R_{\perp\parallel} + p_{\perp\parallel}^c R_{\perp\perp}^A)^2} \cdot \frac{(-R_{\perp}^c)}{\sigma_2} + \frac{\sigma_2}{(-R_{\perp}^c)} = 1 \quad (\text{Eq. 92})$$

for $\sigma_2 < 0$ and $0 \leq \left|\frac{\tau_{21}}{\sigma_2}\right| \leq \left|\frac{\tau_{21c}}{R_{\perp\perp}^A}\right|$

(Eq. 92) is equivalent to (Eq. 77). The following coupling of inclination parameters was used in deriving equation (Eq. 92):

$$\frac{p_{\perp\perp}^c}{R_{\perp\perp}^A} = \frac{p_{\perp\parallel}^c}{R_{\perp\parallel}} \quad (\text{Eq. 93})$$

For this reason $R_{\perp\perp}^A$ needs to be calculated using equation (Eq. 94):

$$R_{\perp\perp}^A = \frac{R_{\perp\parallel}}{2p_{\perp\parallel}^c} \cdot \left(\sqrt{1 + 2p_{\perp\parallel}^c \frac{R_{\perp}^c}{R_{\perp\parallel}}} - 1 \right) \quad (\text{Eq. 94})$$

The fracture conditions for IFF – equations (Eq. 71), (Eq. 73) and (Eq. 77) ((Eq. 92) respectively) – describe in the $(\sigma_1, \sigma_2, \tau_{21})$ stress space the circumferential surface of a ‘cylindrical’ fracture body (see Fig. 50) whose constant cross-sectional contour is the fracture curve for (σ_2, τ_{21}) stress combinations shown in Fig. 45 which has been completed symmetrically with respect to the σ_2 axis. This body extends to infinity in both the positive and negative σ_1 directions; its real importance ceases, however, no later than at the two fiber fracture limits at $\sigma_1 = R_{\perp}^t$ and $\sigma_1 = -R_{\perp}^c$.

Any influence of σ_1 on the IFF is taken into account by introducing a weakening factor $\eta_{w1} < 1$ (see above) in the case of the strengths R_{\perp}^t, R_{\perp}^c ,

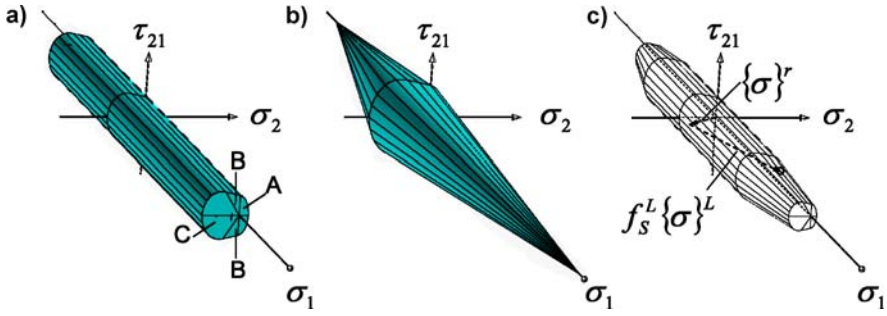


Fig. 50. Creation of the $(\sigma_1, \sigma_2, \tau_{21})$ fracture body for IFF. a) $(\sigma_1, \sigma_2, \tau_{21})$ fracture body for IFF without σ_1 influence according to (Eq. 71), (Eq. 73) and (Eq. 92). This fracture body which theoretically extends to infinity in both the positive and negative σ_1 direction is of practical relevance only between the fiber fracture limits at $\sigma_1 = R_{||}^t$ and $\sigma_1 = (-R_{||}^c)$. b) IFF fracture body calculated with weakening σ_1 influence using (Eq. 101), (Eq. 102) and (Eq. 103). c) Valid remaining fracture body as intersection of the bodies in accordance with a) and b) and following removal of the invalid parts

$R_{\perp||}$ which are of primary, decisive importance to the IFF. These strengths do not weaken until a threshold value of σ_1 is passed. This value must be determined on the basis of experimental experience and is given as a fraction of the stress $(\sigma_1)_{fr} = R_{||}^t$ or $(\sigma_1)_{fr} = (-R_{||}^c)$ leading to fiber fracture. In chapter 4.3.1.1 an ellipse has been selected for the course of the weakening factor η_{w1} as a function $\eta_{w1}(\sigma_1)$. In order to obtain a closed solution for f_s^L , and that in the form of the solution of a quadratic equation, it will be necessary to linearize the function for η_{w1} (see equation (Eq. 95) and Fig. 51). Weakening of the strengths R_{\perp}^t , R_{\perp}^c , $R_{\perp||}$ increases as FF stress exposure $f_{E,FF}$ increases; in other words, the weakening factor η_{w1} becomes smaller as $f_{E,FF}$ increases. Here the following linear equation is used:

$$\eta_{w1} = \eta_{w1,0} - \eta'_{w1} \cdot f_{E,FF} \quad (\text{Eq. 95})$$

$\eta_{w1,0}$ is a hypothetical value of η_{w1} when $\sigma_1 = 0$, and η'_{w1} is the slope of the straight line for η_{w1} according to equation (Eq. 95).

By definition, the stress exposure $f_{E,FF}$ is the ratio of the acting stress and the stress leading to fracture (cf. discussion). Accordingly, from the FF condition equation (Eq. 15) we obtain:

$$f_{E,FF} = \frac{\sigma_1}{(\sigma_1)_{fr}} \quad \text{with} \quad \begin{cases} (\sigma_1)_{fr} = R_{||}^t & \text{for } \sigma_1 \geq 0 \\ (\sigma_1)_{fr} = -R_{||}^c & \text{for } \sigma_1 < 0 \end{cases} \quad (\text{Eq. 96})$$

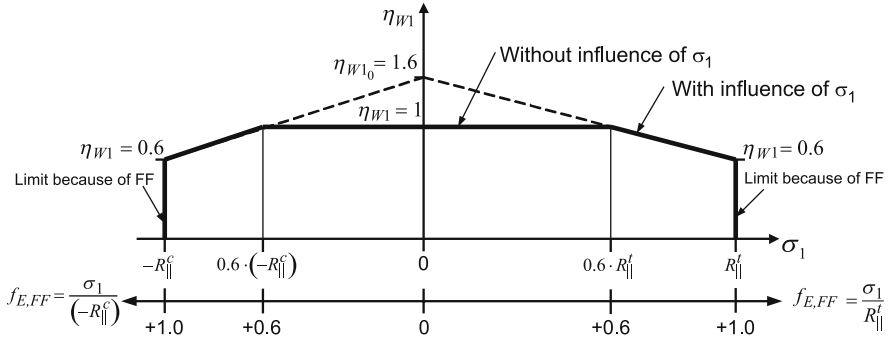


Fig. 51. Course of the weakening factor η_{w1} as a function of σ_1 or as a function of $f_{E,FF}$ in the range $-R_{||}^c \leq \sigma_1 \leq R_{||}^t$ or $0 < f_{E,FF} < 1.0$ respectively. In order to approximate the ellipse with parameters $s = m = 0.5$ as recommended in chapter 4.3.1.1, the values $\eta_{w1_0} = 1.6$ and $\eta'_{w1} = 1$ are chosen ($S = M = 0.6$).

The reason for using different signs with $R_{||}^t$ and $(-R_{||}^c)$ lies in the international convention whereby compressive stresses are expressed as negative values while all strengths (even compressive strengths) are expressed as positive values.

Now, with the aid of the weakening factor $\eta_{w1} = \eta_{w1}(\sigma_1)$ which we introduced in the case of the three strengths R_{\perp}^t , R_{\perp}^c , $R_{\perp||}$ a description is obtained of that (conical) part of the fracture body whose surface equation depends not only on σ_2 and τ_{21} but also on σ_1 (Fig. 50b).

To do so, it is necessary to select numerical values for the two parameters η_{w1_0} and η'_{w1} in the linear equation (Eq. 95) for the weakening factor η_{w1} . In chapter 4.3.1.1 the “starting point” of the “elliptical” weakening was defined by the value s and the minimum value of the weakening factor at the FF limit by the value m . If the corresponding values for the linearized course of $\eta_{w1}(f_{E,FF})$ are designed by S and M this delivers the following relationships:

$$\eta_{w1_0} = \frac{1 - S \cdot M}{1 - S} \quad (\text{Eq. 97})$$

$$\eta'_{w1} = \frac{1 - M}{1 - S} \quad (\text{Eq. 98})$$

In chapter 4.3.1.1 the recommendation was made, should experimental results be lacking, that the values $s = 0.5$ and $m = 0.5$ should be selected when η_{w1} has an elliptical course. A good approximation to this ellipse may be obtained by using $S = 0.6$ and $M = 0.6$ for the straight line. On the basis

of (Eq. 97) this yields $\eta_{w10} = 1.6$ and on the basis of (Eq. 98) $\eta_{w1}' = 1.0$. From this we obtain the course of the weakening factor η_{w1} shown in Fig. 51 as a function of σ_1 or $f_{E, FF}$. (In principle even different pairs of values (S and M) can be used for the ranges $\sigma_1 > 0$ and $\sigma_1 < 0$.)

By applying an equally high weakening factor η_{w1} to all three strengths R_{\perp}^t , R_{\perp}^c , $R_{\perp\parallel}$ which have a decisive influence on IFF we obtain (σ_2, τ_{21}) fracture curves which represent a geometrically similar reduction by a factor $\eta_{w1} < 1$ of the (σ_2, τ_{21}) fracture curve shown in Fig. 45 which was completed symmetrically to the σ_2 axis. As a consequence, therefore, of the linear equation for $\eta_{w1}(\sigma_1)$, in the $(\sigma_1, \sigma_2, \tau_{21})$ stress space we find a fracture body for IFF which has the shape of a double cone (Fig. 50b). Its cross sections perpendicular to the σ_1 axis are geometrically similar.

The “cylindrical” fracture body shown in Fig. 50a and the double-conical fracture body intersect each other at $\sigma_1 = S \cdot R_{\parallel}^t$ and $\sigma_1 = S \cdot (-R_{\parallel}^c)$ in two sections which are vertical with respect to the σ_1 axis. The validity of the cylindrical fracture body extends from the coordinates origin as far as these intersection planes. The conical circumferential surfaces of the double-conical fracture body for IFF as shown in Fig. 50b are valid in the range between the intersection planes and the planes at $\sigma_1 = R_{\parallel}^t$ and $\sigma_1 = -R_{\parallel}^c$ which are vertical to the σ_1 axis and assigned to FF.

Calculation of the desired stretch factor f_s^L for the load-determined stresses σ_1^L , σ_2^L , τ_{21}^L – from the geometrical point of view – requires determination of the point where the resulting stress vector $\{\sigma\}$ makes contact with the valid range of the surface of the $(\sigma_1, \sigma_2, \tau_{21})$ fracture body for IFF (Fig. 50c). The resulting stress vector $\{\sigma\}$ comes from the “geometrical sum” of the residual stress vector $\{\sigma\}^r$ and the load stress vector $\{\sigma\}^L$ elongated (stretched) by the factor f_s^L . The shape of the $(\sigma_1, \sigma_2, \tau_{21})$ fracture body as shown in Fig. 50c and the requirement that the load-determined vector $\{\sigma\}^L$ may only be stretched in its specified direction means that there is only one possible point of contact between the vector and the surface of the fracture body. In most cases this point of contact will be located on the cylindrical or conical part of the circumferential surface applicable to IFF. It can, however, also be located on one of the two “end faces” which are valid for FF.

4.3.2.2 Derivation of the formulae required for calculating f_s^L

In the fracture conditions for IFF – equations (Eq. 71), (Eq. 73) and (Eq. 92) – the same weakening factor $\eta_{w1}(\sigma_1)$ is used with the strengths

$R_{\perp}^t, R_{\perp}^c, R_{\perp\parallel}$. Using IFF stress exposure f_{E_1} with weakening due to σ_1 we therefore have as *fracture condition* with weakening:

$$f_{E_1}(\sigma_2, \tau_{21}, \sigma_1) = \frac{f_{E_0}(\sigma_2, \tau_{21})}{\eta_{w1}(\sigma_1)} = 1 \quad (\text{Eq. 99})$$

$$\text{or also } f_{E_0}(\sigma_2, \tau_{21}) = \eta_{w1}(\sigma_1) \quad (\text{Eq. 100})$$

For the three IFF modes this therefore yields:

For mode A

$$\frac{1}{R_{\perp\parallel}} \left[\sqrt{\left(\frac{R_{\perp\parallel}}{R_{\perp}^t} - p_{\perp\parallel}^t \right)^2 \sigma_2^2 + \tau_{21}^2 + p_{\perp\parallel}^t \sigma_2} \right] = \eta_{w1}(\sigma_1) \quad (\text{Eq. 101})$$

For mode B

$$\frac{1}{R_{\perp\parallel}} \left(\sqrt{\tau_{21}^2 + (p_{\perp\parallel}^c \sigma_2)^2} + p_{\perp\parallel}^c \sigma_2 \right) = \eta_{w1}(\sigma_1) \quad (\text{Eq. 102})$$

For mode C

$$\frac{\tau_{21}^2}{4(R_{\perp\parallel} + p_{\perp\parallel}^c R_{\perp\perp}^A)^2} \cdot \frac{(-R_{\perp}^c)}{\sigma_2} + \frac{\sigma_2}{(-R_{\perp}^c)} = \eta_{w1}(\sigma_1) \quad (\text{Eq. 103})$$

$$\text{with } \eta_{w1} = \eta_{w1_0} - \eta_{w1}' \cdot \frac{\sigma_1}{(\sigma_1)_{fr}},$$

$$\text{where } (\sigma_1)_{fr} = R_{\parallel}^t \text{ for } \sigma_1 > 0$$

$$\text{and } (\sigma_1)_{fr} = -R_{\parallel}^c \text{ for } \sigma_1 < 0.$$

The validity ranges of fracture conditions (Eq. 101) to (Eq. 103) are the same as those for equations (Eq. 71), (Eq. 73) and (Eq. 77) (see also Table 3). In the equations (Eq. 101) to (Eq. 103) the stresses σ_2 and τ_{21} are the *stresses at the fracture limit*.

The strengths $R_{\perp}^t, R_{\perp}^c, R_{\perp\parallel}$ appearing in equations (Eq. 101) to (Eq. 103) are the “unweakened” strengths. For the stresses $(\sigma_1, \sigma_2, \tau_{21})$ occurring in

them we use the stress components corresponding to the contact point of the resultant *fracture vector* $\{\sigma_{fr}\} = \{\sigma\}^r + f_s^L \{\sigma\}^L$:

$$\sigma_1 = \sigma_1^r + f_s^L \sigma_1^L, \quad (\text{Eq. 104})$$

$$\sigma_2 = \sigma_2^r + f_s^L \sigma_2^L, \quad (\text{Eq. 105})$$

$$\tau_{21} = \tau_{21}^r + f_s^L \tau_{21}^L. \quad (\text{Eq. 106})$$

In this way we obtain equations whose only unknown is the desired stretch factor f_s^L of the load-determined stresses. After necessary reformulation, which in particular includes the removal of the root expressions, we obtain for each of the modes A, B, C a quadratic equation for f_s^L to which can be applied the known solution formula:

$$f_s^L = \frac{1}{2q} \left(\sqrt{l^2 - 4qc} - l \right). \quad (\text{Eq. 107})$$

Quantities q and l are the coefficients of the quadratic terms or of the linear terms of f_s^L , and in c are grouped the corresponding (constant) terms which are independent of f_s^L . Table 2 shows quantities q , l and c in each case for IFF modes A, B and C.

4.3.2.3 Procedure for calculating f_s^L and evaluation of results

With this task the starting situation is generally the following. The component design process came up with a laminate whereby specification of fiber directions and fiber quantities has been brought to a stage whereby the next step is to try to improve the laminate structure with regard to homogenizing the “safety” to IFF in the individual laminae. The load-determined stresses which need to be taken into account here in most cases relate to the maximum loading to be expected when the component is in service. With this maximum loading an addition safety margin with respect to IFF is to be provided and generally a larger safety margin with respect to FF. When considerable residual stresses are present, it is not possible on the basis of calculated stress exposure values f_{E_1} to come to any useful conclusions regarding these safety margins for the individual lamina, instead this is entirely possible on the basis of the stretch factors f_s^L of the load-determined stresses.

Before commencing with determining f_s^L with regard to IFF, it appears to be advisable to clarify whether an IFF can even occur in the lamina under consideration or whether a FF will appear first before an IFF.

From the simple FF condition given in (Eq. 14) it follows that it is solely stress σ_1 which is responsible for the FF. At FF:

$$f_{E,FF} = \frac{\sigma_1}{(\sigma_1)_{fr}} = \frac{\sigma_1^r + f_{S(FF)}^L \cdot \sigma_1^L}{(\sigma_1)_{fr}} = 1. \quad (\text{Eq. 108})$$

where $(\sigma_1)_{fr} = R_{\parallel}^t$ for $\sigma_1 > 0$

and $(\sigma_1)_{fr} = -R_{\parallel}^c$ for $\sigma_1 < 0$.

If σ_1^r and σ_1^L have the same sign, $\sigma_1 = \sigma_1^r + f_{S(FF)}^L \cdot \sigma_1^L$ can also only have the same sign. If σ_1^r and σ_1^L have different signs, it can be assumed that σ_1^r alone will not yet cause a FF. This is because a FF due solely to σ_1^r must not even be permitted and will have already been ruled out by the designer's pre-dimensioning. Should a stress $f_{S(FF)}^L \cdot \sigma_1^L$ with a different sign appear in addition to σ_1^r , then as it increases it will initially work in opposition to the residual stress σ_1^r . Not until after the "disappearance" of σ_1^r will the resulting stress σ_1 increase with the same sign as σ_1^L until the FF limit at $\sigma_1 = (\sigma_1)_{fr}$ is reached and FF finally occurs. Consequently the decision regarding the quantity $(\sigma_1)_{fr}$ to be used in equation (Eq. 108) can be made as follows:

$$\begin{aligned} (\sigma_1)_{fr} &= R_{\parallel}^t \text{ for } \sigma_1^L > 0 \\ (\sigma_1)_{fr} &= -R_{\parallel}^c \text{ for } \sigma_1^L < 0. \end{aligned} \quad (\text{Eq. 109})$$

The stretch factor $f_{s(FF)}^L$ of the load-determined stresses *with regard to FF* is thus obtained from equations (Eq. 108) and (Eq. 109):

$$f_{S(FF)}^L = \frac{(\sigma_1)_{fr} - \sigma_1^r}{\sigma_1^L}. \quad (\text{Eq. 110})$$

The three components σ_1^L , σ_2^L , τ_{21}^L of the load-determined stress vector are all increased by the same stretch factor. Once the FF limit is reached, the resulting stresses will therefore have these magnitudes:

$$\sigma_1 = \sigma_1^r + f_{S(FF)}^L \sigma_1^L, \quad (\text{Eq. 111})$$

$$\sigma_2 = \sigma_2^r + f_{S(FF)}^L \sigma_2^L, \quad (\text{Eq. 112})$$

$$\tau_{21} = \tau_{21}^r + f_{S(FF)}^L \tau_{21}^L. \quad (\text{Eq. 113})$$

With the aid of these stresses a check is made as to whether the contact point of the resulting stress vector (at $\sigma_1 = R_{\parallel}^t$ or $\sigma_1 = -R_{\parallel}^c$) lies inside or outside the contour line of the fracture body end face as shown in Fig. 50c. This contour line is the intersection line of the conical circumferential surface for IFF and the FF plane. It is a reduced (σ_2, τ_{21}) fracture curve for IFF which is geometrically similar reduced by the minimum weakening factor $\eta_{w1} = M$ valid at the FF limit.

With stresses σ_2 and τ_{21} calculated at the FF limit on the basis of equations (Eq. 112) and (Eq. 113) and $\eta_{w1} = M$, the IFF stress exposure with σ_1 influence can be calculated from:

$$f_{E_1} = \frac{f_{E_0}}{\eta_{w1}} = \frac{f_{E_0}}{M}, \quad (\text{Eq. 114})$$

doing so with the equation for mode A, B or C which is valid for the stress state under consideration (see equations (Eq. 71), (Eq. 73) and (Eq. 92)).

If the result $f_{E_1} = 1$ were obtained from equation (Eq. 114), the contact point would be located exactly on the IFF curve and simultaneously in the plane for FF. In theory this would therefore mean that both IFF and FF would occur. If $f_{E_1} < 1$ is the result, the vector passes through the FF plane without having previously touched an IFF circumferential surface – in other words, a f_s^L value cannot be calculated for IFF.

Should the result be $f_{E_1} > 1$, this means that the vector must pierce the IFF circumferential surface before it reaches the FF limit. In this case f_s^L is calculated for IFF using the procedure shown in the flow chart in Fig. 52.

Instead of the sequence shown in this flow chart, the computational operations and inquiries could also be carried out in a different order. Whatever the case, it ends up to a procedure whereby arbitrary assumptions are made first (for example, about which IFF mode is to be expected, A, B or C and $(\sigma_1)_{fr} = R_{\parallel}^t$ or $(\sigma_1)_{fr} = -R_{\parallel}^c$ as well as an assumption as to whether a σ_1 influence is already becoming effective or not. A decision is then made on the basis of the computational results as to whether the assumptions made were justified or not. If this does not appear to be the case, f_s^L is recalculated using modified assumptions. The procedure in the flow chart (Fig. 52) is that in each case the investigation is carried out for a selected mode A, B or C until the result is accepted or rejected. The final test is to check to see whether the calculated contact point actually falls within the range of validity of the equations associated with the mode under consideration.

If the result for a mode passes in addition to all proceeding tests also this final one, this means that the result is the correct and only possible result, because only one contact point exists.

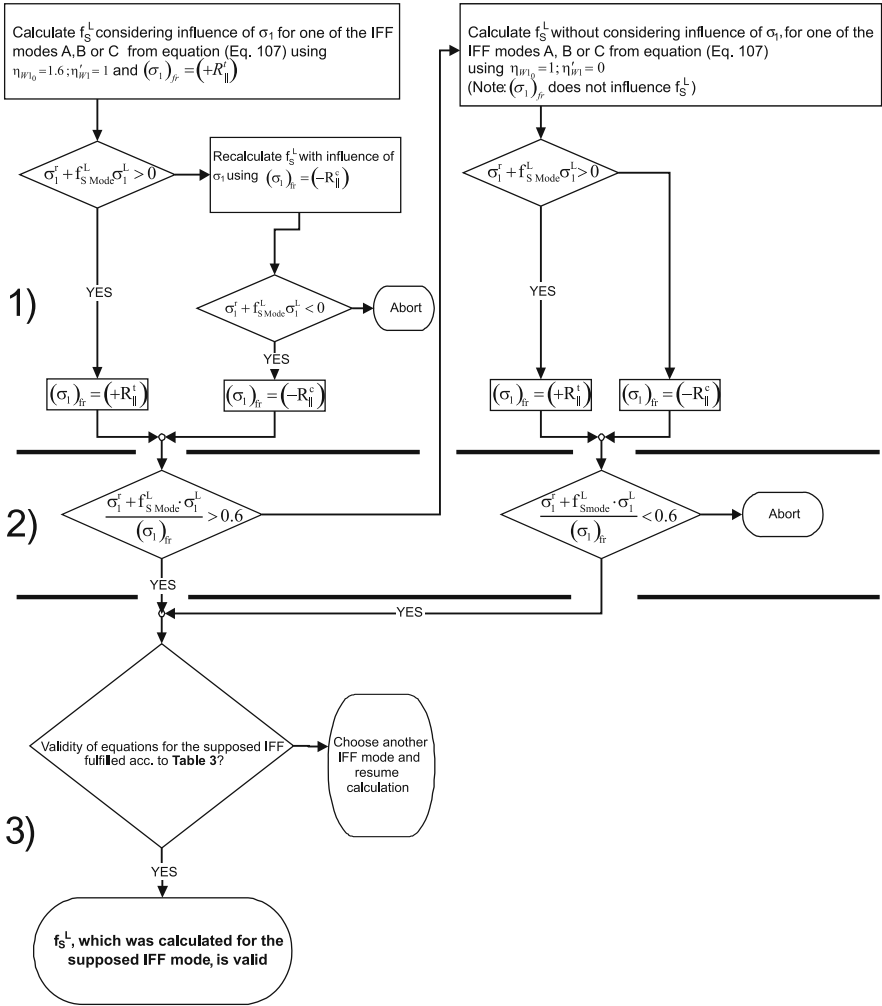


Fig. 52. Checks which have to be carried out during calculation of the stretch factor f_s^L for an IFF mode A, B or C in order to decide whether the weakening influence of σ_1 needs to be considered for the IFF modes, as well as the final check, whether the contact point to the fracture body surface falls within the range of validity of the equations for the considered IFF-mode A, B or C.

Table 2. Terms of equation (Eq. 107) for the calculation of f_S^L

IFF mode	
A	$q_A = \frac{(\tau_{21}^L)^2}{R_{\perp\parallel}^2} - \frac{2p_{\perp\parallel}' \eta_{w1}' \sigma_1^L \sigma_2^L}{R_{\perp\parallel} (\sigma_1)_{fr}} + \left(1 - \frac{2p_{\perp\parallel}' R_{\perp}^L}{R_{\perp\parallel}^2}\right) \cdot \frac{(\sigma_2^L)^2}{(R_{\perp\parallel})^2} - \frac{(\eta_{w1}')^2 (\sigma_1^L)^2}{(\sigma_1)_{fr}^2}$ $l_A = -\frac{2p_{\perp\parallel}' \eta_{w1}' \sigma_1^L \sigma_2^L}{R_{\perp\parallel} (\sigma_1)_{fr}} + \frac{2p_{\perp\parallel}' \sigma_2^L}{R_{\perp\parallel}} \cdot \left(\eta_{w1_0} - \eta_{w1}' \cdot \frac{\sigma_1^r}{(\sigma_1)_{fr}}\right) + \frac{2\sigma_2^r \sigma_2^L}{(R_{\perp\parallel}^2)^2} \cdot \left(1 - \frac{2p_{\perp\parallel}' R_{\perp}^L}{R_{\perp\parallel}^2}\right) +$ $+ \frac{2\eta_{w1}' \sigma_1^L}{(\sigma_1)_{fr}} \cdot \left(\eta_{w1_0} - \eta_{w1}' \cdot \frac{\sigma_1^r}{(\sigma_1)_{fr}}\right) + \frac{2\tau_{21}^r \tau_{21}^L}{R_{\perp\parallel}^2}$ $c_A = \left(1 - \frac{2p_{\perp\parallel}' R_{\perp}^L}{R_{\perp\parallel}^2}\right) \cdot \frac{(\sigma_2^L)^2}{(R_{\perp\parallel}^2)^2} - \left(\eta_{w1_0} - \eta_{w1}' \cdot \frac{\sigma_1^r}{(\sigma_1)_{fr}}\right)^2 + \frac{(\tau_{21}^r)^2}{R_{\perp\parallel}^2} + \frac{2p_{\perp\parallel}' \sigma_2^L}{R_{\perp\parallel}} \cdot \left(\eta_{w1_0} - \eta_{w1}' \cdot \frac{\sigma_1^r}{(\sigma_1)_{fr}}\right)$
B	$q_B = \frac{(\tau_{21}^L)^2}{R_{\perp\parallel}^2} - \frac{2p_{\perp\parallel}^c \eta_{w1}' \sigma_1^L \sigma_2^L}{R_{\perp\parallel} (\sigma_1)_{fr}} - \frac{(\eta_{w1}')^2 (\sigma_1^L)^2}{(\sigma_1)_{fr}^2}$ $l_B = \frac{2\tau_{21}^r \tau_{21}^L}{R_{\perp\parallel}^2} - \frac{2p_{\perp\parallel}^c \eta_{w1}' \sigma_1^L \sigma_2^L}{R_{\perp\parallel} (\sigma_1)_{fr}} + \frac{2p_{\perp\parallel}^c \sigma_2^L}{R_{\perp\parallel}} \cdot \left(\eta_{w1_0} - \eta_{w1}' \cdot \frac{\sigma_1^r}{(\sigma_1)_{fr}}\right) +$ $+ \frac{2\eta_{w1}' \sigma_1^L}{(\sigma_1)_{fr}} \cdot \left(\eta_{w1_0} - \eta_{w1}' \cdot \frac{\sigma_1^r}{(\sigma_1)_{fr}}\right)$ $c_B = \frac{(\tau_{21}^r)^2}{R_{\perp\parallel}^2} - \left(\eta_{w1_0} - \eta_{w1}' \cdot \frac{\sigma_1^r}{(\sigma_1)_{fr}}\right)^2 + \frac{2p_{\perp\parallel}^c \sigma_2^L}{R_{\perp\parallel}} \cdot \left(\eta_{w1_0} - \eta_{w1}' \cdot \frac{\sigma_1^r}{(\sigma_1)_{fr}}\right)$
C	$q_C = \frac{1}{4} \cdot \frac{(\tau_{21}^L)^2}{(R_{\perp\parallel} + p_{\perp\parallel}^c R_{\perp\perp}^A)^2} + \frac{(\sigma_2^L)^2}{(R_{\perp\perp}^c)^2} - \frac{\eta_{w1}' \sigma_1^L \sigma_2^L}{R_{\perp\perp}^c (\sigma_1)_{fr}}$ $l_C = \frac{\tau_{21}^r \tau_{21}^L}{2(R_{\perp\parallel} + p_{\perp\parallel}^c R_{\perp\perp}^A)^2} - \frac{\eta_{w1}' \sigma_1^L \sigma_2^L}{R_{\perp\perp}^c (\sigma_1)_{fr}} - \frac{\eta_{w1}' \sigma_1^L \sigma_2^r}{R_{\perp\perp}^c (\sigma_1)_{fr}} + \frac{\eta_{w1_0} \sigma_2^L}{R_{\perp\perp}^c} + \frac{2\sigma_2^r \sigma_2^L}{(R_{\perp\perp}^c)^2}$ $c_C = \frac{1}{4} \cdot \frac{(\tau_{21}^r)^2}{(R_{\perp\parallel} + p_{\perp\parallel}^c R_{\perp\perp}^A)^2} + \frac{\eta_{w1_0} \sigma_2^r}{R_{\perp\perp}^c} + \frac{(\sigma_2^r)^2}{(R_{\perp\perp}^c)^2} - \frac{\eta_{w1}' \sigma_2^r \sigma_1^r}{R_{\perp\perp}^c (\sigma_1)_{fr}}$
<p>Note: Because of the parameter coupling $p_{\perp\perp}^c R_{\perp\parallel} = p_{\perp\parallel}^c \cdot R_{\perp\perp}^A$ according to (Eq. 93) $R_{\perp\perp}^A$ needs to be calculated using (Eq. 94):</p> $R_{\perp\perp}^A = \frac{R_{\perp\parallel}}{2p_{\perp\parallel}^c} \left(\sqrt{1 + 2p_{\perp\parallel}^c \frac{R_{\perp\perp}^c}{R_{\perp\parallel}}} - 1 \right)$	
$(\sigma_1)_{fr} = \begin{cases} (\sigma_1)_{fr} = R_{\parallel}' & \text{for } \sigma_1 > 0 \\ (\sigma_1)_{fr} = -R_{\parallel}^c & \text{for } \sigma_1 < 0 \end{cases}$	
<p>The relations given in Table 2 are also suitable for the calculation of f_S^L without influence of σ_1 by setting $\eta_{w1_0} = 1.0$ and $\eta_{w1}' = 0$</p>	

Table 3. Range of validity of the equations for IFF modes A, B, C

IFF mode	Range of validity
A	$\sigma_2^r + f_{S\ A}^L \cdot \sigma_2^L \geq 0$
B	$\sigma_2^r + f_{S\ B}^L \cdot \sigma_2^L < 0$ and $0 \leq \left \frac{\sigma_2^r + f_{S\ B}^L \cdot \sigma_2^L}{\tau_{21}^r + f_{S\ B}^L \cdot \tau_{21}^L} \right \leq \frac{R_{\perp\perp}^A}{ \tau_{21c}^L }$
C	$\sigma_2^r + f_{S\ C}^L \cdot \sigma_2^L < 0$ and $0 \leq \left \frac{\tau_{21}^r + f_{S\ C}^L \cdot \tau_{21}^L}{\sigma_2^r + f_{S\ C}^L \cdot \sigma_2^L} \right \leq \frac{ \tau_{21c}^L }{R_{\perp\perp}^A}$ with $\tau_{21c}^L = R_{\perp\perp} \cdot \sqrt{1 + 2p_{\perp\perp}^c}$ ($p_{\perp\perp}^c$ according to (Eq. 93) and $R_{\perp\perp}^A$ according to (Eq. 94))

With the coordinates σ_1 , σ_2 , τ_{21} of this contact point on the fracture body surface, the value $f_{E_1} = 1$ for the IFF stress exposure f_{E_1} must result from equation (Eq. 99) when applying the relevant equation (Eq. 101), (Eq. 102) or (Eq. 103). This can be used for checking purposes.

If a value is calculated for $f_{S\ }^L$ which is <1 , this indicates that the IFF limit will have already been exceeded with the existing load stresses $\sigma_1^L, \sigma_2^L, \tau_{21}^L$ used in the calculation!

4.4 Visualization of fracture bodies

The visualization of fracture conditions for FRP has been treated by Kopp [Kopp and Michali 1999]. This visualization can very much help to see and comprehend the characteristics of different fracture conditions. For the principal understanding it is important to recall the remarks on the coordinate systems in the chapter 3.

The visualization of fracture conditions for isotropic material is not difficult at all. In this case the 6 stress components σ_1 , σ_2 , σ_3 , τ_{23} , τ_{31} , τ_{21} are substituted by 3 principal normal stresses σ_{IP} , σ_{IIP} , σ_{IIIP} . For fibrous transversely isotropic materials such a change of the coordinate systems is not possible, as a rotation is only allowed in the so called transversely isotropic (x_2 , x_3)-plane. The x_1 -axis must remain parallel to the fiber direction, because only for these 'natural directions' the basic strength parameters of the UD-layer are known.

The following investigations will only consider stresses having a direct influence on IFF. The fiber parallel stress σ_1 is disregarded, since IFF occurs in a fiber parallel plane [2, 3] and with that the fracture plane is parallel to σ_1 . The corresponding situation for an isotropic material is that $\sigma_1 = \sigma_{IP}$ is neither the minimal nor the maximal principal normal stress. According to *Mohr* only the extreme values of the principal stresses σ_{IIP} and σ_{IIIP} do have an influence on the fracture process; for this reason fracture occurs parallel to the direction of σ_{IP} similar to the IFF in an UD-lamina.

For human imagination it is necessary to restrict fracture bodies to three dimensions. Therefore it seems reasonable in a first step to transform the $(\sigma_2, \sigma_3, \tau_{23}, \tau_{31}, \tau_{21})$ -stress state in consideration of the transverse isotropy into a $(\sigma_{II}, \sigma_{III}, 0, \tau_{III}, \tau_{II})$ -stress state (Fig. 20). By no means σ_{II} and σ_{III} are 'real' principal stresses σ_{IIP} and σ_{IIIP} , because also the shear stresses τ_{III}, τ_{II} occur on their action planes (Fig. 20). Using the following transformation rule one is enabled to substitute any stress component appearing in a fracture condition in the way wanted:

$$\begin{Bmatrix} \sigma_2 \\ \sigma_3 \\ \tau_{23} \\ \tau_{31} \\ \tau_{21} \end{Bmatrix} = \begin{bmatrix} \cos^2 \varphi & \sin^2 \varphi & -2 \cdot \sin \varphi \cdot \cos \varphi & 0 & 0 \\ \sin^2 \varphi & \cos^2 \varphi & 2 \cdot \sin \varphi \cdot \cos \varphi & 0 & 0 \\ \sin \varphi \cdot \cos \varphi & -\sin \varphi \cdot \cos \varphi & \cos^2 \varphi - \sin^2 \varphi & 0 & 0 \\ 0 & 0 & 0 & \cos \varphi & \sin \varphi \\ 0 & 0 & 0 & -\sin \varphi & \cos \varphi \end{bmatrix} \cdot \begin{Bmatrix} \sigma_{II} \\ \sigma_{III} \\ 0 \\ \tau_{III} \\ \tau_{II} \end{Bmatrix} \quad (\text{Eq. 115})$$

$$\text{with } \varphi = \frac{1}{2} \arctan \frac{2 \cdot \tau_{23}}{\sigma_2 - \sigma_3}$$

The next step is to replace the shear stresses τ_{III} and τ_{II} by the resulting longitudinal shear stress $\tau_{\omega 1}$ as shown in (Fig. 53). The Figure clarifies that τ_{III} and τ_{II} are nothing else but the components of a longitudinal shear stress $\tau_{\omega 1}$ acting on a plane perpendicular to the x_1 -direction [Puck 1997]:

$$\tau_{\omega 1} = \sqrt{\tau_{III}^2 + \tau_{II}^2} = \sqrt{\tau_{III}^2 + \tau_{II}^2} = \tau_{\omega 1} \quad (\text{Eq. 116})$$

The direction of $\tau_{\omega 1}$ is defined by the angle δ :

$$\delta = \arctan \frac{\tau_{III}}{\tau_{II}} = \arctan \frac{\tau_{III}}{\tau_{II}} \quad (\text{Eq. 117})$$

δ is called the difference angle or deviation angle because its value is a measure for the deviation of the action planes of $\tau_{\omega 1}$ and σ_{II} . Stress states

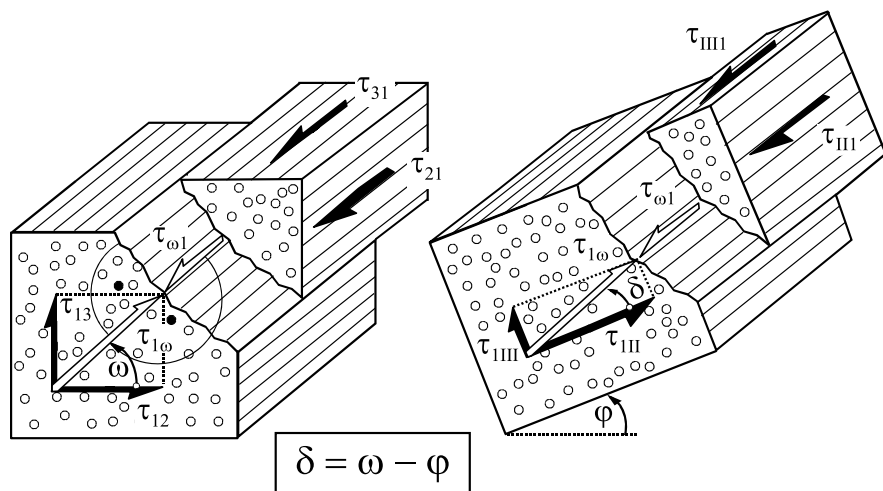


Fig. 53. Resulting shear stress $\tau_{\omega 1}$ and deviation angle δ

without transversal stresses σ_{II} and σ_{III} will lead to an IFF in the fiber parallel plane the resultant shear stress $\tau_{\omega 1}$ is acting in. In this special case the fracture angle is $\theta_{fp} = \omega = \arctan \tau_{31}/\tau_{21}$ and fracture takes place when $\tau_{\omega 1}$ has reached the longitudinal shear strength $R_{\perp\parallel}$. One can imagine that in general the deviation angle δ between the action planes of $\tau_{\omega 1}$ and σ_{II} is of main importance for the fracture process. It is obvious that in dependence of δ the interaction between the transverse extreme stresses σ_{II} , σ_{III} and the resulting shear stress $\tau_{\omega 1}$ is more or less distinct. As an example one can regard a $(\sigma_{II} > 0, 0, \tau_{\omega 1}, \delta)$ -stress state with $\delta = 0^\circ$ on the one hand and $\delta = 90^\circ$ on the other hand. In contrast to the complete interaction of σ_{II} and $\tau_{\omega 1}$ for $\delta = 0^\circ$ there is no interaction at all for $\delta = 90^\circ$ and fracture does not take place as long as either σ_{II} reaches the transverse tension strength R_{\perp}^t or $\tau_{\omega 1}$ reaches $R_{\perp\parallel}$. It is inevitable to consider δ as a parameter for the visualization of fracture conditions. From an academic point of view this leads to an infinite number of fracture bodies in the $(\sigma_{II}, \sigma_{III}, \tau_{\omega 1})$ -stress space, as any small change of δ might modify the fracture body slightly. For the comparison of different fracture conditions it is absolutely sufficient to make a $\Delta\delta = 22,5^\circ$ grading.

All fracture conditions visualized in this chapter were calculated with the same set of basic strength values published in [Cuntze et al. 1997]. If a criterion is complemented by additional material coefficients the suggestions of the accompanying developer were fulfilled.

4.4.1.1 Tsai,Wu-criterion

A classical representative of a global strength criterion is the well-known criterion of *Tsai* and *Wu* (Tsai and Wu 1971). It is a pure interpolation polynomial deduced from the basic strength values of the UD-layer, not regarding the fact that some strength values are dominated by fiber strength and others by matrix or interface strength.

The result is a smooth fracture body without any edges. Most certainly the fracture body does not change its shape if the influence of σ_I is neglected. According to expectations the *Tsai,Wu*-criterion takes on the shape of an ellipsoid in the $(\sigma_{II}, \sigma_{III}, \tau_{\omega I})$ -stress space, too (Fig. 54). There is no dependence on the deviation angle δ . As σ_{II} and σ_{III} are treated absolutely equally in the invariant formulation of the criterion the fracture body is moreover symmetrical with regard to the $(\sigma_{II} = \sigma_{III})$ -plane. Therefore stress states having a transverse normal stress and a longitudinal shear stress acting on the same plane are treated equally to those having their action planes perpendicular to each other. Another remarkable aspect of this fracture body is that it is closed for biaxial compressive stresses $\sigma_{II} \approx \sigma_{III}$. From a macro mechanical point of view – which is the basis of all strength criteria investigated here – the shear fracture due to transverse compression is not possible for $\sigma_{II} = \sigma_{III}$ as the maximum transverse shear

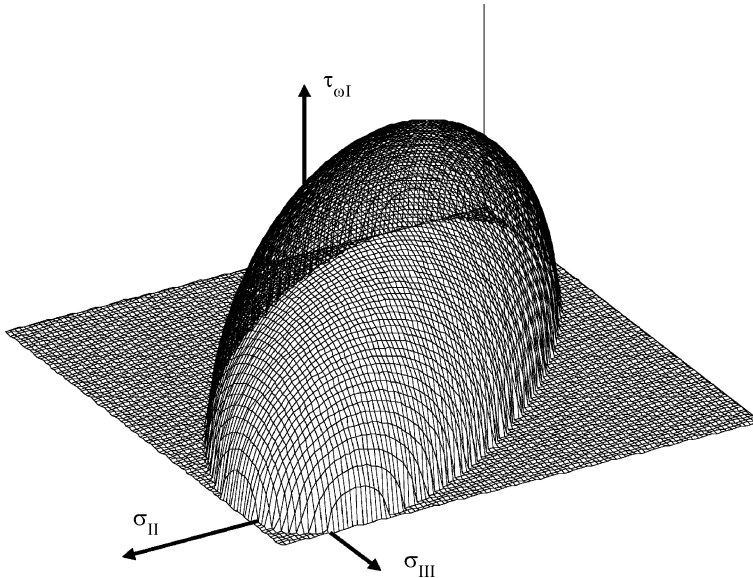


Fig. 54. Fracture body of the Tsai,Wu-criterion

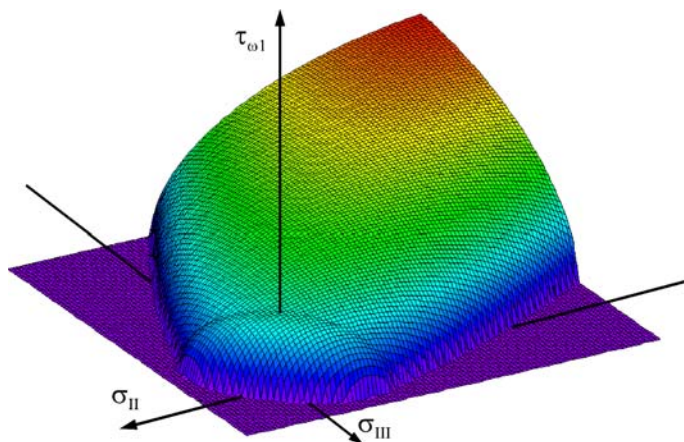


Fig. 55. Fracture body of the Hashin-criterion

stress $\tau_{\perp\perp\max} = \frac{1}{2}(\sigma_{II} - \sigma_{III})$ always remains zero. However – because of micromechanical inhomogeneity – a ‘damage limit’ for biaxial transverse compressive stresses must be expected ([Kopp et al. 1997]). After exceeding this ‘damage limit’ the micro-cracks in the matrix will reduce the original mechanical properties noticeably but a real material separation does not happen.

4.4.1.2 Hashin-criterion

Usually the term Hashin-criterion for IFF is related to two invariant fracture conditions published in (Hashin 1980), although in the same publication an action plane related approach is discussed too, which gave Puck the impulse to develop his action plane related IFF-criterion (Puck 1992). As Hashin was aware of the importance of the sign of the normal stress σ_n on the fracture plane, his invariant formulations differentiate between the cases $\sigma_n \geq 0$ and $\sigma_n < 0$. Unfortunately the fracture plane is not known a priori and cannot be found by using invariant formulations. Therefore Hashin had to define a more practical condition to delimit his fracture conditions from each other. He fixed the boundary of the sections for $\sigma_n \geq 0$ and for $\sigma_n < 0$ in the plane $\sigma_{III} = -\sigma_{II}$. However he simultaneously pointed out the severe physical contradictions, which result from this rather arbitrary boundary.

The corresponding fracture body is composed of a paraboloid with elliptical cross sections for $\sigma_n < 0$ and a crosswise oriented ellipsoid for $\sigma_n \geq 0$. Both are symmetric to the $(\sigma_{II} = \sigma_{III})$ -plane and intersect each other in the

($\sigma_{III} = -\sigma_{II}$)-plane in an elliptical borderline. The fracture curve for $\tau_{\omega I} = 0$ and $\sigma_n \geq 0$ contradicts to the theory of Paul (Paul 1961), which assumes no interactions of the principal stresses in this area, but Hashin already takes into account that a real fracture due to biaxial transverse compression is not possible. Accordingly the fracture body is not closed for $\sigma_{II} \approx \sigma_{III}$. Again it has to be emphasized that the Hashin fracture body is independent of the deviation angle δ .

4.4.1.3 Puck criterion

Figure 56 displays the fracture bodies of Puck's IFF-criterion in the (σ_{II} , σ_{III} , $\tau_{\omega I}$)-stress space in dependence on δ . Of course all fracture bodies show the same base in the (σ_{II} , σ_{III})-plane, which has – except of the compression/compression domain – the shape of Paul's fracture envelope for intrinsically brittle isotropic material (Paul 1961). Comparable to Hashin's approach in the third quadrant fracture due to biaxial transverse compression is not possible.

Particularly interesting is the shape of the fracture bodies for $\delta = 0^\circ$ and $\delta = 90^\circ$. Here the components of the fracture surface, which belong to the different fracture modes marked in the figure, touch each other in sharp edges. (A fracture mode is defined by the combination of stressings acting on the fracture plane (Puck 1997)). It is remarkable that Puck's fracture

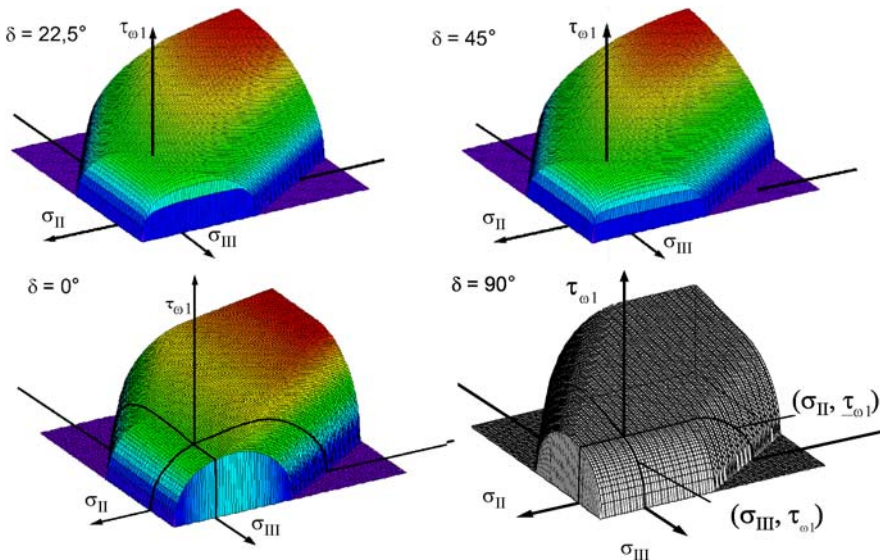


Fig. 56. Fracture bodies of the action plane related criterion by Puck

conditions, which describe a smooth ellipsoid combined with a smooth paraboloid in the $(\sigma_n, \tau_{nt}, \tau_{nl})$ -stress space (compare Fig. 45), have the ability to describe so many fracture surface portions in the $(\sigma_{II}, \sigma_{III}, \tau_{\omega I})$ -stress space. The reason for this is given by the search of the plane with the highest stress exposure factor. Thereby the criterion corresponds in certain sections to a maximum stress criterion, whereas other stress combinations are assessed in the form of a mixed-mode criterion. These effects can be clarified excellently by means of the fracture envelopes for $\sigma_{II} = 0$ and $\sigma_{III} = 0$ which have been drawn onto the fracture body for $\delta = 90^\circ$. Whereas the $(\sigma_{III}, \tau_{\omega I})$ -fracture envelope corresponds in its complete extent of validity to a mixed-mode criterion, by far the most of the $(\sigma_{II}, \tau_{\omega I})$ -fracture envelope corresponds to a maximum normal stress criterion or a maximum longitudinal shear stress criterion. The explanation for this phenomenon is, that in case of a deviation angle $\delta = 90^\circ$ the stresses $\tau_{\omega I} = \tau_{III}$ and σ_{III} are acting on the same fiber parallel plane and therefore promote fracture together. In contrast $\tau_{\omega I} = \tau_{III}$ is acting on a plane that is perpendicular to the one σ_{II} is acting on; according to *Mohr* an interaction is therefore not possible until an inclined fracture plane occurs and the transverse shear stress τ_{nt} due to high σ_{II}^c co-operates with the longitudinal shear stress τ_{nl} to produce fracture.

Passing over to deviation angles, which differ some degrees from 0° and 90° , the sections comparable to a maximum stress criterion vanish, except for the $(\sigma_{II}, \sigma_{III})$ -base. In case of $\delta = 45^\circ$ the fracture body has to be symmetrical with regard to the $(\sigma_{II} = \sigma_{III})$ -plane, as the action plane of $\tau_{\omega I}$ is equally inclined towards the action planes of σ_{II} and σ_{III} .

The comparison of fracture bodies in the $(\sigma_{II}, \sigma_{III}, \tau_{\omega I}, \delta)$ -stress space clearly demonstrates the shortcomings of criteria that do not account for the deviation angle δ between the action planes of the transverse principal stress σ_{II} and the resulting longitudinal shear stress $\tau_{\omega I}$.

4.5 Summary of chapter

This chapter is the core part of the whole book. Here the Puck criteria are derived and presented in all detail. It is worth to read it from the first line on in order to fully understand the physical background of the criteria and the mathematical derivation.

Puck's criteria are based on the concept of intrinsically brittle materials. As an introduction Mohr's fracture hypotheses, the concept of principal stresses and the visualization in the Mohr circles are recalled and extended to orthotropic materials.

The fiber fracture criteria are presented prior to the IFF-criteria, because their explanation takes less space and the derivation of the criteria is simpler. Puck has developed FF-criteria which take all possible influences of shear and transverse normal stresses into account. However, for most cases the most simple maximum stress criterion is still valid for FF-analysis.

The main focus of Puck's work has always been on Inter Fiber Fracture. Puck's criteria offer not only a perfect calculation of the fracture limit and the stress exposure. In addition the fracture angle is calculated. With this additional information the differentiation between tolerable and non-tolerable IFF becomes possible.

The IFF-criteria are first explained in their general 3D-formulation. The mathematical derivation is made step by step and easy to follow. From the general formulation the equations for plane 2D-states of stress are derived. These 2D-formulations are of interest because they do not need the numerical search of the fracture plane.

Puck's criteria are based on knowledge of the idea that fracture is caused by the stresses on the fracture plane. Therefore in the original formulation of Puck's criteria no influence of fiber parallel stress on IFF is reflected. However, as a matter of fact high σ_1 stress leads to microdamage and reduces the strength of the material against IFF. Puck has developed a way to incorporate this into his criteria. In the same way he has incorporated probabilistic effects. These later developments are discussed under the headline "Extensions to the IFF-criteria". Another chapter is dedicated to the visualization of (IFF-) criteria. This visualization is a very good means to illustrate the characteristics of a creation and to compare different criteria. This comparison is done here for the classical Tsai/Wu-criterion, the Hashin-criterion and the Puck criteria.

Analysis of Failure in Fiber Polymer Laminates

The Theory of Alfred Puck

Knops, M.

2008, XI, 205 p., Hardcover

ISBN: 978-3-540-75764-1